Supplementary information

Effective interplay of donor and acceptor groups for optoelectronic properties tuning in Oligothiophene-Naphthalimide Assemblies

Matías J. Alonso-Navarro[a,c†], Alexandra Harbuzaru[b†], Paula de Echegaray[a,c‡], Iratxe Arrechea-Marcos[b‡], Albert-Harillo-Baños[d], Alejandro de la Peña [a,c] M. Mar Ramos,[c] J. Teodomiro López Navarrete[b], Mariano Campoy-Quiles[d], Rocío Ponce Ortiz[b]*, José L. Segura [a]*

[a]*Department of Organic Chemistry, Complutense University of Madrid, Faculty of Chemistry, Madrid 28040, Spain.*

[b]*Department of Physical Chemistry, University of Málaga, Málaga, 29071, Spain.*

[c]*Chemical and Environmental Technology Department. Univ. Rey Juan Carlos, Móstoles, 28933, Spain.*

[d]*Institut de Ciencia de Materials de Barcelona (ICMAB-CSIC), 08193 Bellaterra, Spain*

† These authors contributed equally to this work
‡ These authors contributed equally to this work

Contents

1. General Information

All the chemicals were purchased from commercial suppliers and used without further purification. **NID**, **NID$_b$**, **1, 2**, **3**, **5** and **6** were obtained as previously described.[1-8] Compounds **4** and **7** are commercially available. ^{1}H-NMR and ^{13}C-NMR spectra were recorded on a Bruker Advance 300 MHz and AMX 500 spectrometer. Chemical shifts are reported in ppm and referenced to the residual non-deuterated solvent frequencies ($CDCl_3$: δ 7.26 ppm for ^{1}H, δ 77.0 ppm for ^{13}C, $C_2D_2Cl_4$: δ 5.91 ppm for ^{1}H, δ 77.8 ppm for ^{13}C, DMSO-d_6: δ 2.50 ppm for ^{1}H, δ 39.5 ppm for ^{13}C). UV–vis absorption spectra of the compounds in HPLC chloroform solutions at 20 ºC were recorded on a Varian Cary 50 UV–vis spectrophotometer. Mass spectra were recorded on a Bruker Reflex 2 (MALDI-TOF). FTIR spectra were carried out in a Shimadzu FTIR 8300 spectrophotometer. Cyclic voltammograms were recorded in an inert atmosphere in electrochemical workstation at a scan rate of 200 mV·s-1 at 20 ºC using tetrabutylammonium hexafluorophosphate (TBAHFP, 0.1 mol L^{-1}) as supporting electrolyte in dichloromethane. Polymer-precoated platinum electrode, platinum–wire electrode, and Ag/Ag^+ electrode were used as working electrode, an auxiliary electrode, and reference electrode, respectively. Potentials were recorded versus Fc/Fc^+.

2. Synthesis of compounds and characterization

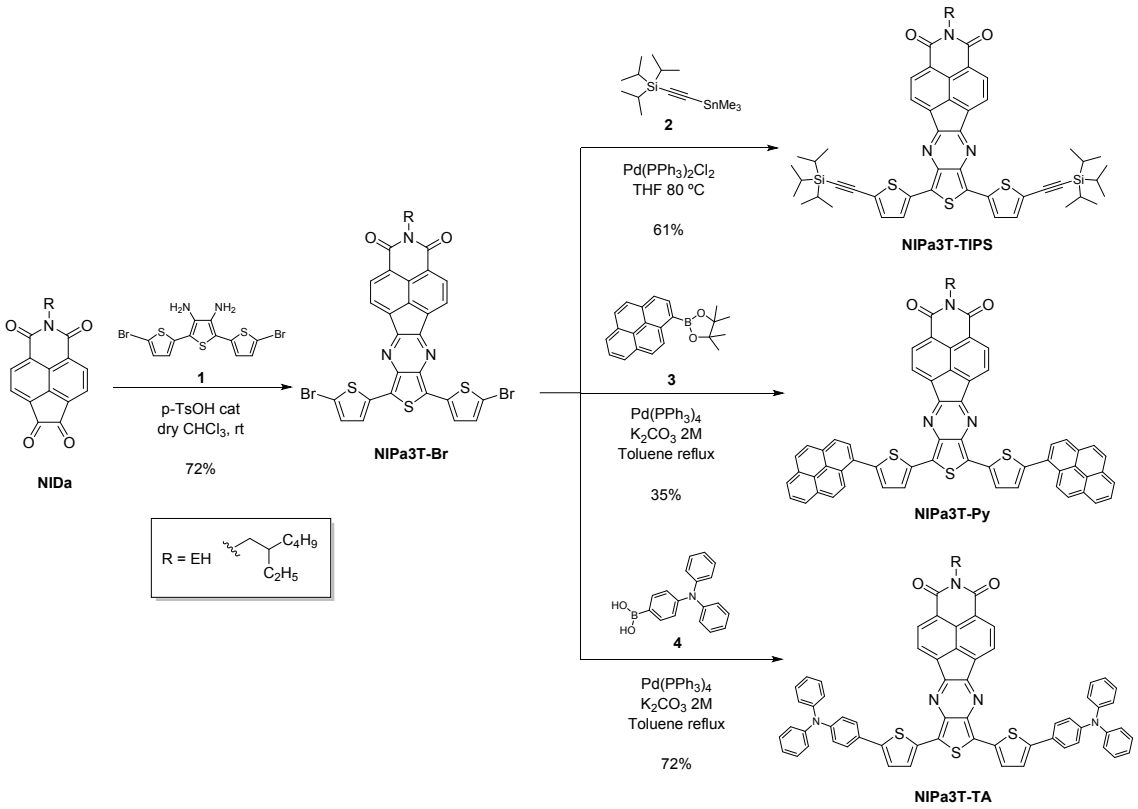

Scheme S1 Synthetic route for the desired D-A1-D compounds.

NIPa3T-Br: To a 30 mL anhydrous chloroform solution of **NID** (271mg, 0.747mmol), a catalytic amount of p-TsOH (10%) was added and the mixture was stirred for 5 min. After that, an anhydrous chloroform solution of **1** (208mg, 0.747mmol) was added. The solution turns instantly to a dark blue color and it was stirred overnight at room temperature. The solvent was evaporated under reduce pressure and the crude was precipitated in MeOH. The solid was filtrated and washed with water, MeOH and hot MeOH to obtain 246mg (72%) of a dark blue solid.

^{1}H-NMR: 8.50 (d, J = 8.47 Hz, 2H), 8.10 (d, J = 8.08 Hz, 2H), 6.95 (d, J= 6.97 Hz, 2H), 6.85 (d, J= 6.86 Hz, 2H), 4.1 (m, 2H), 2 (s, 1H), 1.4 (m, 8H), 0.95 (m, 6H).

FTIR (ATR, $CHCl_3$): υ (cm^{-1}): 3754, 2953, 2923, 2852, 1699, 1664, 1635, 1591, 1450, 1422, 1324, 1232, 1168, 1060, 970, 813, 782, 748, 616.

MALDI-HRMS (m/z): calculated for $C_{34}H_{25}Br_2N_3O_2S_3$: 760.9476, found ($M^+$): 760.9501.

NIPa3T-TIPS: Under argon atmosphere, a mixture of **NIPa3T-Br** (118 mg, 0.1 mmol), **2** (122 mg, 0.35 mmol) and $Pd(PPh_3)Cl_2$ (11 mg, 0.035 mmol) in 12 mL of dry THF were heated at 80º C for 24h. The solvent was then removed under reduced pressure and the residue was dissolved in dichloromethane and washed with water (2 x 15 mL) and 15 mL of an ammonium chloride solution. The organic phase was dried over magnesium sulfate and the solvent was removed under reduced pressure. The solid was purified in flash column chromatography (dichloromethane/hexane 3:7) affording 59 mg (61%) of a deep blue solid.

^{1}H-NMR (300 MHz, $CDCl_3$) δ(ppm) = 8.55 (d, J= 8.54 Hz, 2H), 8.28 (d, J= 8.27 Hz, 2H), 7.44 (d, J= 7.43 Hz, 2H), 7.21 (d, J= 7.2 Hz, 2H), 4.13 (m, 2H), 1.95 (s, 1H), 1.3 (m, 8H), 1.1 (m, 42H), 0.85 (m, 6H).

^{13}C-NMR (75 MHz, $CDCl_3$): δ (ppm) = 163.47, 153.09, 137.43, 135.56, 134.62, 132.89, 132.11, 126.88, 125.50, 125.04, 123.77, 121.74, 99.47, 98.86, 38.24, 30.80, 28.75, 23.19, 18.80, 14.20, 11.44, 10.68.

FTIR (ATR, $CHCl_3$): υ (cm^{-1}) = 2927.08, 2860.73, 2139.37, 1706.81, 1672.80, 1640.45, 1461.26, 1376.08, 1329.54, 1234.55, 1168.35, 1045.50, 999.81, 883.18, 796.12, 755.35, 672.17.

MALDI-HRMS (m/z): calculated for $C_{56}H_{68}N_3O_2S_3Si_2$: 965.3934, found ($M^+$): 966.3991.

NIPa3T-Py: Under argon atmosphere, a mixture of **NIPa3T-Br** (70 mg, 0.092 mmol), **3** (67 mg, 0.21 mmol) and $Pd(PPh_4)$ (11 mg, 0.010 mmol) in 10 mL of dry toluene and 1 mL of K_2CO_3 2M solution were refluxed overnight.. The solvent was then removed under reduced pressure and the residue was dissolved in chloroform and washed with water (2 x 15 mL) and 15 mL of an ammonium chloride solution. The organic phase was dried over magnesium sulfate and the solvent was removed under reduced pressure. The solid was purified in flash column chromatography (chloroform) affording 31 mg (35%) of a green solid.

^{1}H-NMR (300 MHz, $CDCl_3$)= 8.68 – 8.56 (m, 2H), 8.36 (d, *J* = 8.6 Hz, 2H), 8.28 – 7.98 (m, 18H), 7.88 (d, *J* = 8.5 Hz, 2H), 7.66 (d, *J* = 8.6 Hz, 2H), 4.13 (m, 2H), 1.94 (m, 1H), 1.37 (m, 8H), 0.91 (m, 6H).

FTIR (ATR, $CHCl_3$): υ (cm^{-1}) = 2957, 2925, 2855, 1736, 1702, 1666, 1455, 1371, 1233, 844, 757, 718.

MALDI-HRMS (m/z): calculated for $C_{66}H_{43}N_3O_2S_3$: 1005.2517, found (M^+): 1005.2524.

NIPa3T-TA: Under argon atmosphere, a mixture of **NIPa3T-Br** (82 mg, 0.11 mmol), **4** (68 mg, 0.24 mmol) and $Pd(PPh_4)$ (12 mg, 0.010 mmol) in 10 mL of dry toluene and 1 mL of K_2CO_3 2M solution were refluxed overnight. The solvent was then removed under reduced pressure and the residue was dissolved in dichloromethane and washed with

water (2 x 15 mL) and 15 mL of an ammonium chloride solution. The organic phase was dried over magnesium sulfate and the solvent was removed under reduced pressure. The solid was purified in flash column chromatography (dichloromethane/hexane 7:3) affording 85 mg (72%) of a green solid.

^{1}H-NMR (300 MHz, $CDCl_3$): δ (ppm) = 8.02 (d, J= 7.2 Hz, 2H), 7.55 (d, J= 7.2 Hz, 2H), 7.30 (m, 8H), 7.16 (dd, J= 8.6, 1.2 Hz), 7.07 (t, J= 7.3 Hz, 4H), 6.96 (d, J= 8.6 Hz, 4H), 6.85 (d, J= 3.8 Hz, 2H), 6.64 (d, J= 3.8 Hz, 2H), 3.82 (m, 2H), 2.00 (m, 1H), 1.30 (m, 8H), 0.89 (m, 6H).

^{13}C-NMR (75 MHz, $CDCl_3$): δ (ppm) =163.2, 151.5, 147.3, 145.3, 136.2, 135.5, 132.0, 131.5, 129.3, 127.2, 126.2, 126.0, 124.9, 123.3, 122.8, 122.6, 31.9, 29.7, 26.6, 25.7, 23.1, 22.7, 14.2, 10.5.

FTIR (ATR, $CHCl_3$): υ (cm^{-1}) = 2924, 2854, 1700, 1665, 1590, 1490, 1456, 1374, 1324, 1261, 1086, 1019, 796, 753, 696, 614.

MALDI-HRMS (m/z): calculated for $C_{70}H_{53}N_5O_2S_3$: 1091.3361, found (M^+): 1091.3365.

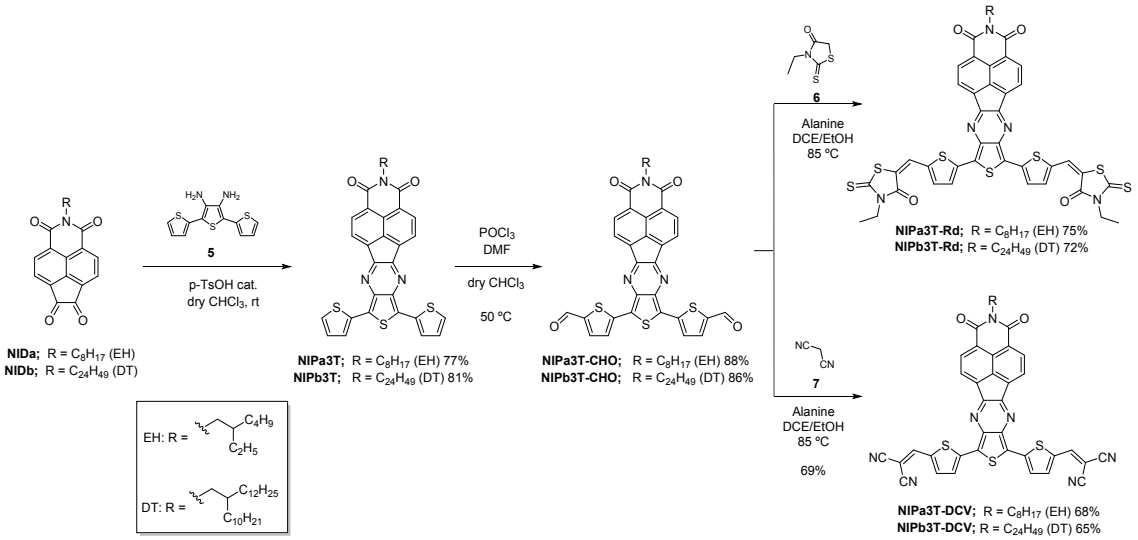

Scheme S2 Synthetic route for the desired A1-D-A2-D-A1 compounds.

General procedure for the synthesis of NIP3T derivatives

To a 30 mL anhydrous chloroform solution of **NIDa** or **NIDb** (1 eq), a catalytic amount of p-TsOH (10%) was added and the mixture was stirred for 5 min. After that, an anhydrous chloroform solution of **5** (1 eq) was added. The solution turns instantly to a dark blue color and it was stirred overnight at room temperature. The solvent was evaporated under reduce pressure and the crude was precipitated in MeOH.

NIPa3T: The solid was filtrated and washed with water, MeOH and hot MeOH to obtain 246 mg (77%) of a dark purple solid.

^{1}H-NMR (300 MHz, $CDCl_3$) = 8.24 (d, *J* = 7.3 Hz, 2H), 7.83 (d, *J* = 7.3 Hz, 2H), 7.35 (d, *J* = 3.5 Hz, 2H), 7.30 (d, *J* = 4.9 Hz, 2H), 6.99 (dd, *J* = 4.9, 3.5 Hz, 2H), 4.14 – 4.05 (m, 2H), 1.98 – 1.90 (m, 1H), 1.46 – 1.33 (m, 8H), 1.04 – 0.86 (m, 6H).

^{13}C-NMR (75 MHz, $CDCl_3$) = 163.65, 152.57, 136.68, 136.16, 135.73, 133.81, 132.01, 27.48, 127.29, 127.01, 125.28, 124.97, 123.54, 121.21, 44.38, 38.38, 30.94, 28.89, 24.21, 23.32, 14.34, 10.81.

FTIR (ATR, $CHCl_3$) υ (cm^{-1}) = 3095, 2926, 2856, 2374, 1738, 1704, 1667, 1637, 1495, 1455, 1424, 1334, 1260, 1233, 1162, 1051, 851, 819, 753, 697, 651.

MALDI-HRMS (m/z): calculated for $C_{34}H_{27}N_3O_2S_3$: 605.1265, found (M^+): 605.1264.

NIPb3T: The precipitate was purified by chromatography column (silica gel flash, DCM/Hex 20:1) to obtain 240mg (81%) of a dark purple solid.

^{1}H-NMR (300 MHz, $CDCl_3$) = 8.37 (d, *J* = 7.3 Hz, 2H), 8.00 (d, *J* = 7.3 Hz, 2H), 7.49 (d, *J* = 3.6 Hz, 2H), 7.37 (d, *J* = 5.0 Hz, 2H), 7.07 (dd, *J* = 5.0, 3.7 Hz, 2H), 4.05 (d, *J* = 7.0 Hz, 2H), 2.02 – 1.91 (m, 1H), 1.24 (m, 40H), 0.86 (dt, *J* = 6.7 Hz, 6H).

^{13}C-NMR (75 MHz, $CDCl_3$) = 163.50, 152.22, 136.35, 135.87, 135.36, 133.70, 131.73, 127.33, 127.14, 126.74, 125.05, 123.35, 120.90, 44.69, 37.17, 32.10, 31.86, 30.36, 29.89, 29.55, 26.66, 22.86, 14.29. (some signals of the alkyl chain are overlapped)

FTIR (ATR, $CHCl_3$) υ (cm^{-1}) = 2922.76, 2852.78, 1703.10, 1667.72, 1635.38, 1454.90, 1326.10, 1231.32, 810.50, 751.23, 695.03

MALDI-HRMS (m/z): calculated for $C_{50}H_{59}N_3O_2S_3$: 829.3769, found (M^+): 829.3749.

General procedure for the synthesis of the dialdehyde derivatives:[9]

To a solution of the corresponding pyrazine derivative (**NIPa3T**, **NIPb3T**, 1eq) in 10 mL of chloroform, DMF was added (1 mL) and the solution was stirred for 5min. After that, $POCl_3$ (1 mL) was added carefully and the reaction was stirred at 50 ºC for 48h. 1M NaOH (20 mL) was added, the mixture was stirred vigorously, and the phases were separated. The aqueous phase was extracted with dichloromethane. The combined organic phases were washed with water and brine and dried over $MgSO_4$. The solvent was evaporated under reduced pressure and the crude was purified by chromatography column (silica gel flash, chloroform) to provide pure product.

NIPa3T-CHO: the product was obtained (66 mg, 88%) as a purple solid.

^{1}H-NMR (300 MHz, $CDCl_3$) = 9.65 (s, 2H), 8.09 (d, *J* = 7.1 Hz, 2H), 7.63 (d, *J* = 7.0 Hz, 2H), 7.31 (d, *J* = 3.6 Hz, 2H), 7.01 (d, *J* = 3.3 Hz, 2H), 3.97 (m, 2H), 1.89 – 1.76 (m, 1H), 1.42 – 1.30 (m, 8H), 1.02 – 0.81 (m, 6H).

^{13}C-NMR (75 MHz, $CDCl_3$) = 182.26, 162.94, 156.54, 153.07, 144.48, 141.22, 137.80, 135.55, 134.09, 131.91, 125.49, 124.55, 124.15, 122.06, 38.35, 30.84, 29.85, 28.80, 24.09, 23.30, 14.34, 10.69.

FTIR (ATR, $CHCl_3$) υ (cm^{-1}) = 3089, 3019, 2957, 2927, 2858, 1702, 1663, 1591, 1517, 1437, 1377, 1328, 1281, 1218, 1168, 1132, 1057, 863, 817, 794, 754, 664.

MALDI-HRMS (m/z): calculated for $C_{36}H_{27}N_3O_4S_3$: 661.1164, found (M^+): 661.1241.

NIPb3T-CHO: the product was obtained (132 mg, 86%) as a purple solid.

^{1}H-NMR (300 MHz, $CDCl_3$) = 9.79 (s, 2H), 8.29 (d, *J* = 7.3 Hz, 2H), 7.92 (d, *J* = 7.3 Hz, 2H), 7.49 (d, *J* = 4.0 Hz, 2H), 7.28 (d, *J* = 4.0 Hz, 2H), 4.02 (d, *J* = 6.4 Hz, 2H), 1.99 – 1.83 (m, 1H), 1.22 (m, 40H), 0.85 (t, *J* = 6.2 Hz, 6H).

^{13}C-NMR (75 MHz, $CDCl_3$) = 163.50, 152.22, 136.35, 135.87, 135.36, 133.70, 131.73, 127.33, 127.14, 126.74, 125.05, 123.35, 120.90, 44.69, 37.17, 32.10, 31.86, 30.36, 29.89, 29.55, 26.66, 22.86, 14.29 (some signals of the alkyl chain are overlapped).

FTIR (ATR, $CHCl_3$) υ (cm^{-1}) = 2921.00, 2851.56, 1740.19, 1703.55, 1659.05, 1456.17, 1437.92, 1259.49, 1221.02, 1058.41, 801.67.

MALDI-HRMS (m/z): calculated for $C_{52}H_{59}N_3O_4S_3$: 885.3668, found (M^+): 885.3710.

General procedure for the synthesis of the rhodanine end-capped derivatives:[10]

To a solution of the corresponding dialdehyde derivative (1eq) in 21 mL of a mixture of DCE/EtOH (5:2), **β-Alanine** (1.75eq) and **6** (3,25eq) was added and the mixture was stirred under reflux for 48h. The solvent was removed under reduced pressure and the residue was redisolved in DCM and precipitated in MeOH.

NIPa3T-RD: The solid was filtered and washed with water, MeOH and hot MeOH to obtain the product (46 mg, 75 %) as a black powder.

^{1}H-NMR (300 MHz, $C_2D_2Cl_4$, 343 K) = 8.14 (d, *J* = 7.2 Hz, 2H), 7.62 (d, *J* = 7.2 Hz, 2H), 7.37 (s, 2H), 7.04 (d, *J* = 3.7 Hz, 2H), 6.87 (d, *J* = 3.8 Hz, 2H), 4.19 – 4.05 (m, 4H), 4.02 – 3.87 (m, 2H), 1.91 – 1.79 (m, 1H), 1.39 – 1.18 (m, 14H), 1.01 – 0.80 (m, 6H).

^{13}C-NMR (175 MHz, $C_2D_2Cl_4$) = 190.33, 165.94, 162.05, 151.93, 139.31, 139.09, 136.91, 135.05, 133.42, 132.80, 131.22, 125.87, 125.48, 123.81, 123.26, 122.60, 121.14, 120.83, 119.77, 39.60, 37.54, 30.26, 29.41, 28.04, 23.54, 22.54, 13.63, 11.75, 10.04.

FTIR (ATR, $CHCl_3$) υ (cm^{-1}) = 3017, 2961, 2929, 2903, 1739, 1702, 1667, 1575, 1455, 1431, 1374, 1351, 1327, 1231, 1129, 1108, 1051, 1022, 877, 818, 759, 609, 565.

MALDI-HRMS (m/z): calculated for $C_{46}H_{37}N_5O_4S_7$: 947.0890, found (M^+): 947.0927.

NIPb3T-RD: the precipitate was purified in a chromatography column ($CHCl_3$/Hex 20:1), obtaining the pure product (46 mg, 72 %) as a black powder.

^{1}H-NMR (300 MHz, $CDCl_3$) = 7.97 (d, *J* = 7.0 Hz, 2H), 7.35 (d, *J* = 7.2 Hz, 2H), 7.14 (bs, 2H), 6.70 (bs, 2H), 6.64 (bs, 2H), 4.09 (bs, 4H), 3.85 (bs, 2H), 1.86 (m, 1H), 1.49-1.03 (m, 46H), 0.90 (t, *J* = 5.4 Hz, 6H).

^{13}C-NMR (75 MHz, $CDCl_3$) = 190.66, 166.45, 162.51, 152.29, 137.20, 135.49, 133.71, 133.31, 131.70, 124.29, 123.79, 121.75, 121.26, 49.40, 40.12, 31.97, 31.64, 30.33, 29.80, 29.46, 26.30, 22.75, 22.65, 14.19, 12.32. (some signals of the alkyl chain are overlapped)

FTIR (ATR, $CHCl_3$) υ (cm^{-1}) = 2923.01, 2852.90, 1704.82, 1667.20, 1567.26, 1455.38, 1323.47, 1238.10

MALDI-HRMS (m/z): calculated for $C_{62}H_{69}N_5O_4S_7$: 1171,3395, found (M^+): 1171.3437.

General procedure for the synthesis of the dicyanovinylene end-capped derivatives:[10]

To a solution of the corresponding dialdehyde derivative (1eq) in 21 mL of a mixture of DCE/EtOH (5:2), **β-Alanine** (1.75eq) and **7** (3,25eq) was added and the mixture was stirred under reflux for 48h. The solvent was removed under reduced pressure and the residue was dissolved in DCM and precipitated in MeOH. The solid was filtered and washed with water, MeOH and hot MeOH to obtain the product.

NIPa3T-DCV: the pure product was isolated (46 mg, 68 %) as a dark green powder.

^{1}H-NMR (700 MHz, DMSO-d6 333 K) = 8.01 (bs, 2H), 7.43 (bs, 2H), 7.06 (bs, 2H), 6.61 (bs, 2H), 6.56 (bs, 2H), 3.73 (m, 2H), 1.75 (m, 1H), 1.40 – 1.21 (m, 8H), 0.89 (m, 6H).

FTIR ($CHCl_3$) υ (cm^{-1}) = 2955, 2922, 2853, 2219, 1707, 1667, 1637, 1589, 1562, 1484, 1456, 1429, 1377, 1331, 1277, 1260, 1235, 1166, 1129, 1083, 1065, 1018, 868, 798, 752, 608.

MALDI-HRMS (m/z): calculated for $C_{42}H_{27}N_7O_2S_3$: 757.1388, found (M^+): 757.1389.

NIPb3T-DCV: the pure product was isolated (37 mg, 65 %) as a dark green powder.

^{1}H-NMR (300 MHz, $CDCl_3$) = 8.61 (d, J = 7.3 Hz, 2H), 8.28 (d, J = 7.3 Hz, 2H), 7.86 (s, 2H), 7.71 (d, J = 4.2 Hz, 2H), 7.67 (d, J = 4.1 Hz, 2H), 4.14 (d, J = 7.0 Hz, 2H), 1.97 (m, 1H), 1.24 (m, 46H), 0.85 (t, J = 6.7 Hz, 6H).

FTIR (ATR, $CHCl_3$) υ (cm^{-1}) = 2921.54, 2852.25, 2220.20, 1739.66, 1706.37, 1669.65, 1638.32, 1561.61, 1460.02, 1428.54, 1330.11, 1259.46, 1235.06, 1066.47, 1023.54, 842.89

MALDI-HRMS (m/z): calculated for $C_{58}H_{59}N_7O_2S_3$: 981.3892, found (M^+): 981.3940.

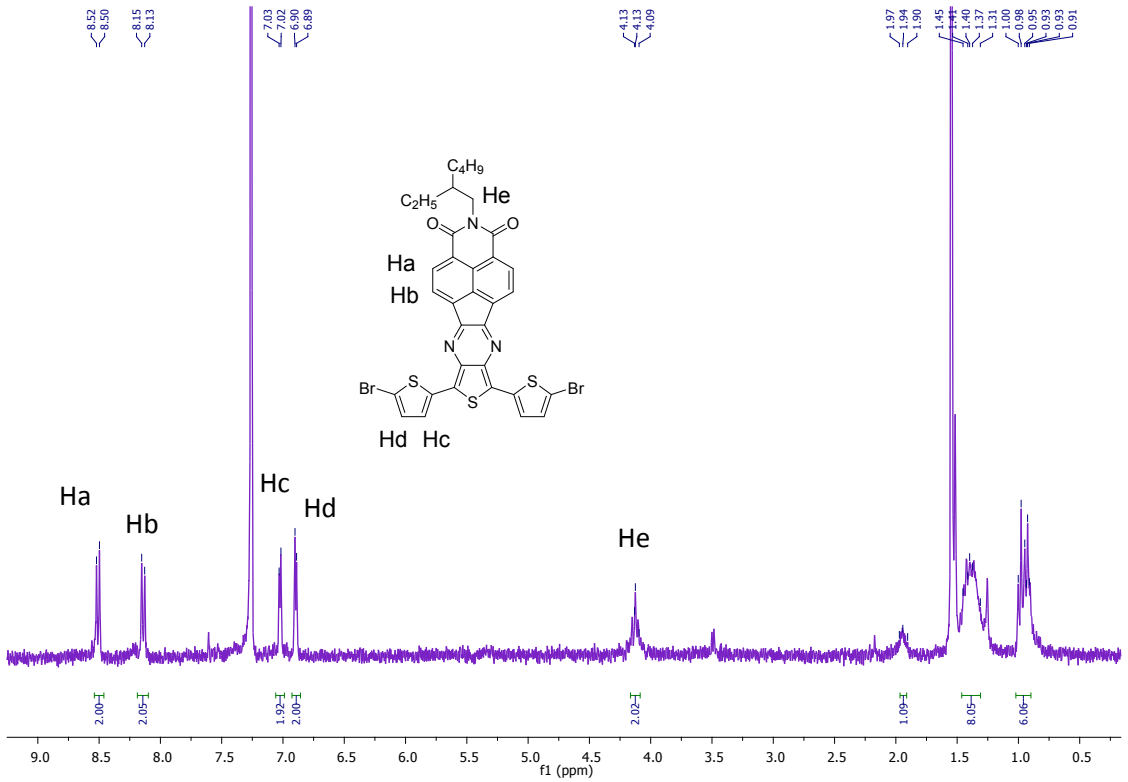

Figure S1 ^{1}H-NMR spectrum of **NIPa3T-Br** in $CDCl_3$.

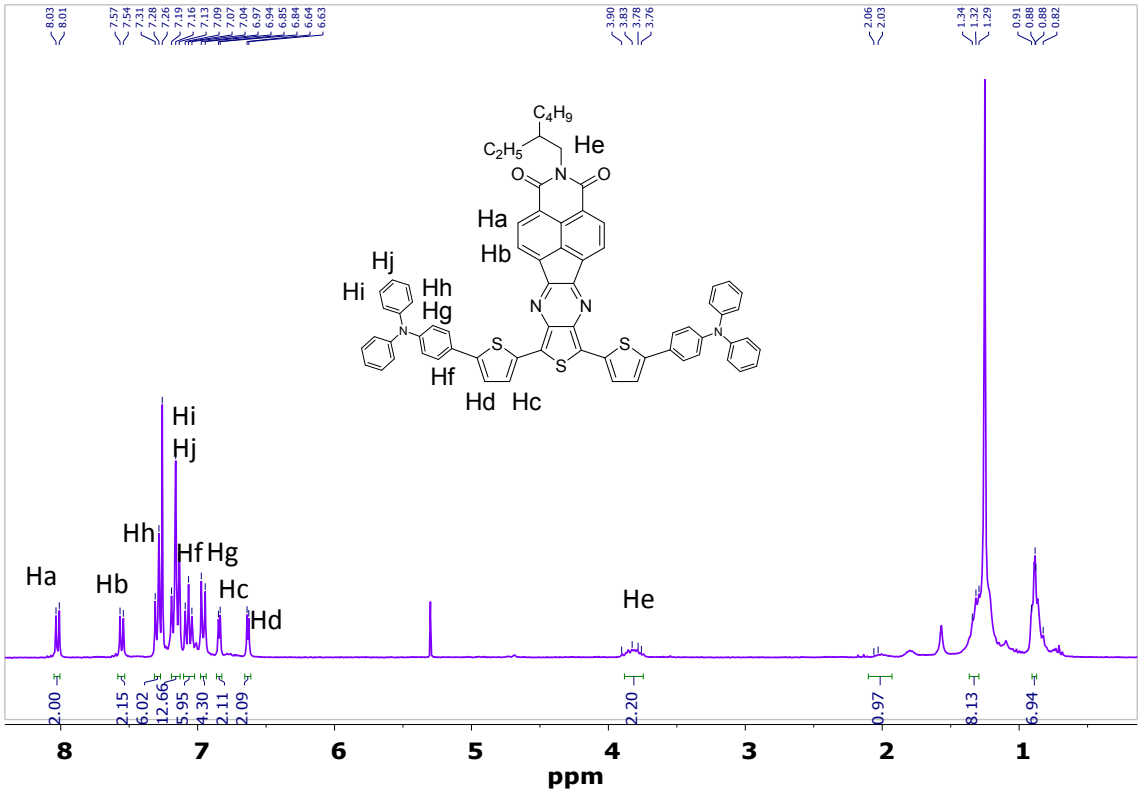

Figure S2 ^{1}H-NMR spectrum of **NIPa3T-TA** in $CDCl_3$.

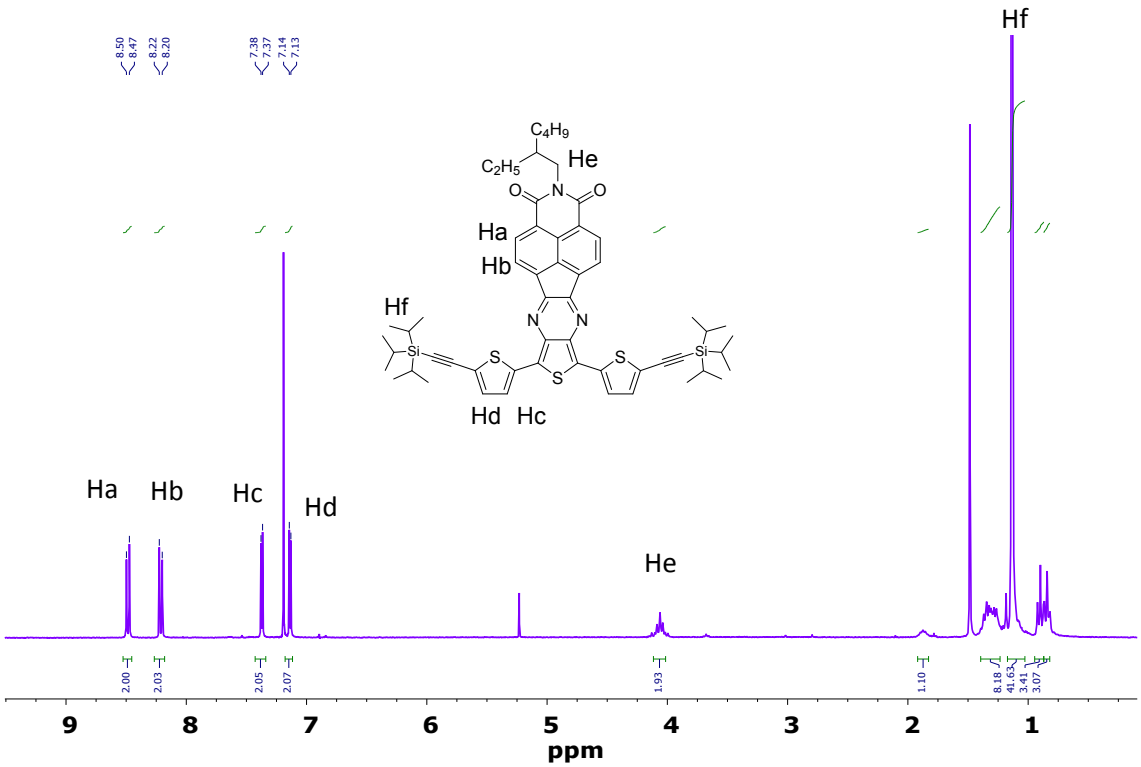

Figure S3 ^{1}H-NMR spectrum of **NIPa3T-TIPS** in $CDCl_3$.

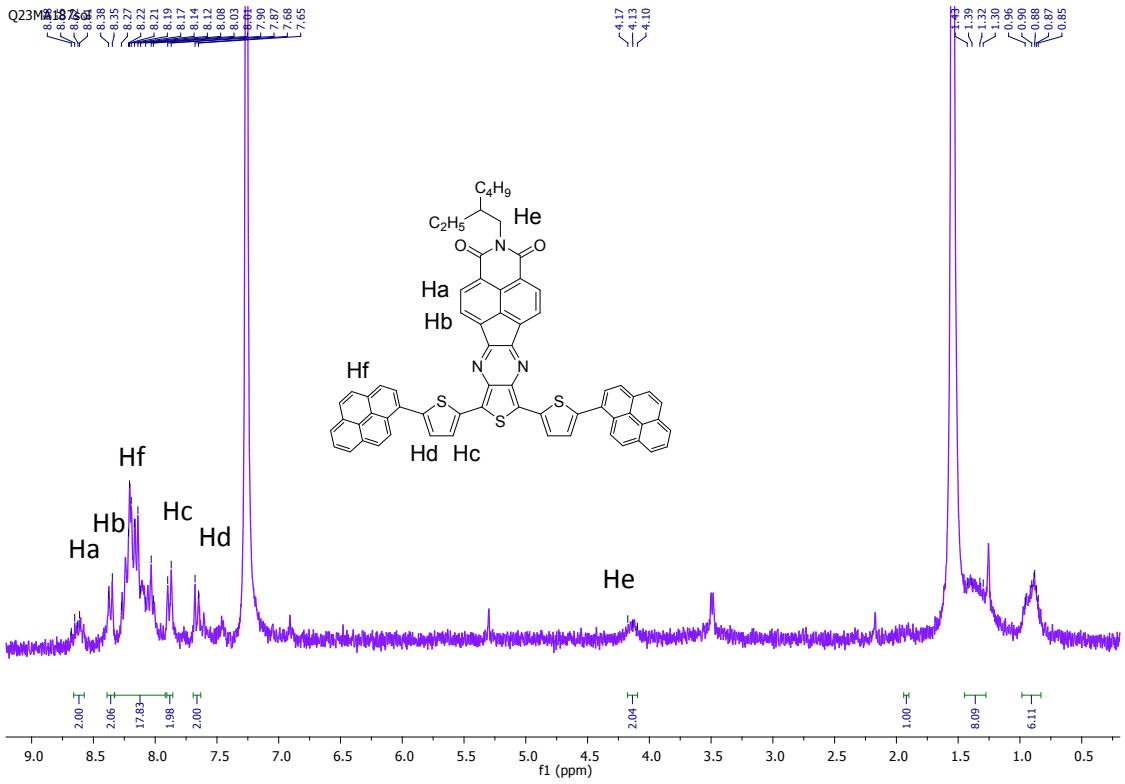

Figure S4 ^{1}H-NMR spectrum of **NIPa3T-Py** in $CDCl_3$.

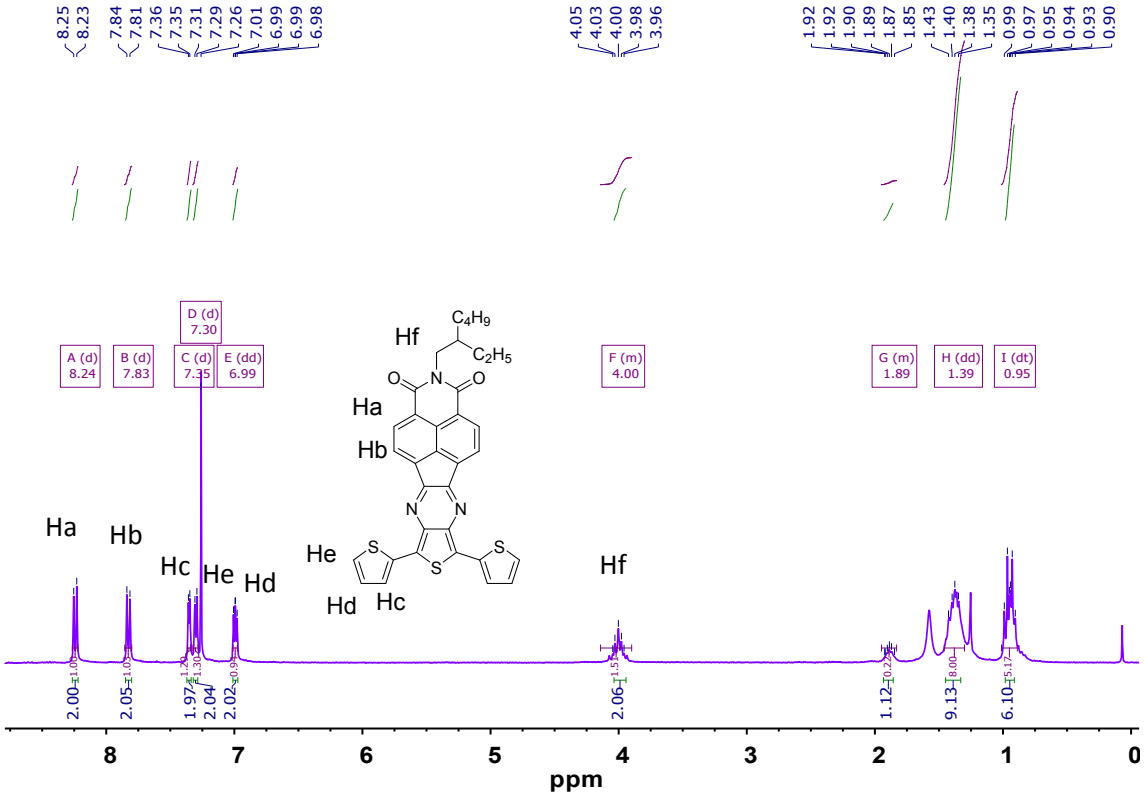

Figure S5 ^{1}H-NMR spectrum of **NIPa3T** in $CDCl_3$.

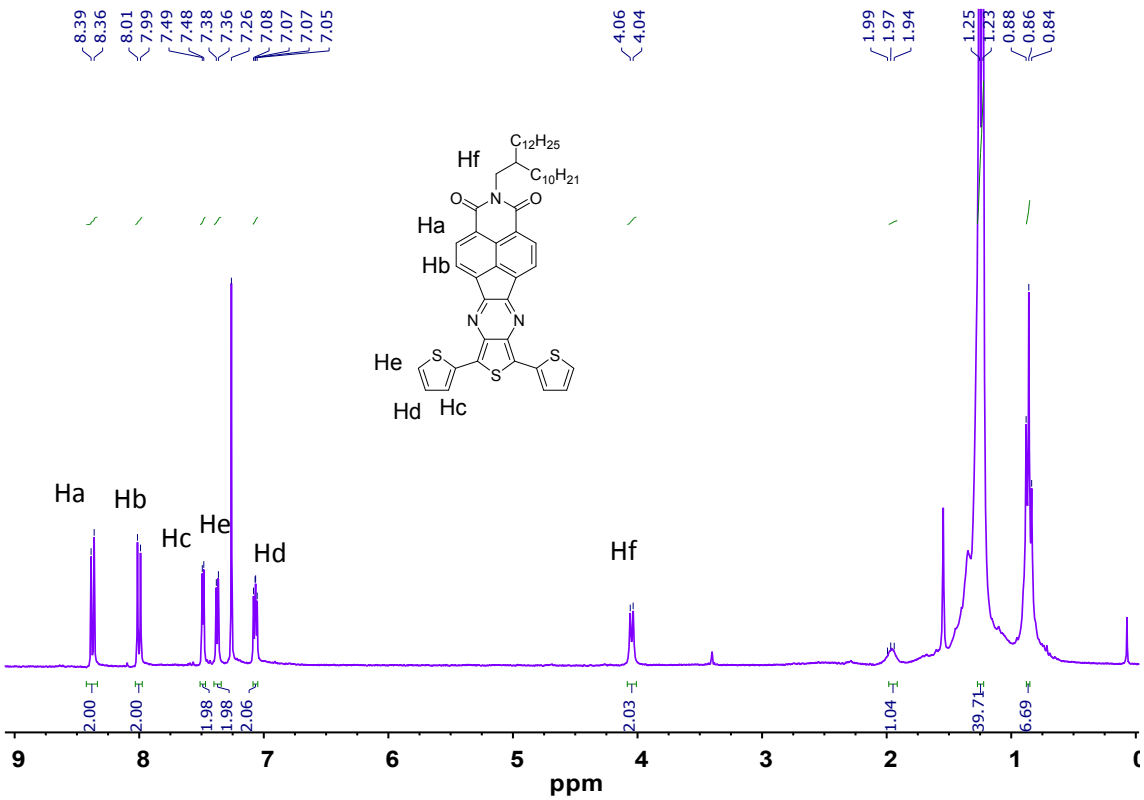

Figure S6 ^{1}H-NMR spectrum of **NIPb3T** in $CDCl_3$.

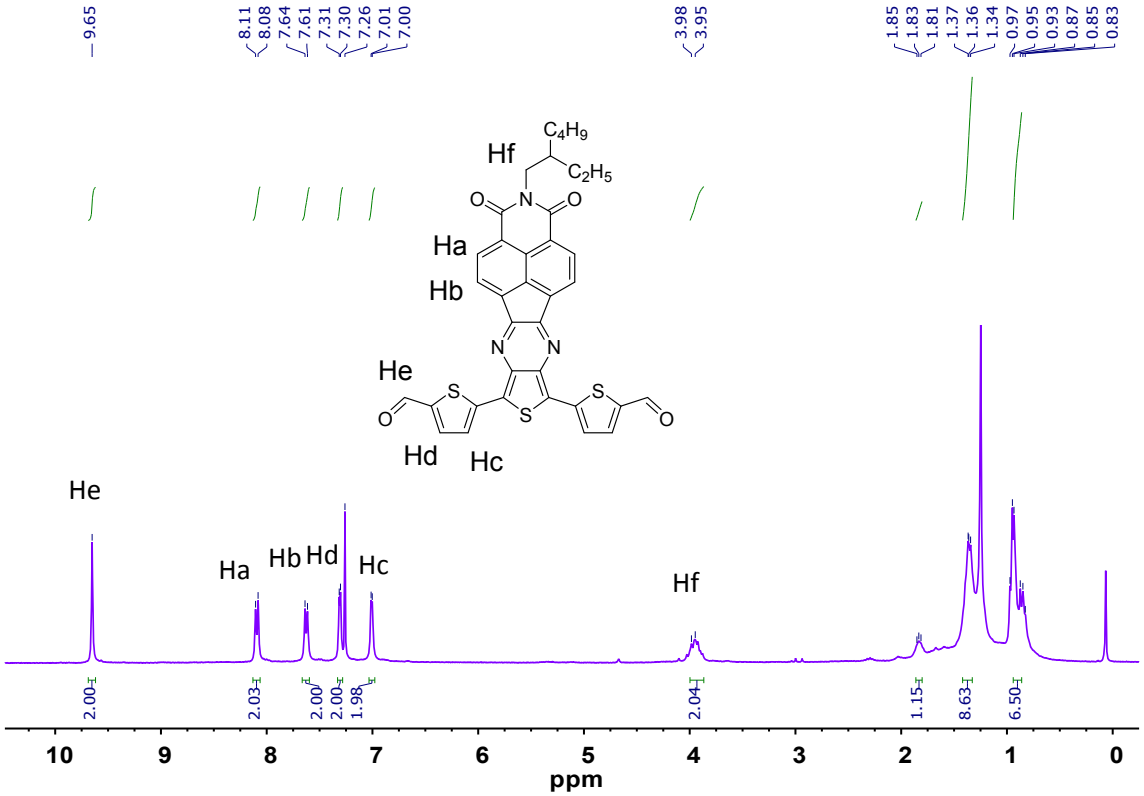

Figure S7 ^{1}H-NMR spectrum of **NIPa3T-CHO** in $CDCl_3$.

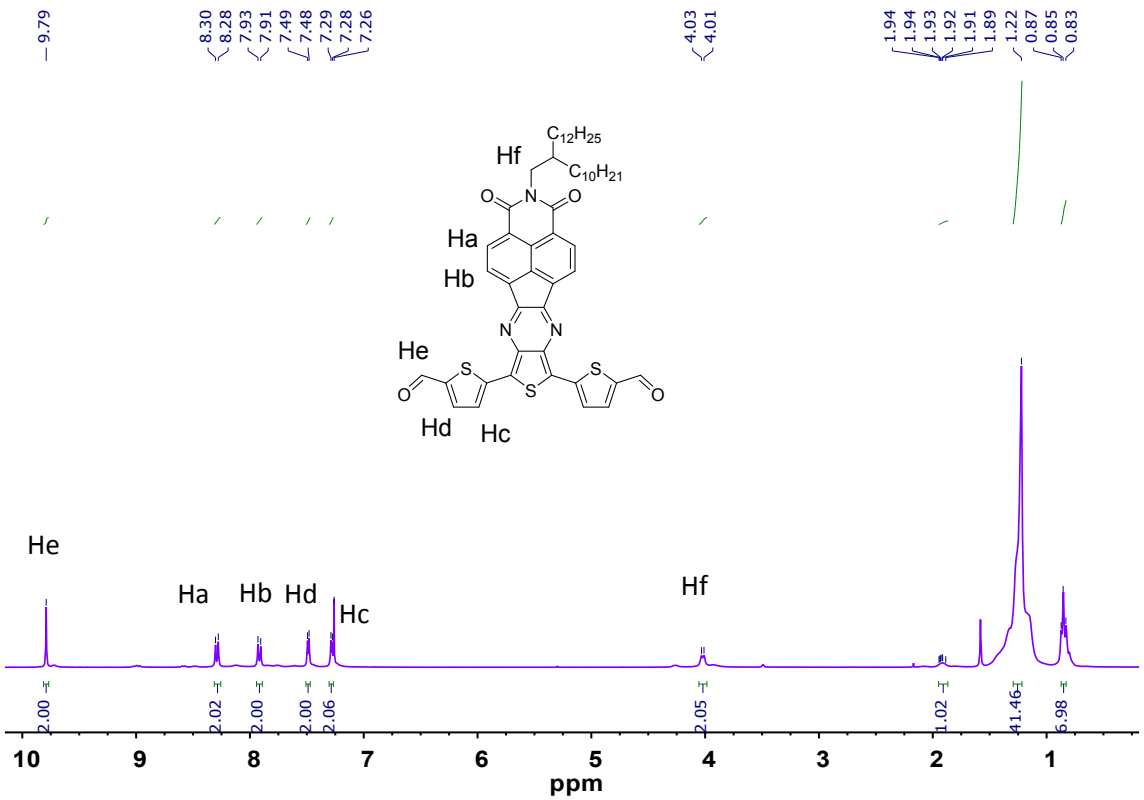

Figure S8 ^{1}H-NMR spectrum of **NIPb3T-CHO** in $CDCl_3$.

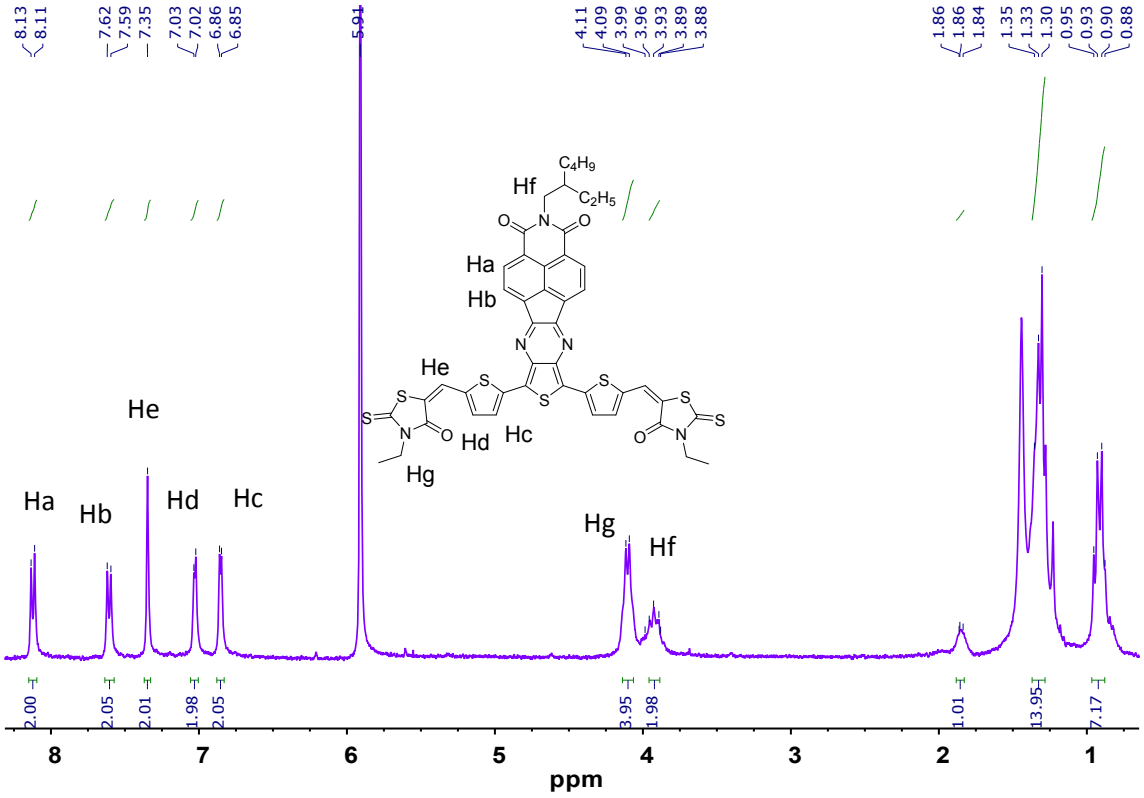

Figure S9 ^{1}H-NMR spectrum of **NIPa3T-Rd** in $C_2D_2Cl_4$ at 343 K.

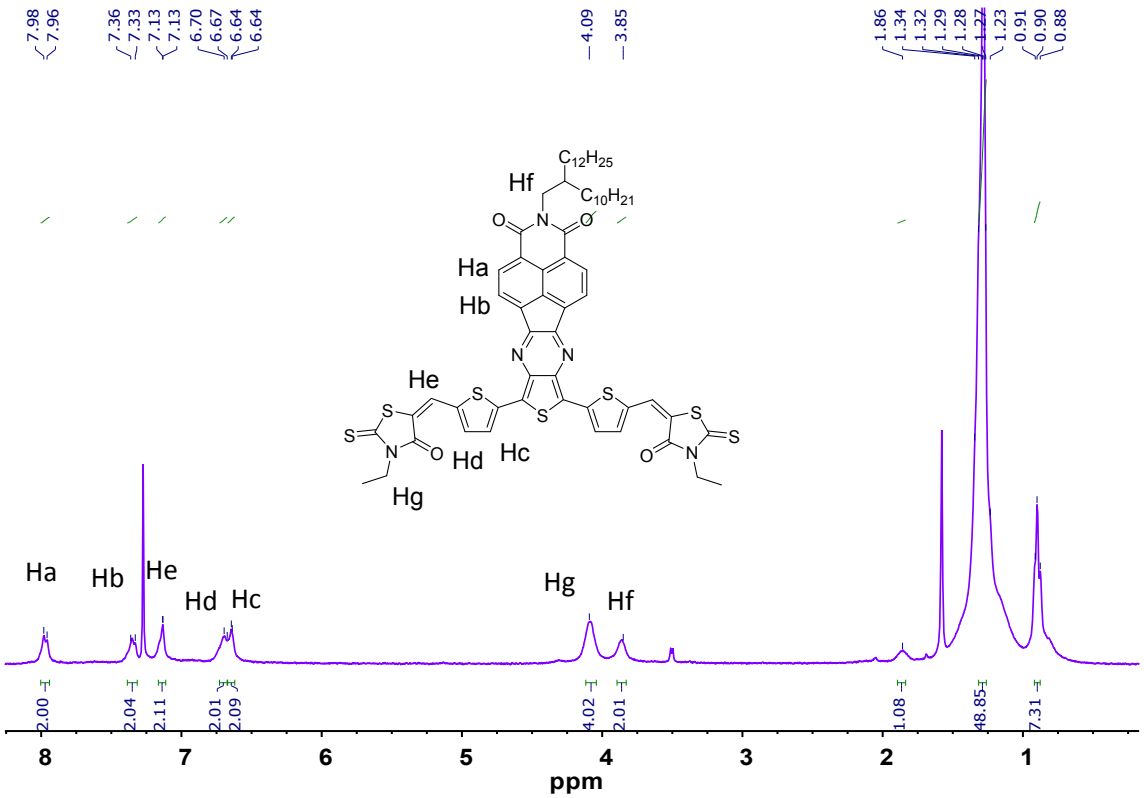

Figure S10 ^{1}H-NMR spectrum of **NIPb3T-Rd** in $CDCl_3$.

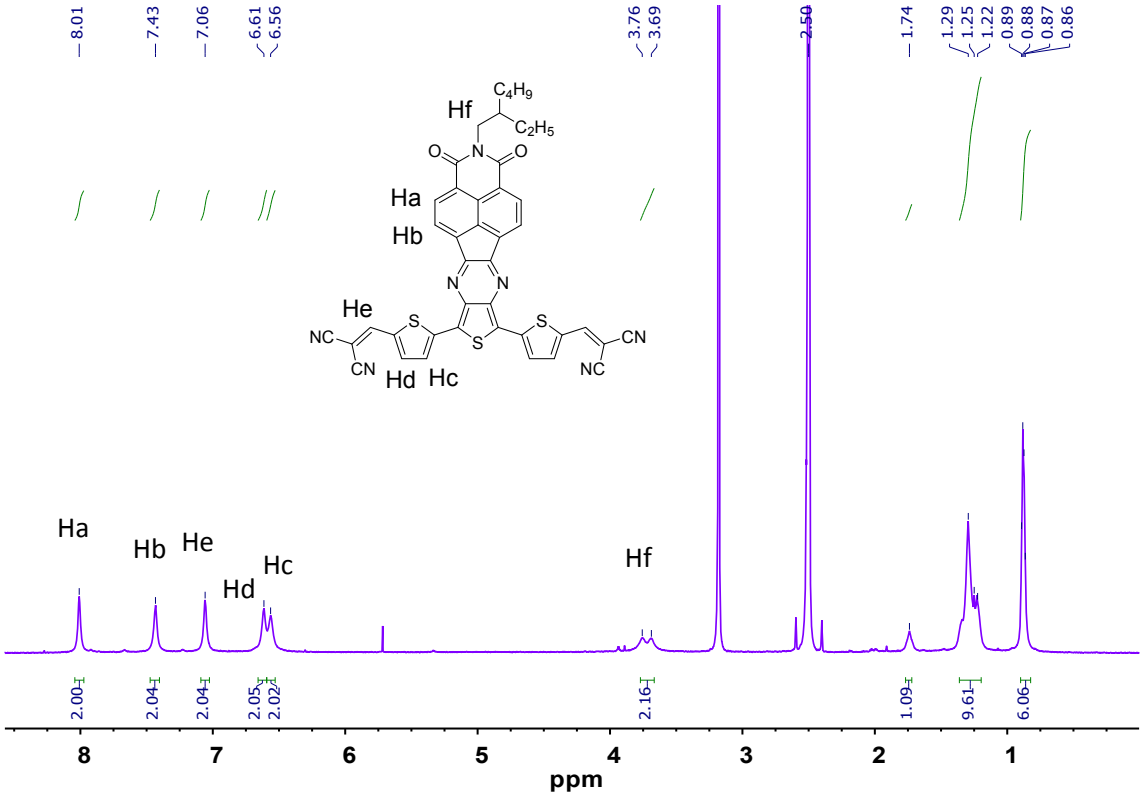

Figure S11 ^{1}H-NMR spectrum of **NIPa3T-DCV** in DMSO-d_6 at 343 K.

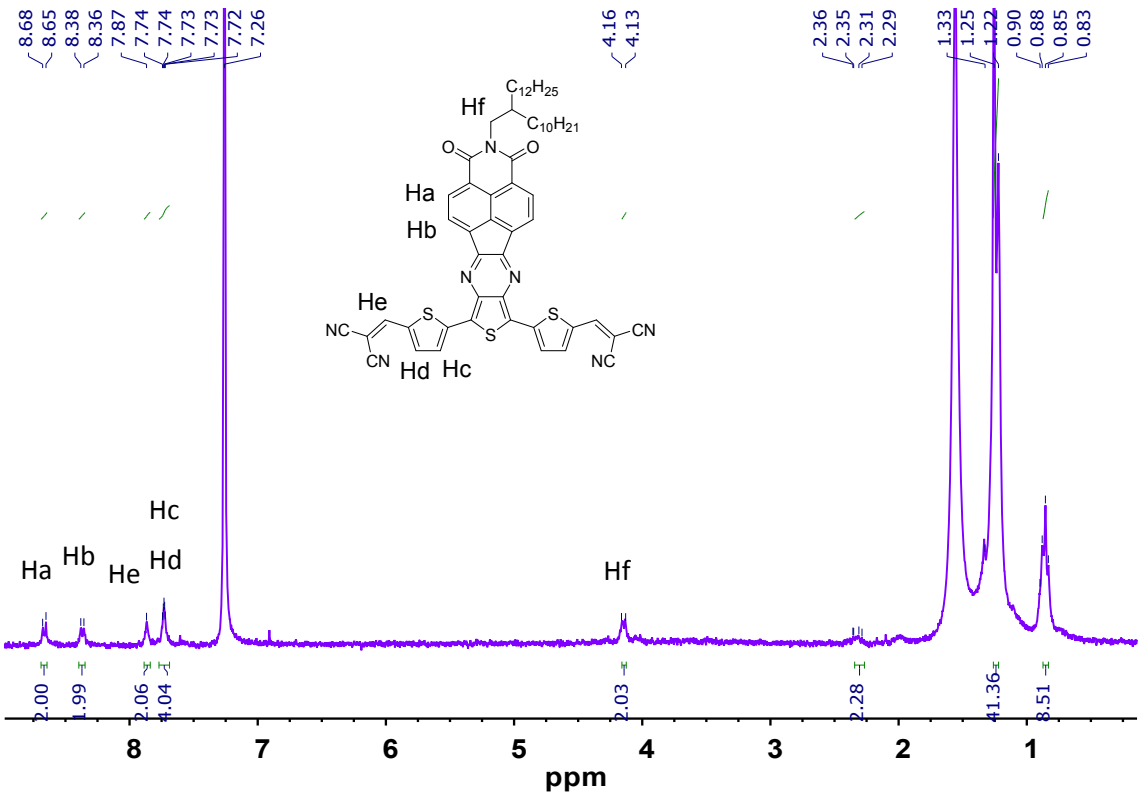

Figure S12 ^{1}H-NMR spectrum of **NIPb3T-DCV** in $CDCl_3$.

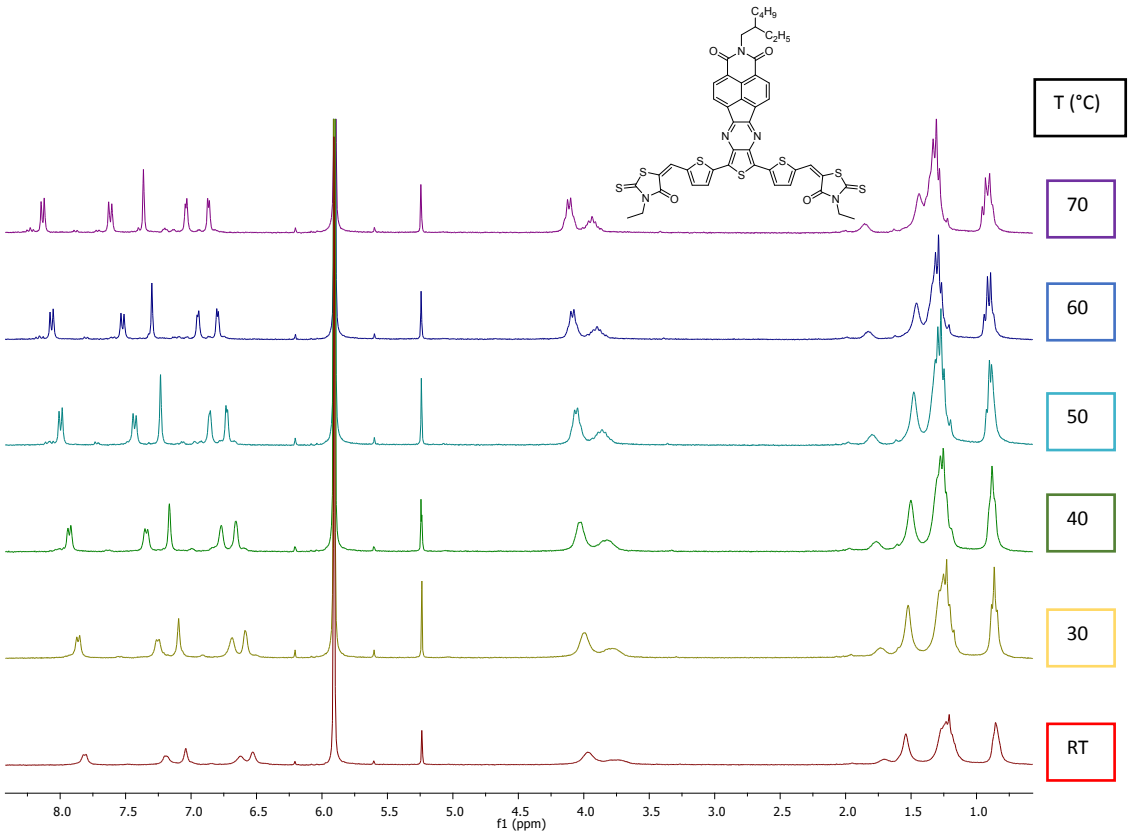

Figure S13 ^{1}H-NMR temperature dependent experiment spectrum of **NIPa3T-Rd** in $C_2D_2Cl_4$.

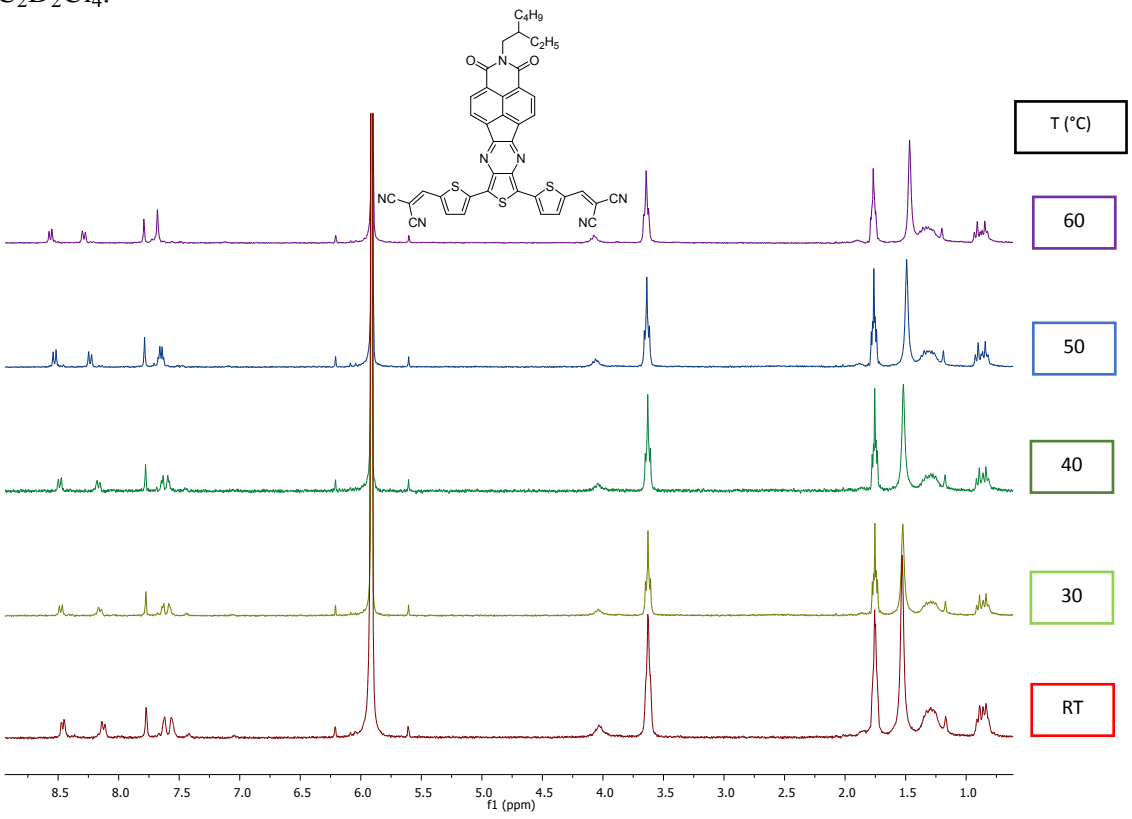

Figure S14 ^{1}H-NMR temperature dependent experiment spectrum of **NIPa3T-DCV** in $C_2D_2Cl_4$.

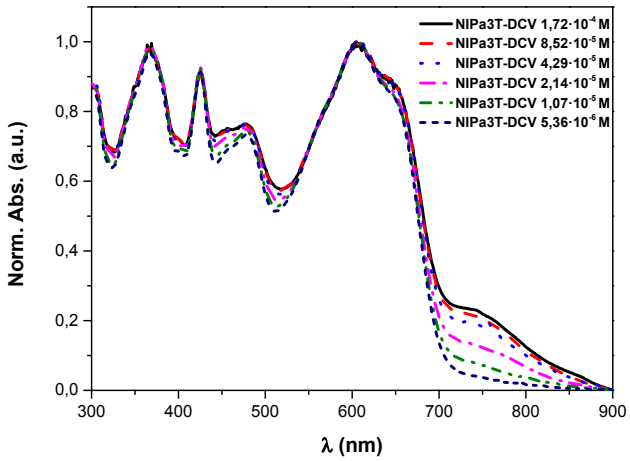

Figure S15 UV-Vis concentration dependent experiment of **NIPa3T-DCV** in $CDCl_3$.

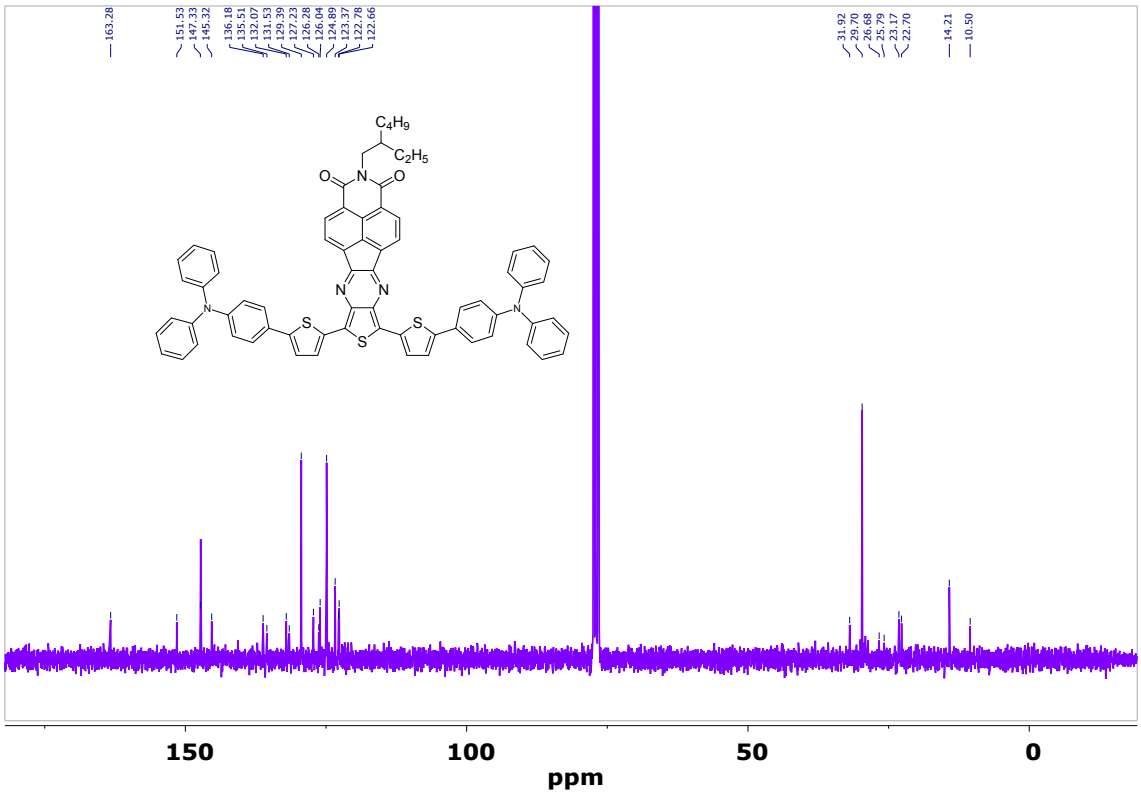

Figure S16 ^{13}C-NMR spectrum of **NIPa3T-TA** in $CDCl_3$.

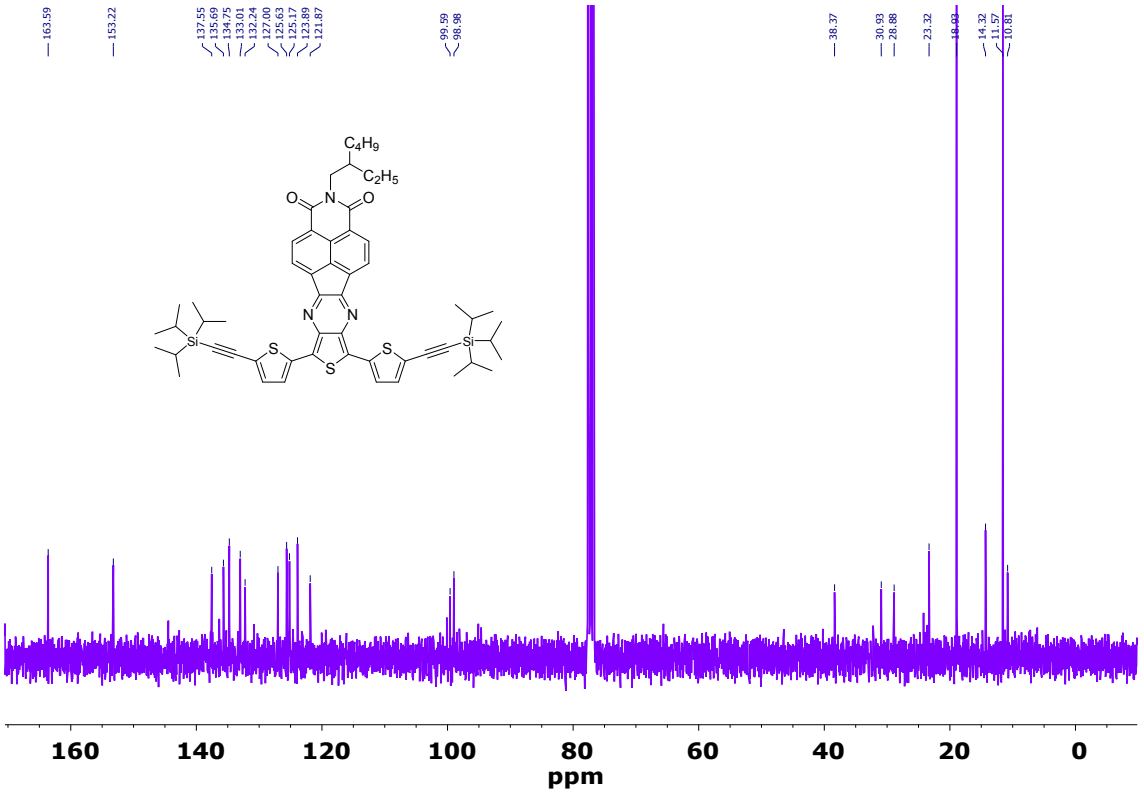

Figure S17 ^{13}C-NMR spectrum of **NIPa3T-TIPS** in $CDCl_3$.

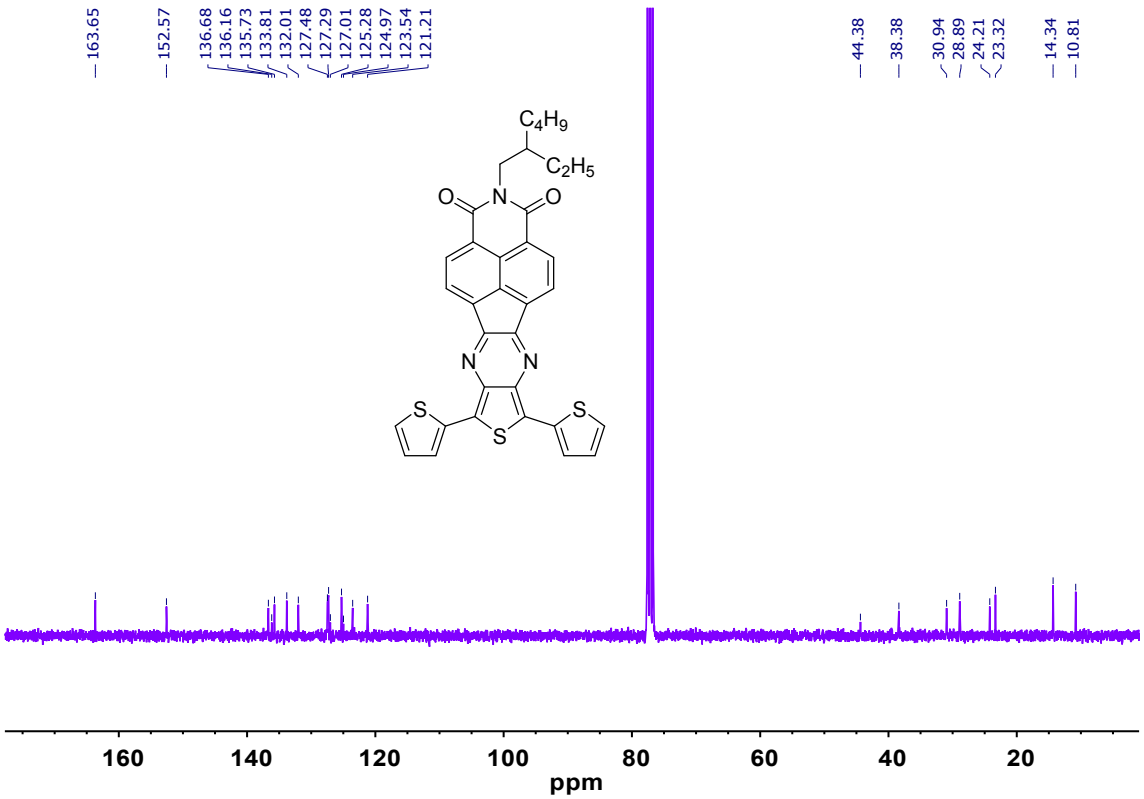

Figure S18 ^{13}C-NMR spectrum of **NIPa3T** in $CDCl_3$.

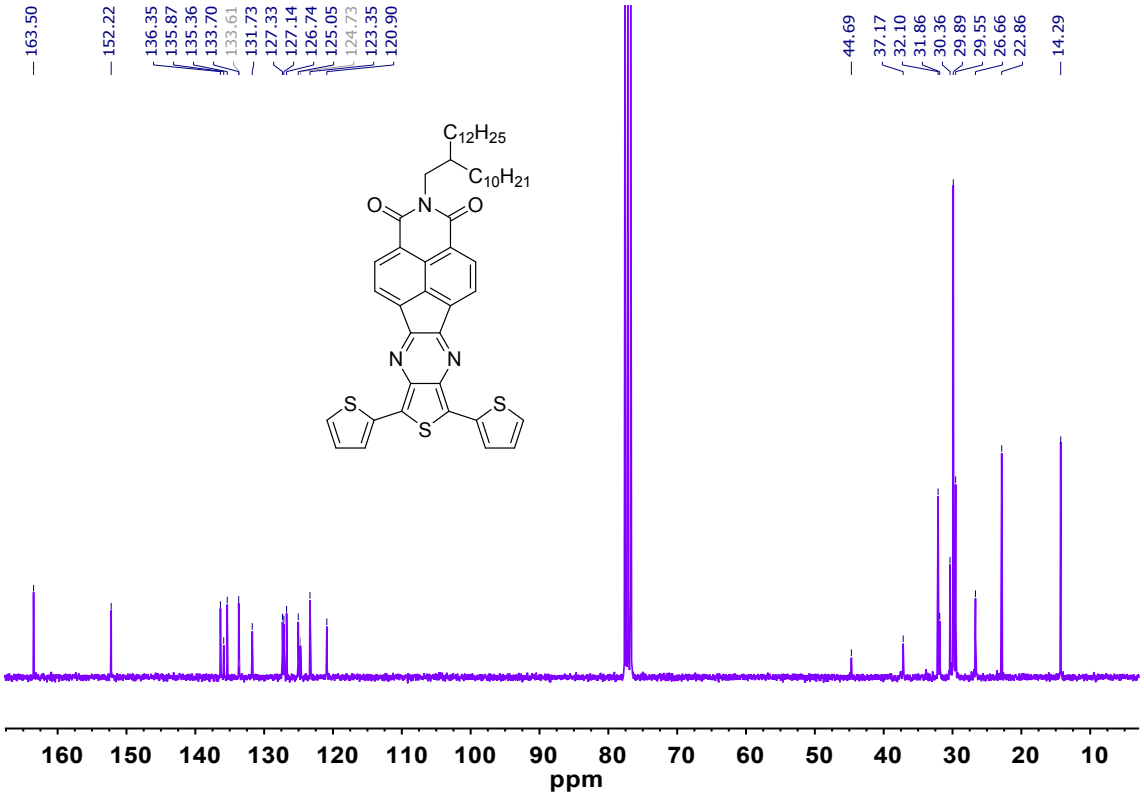

Figure S19 ^{13}C-NMR spectrum of **NIPb3T** in $CDCl_3$.

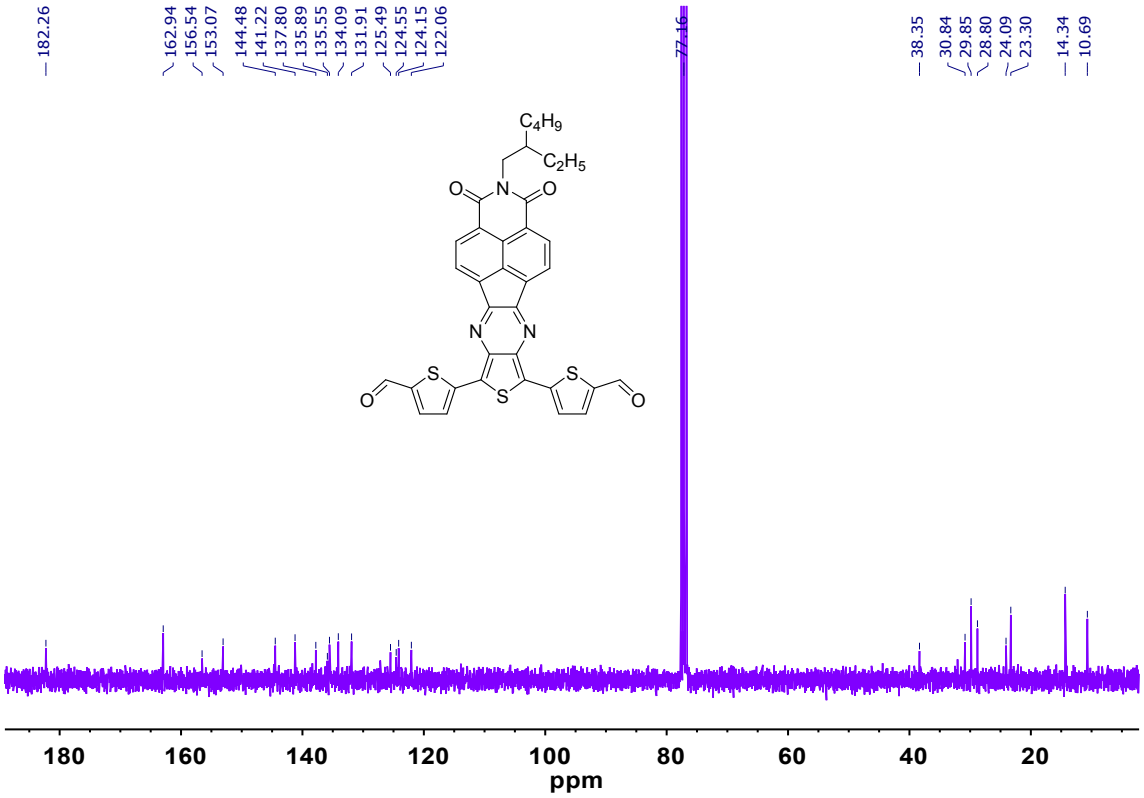

Figure S20 ^{13}C-NMR spectrum of **NIPa3T-CHO** in $CDCl_3$.

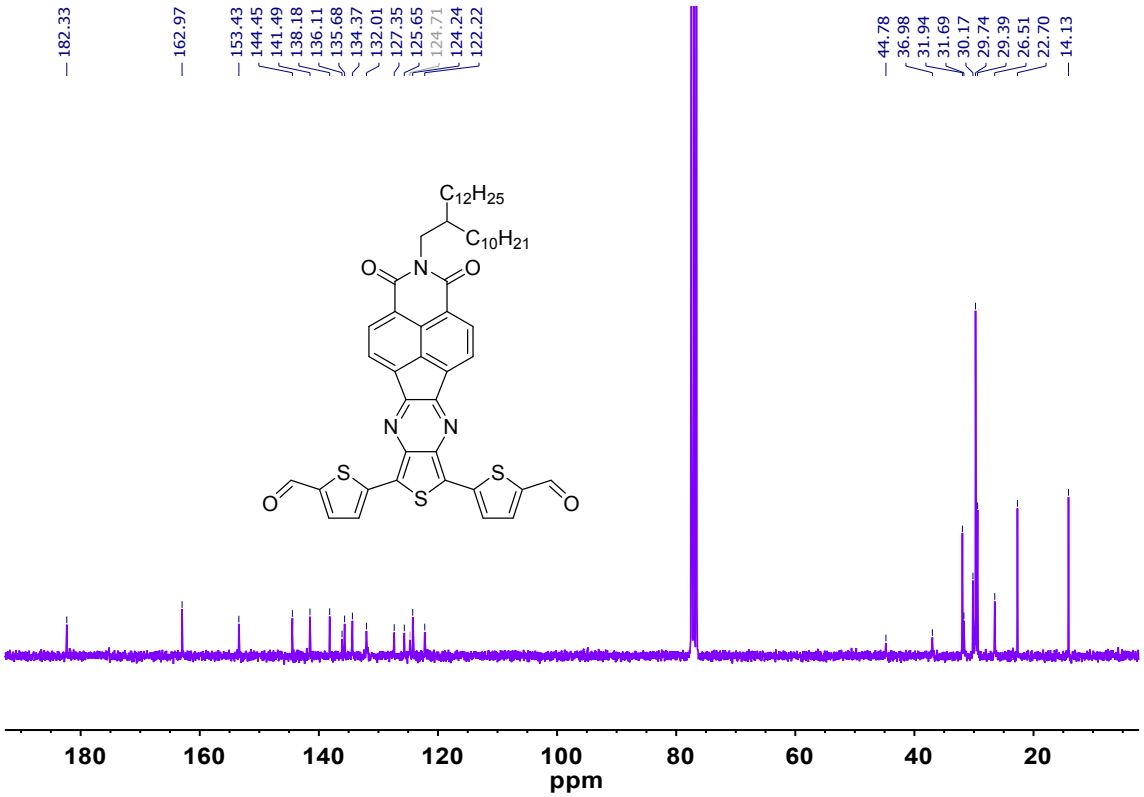

Figure S21 ^{13}C-NMR spectrum of **NIPb3T-CHO** in $CDCl_3$.

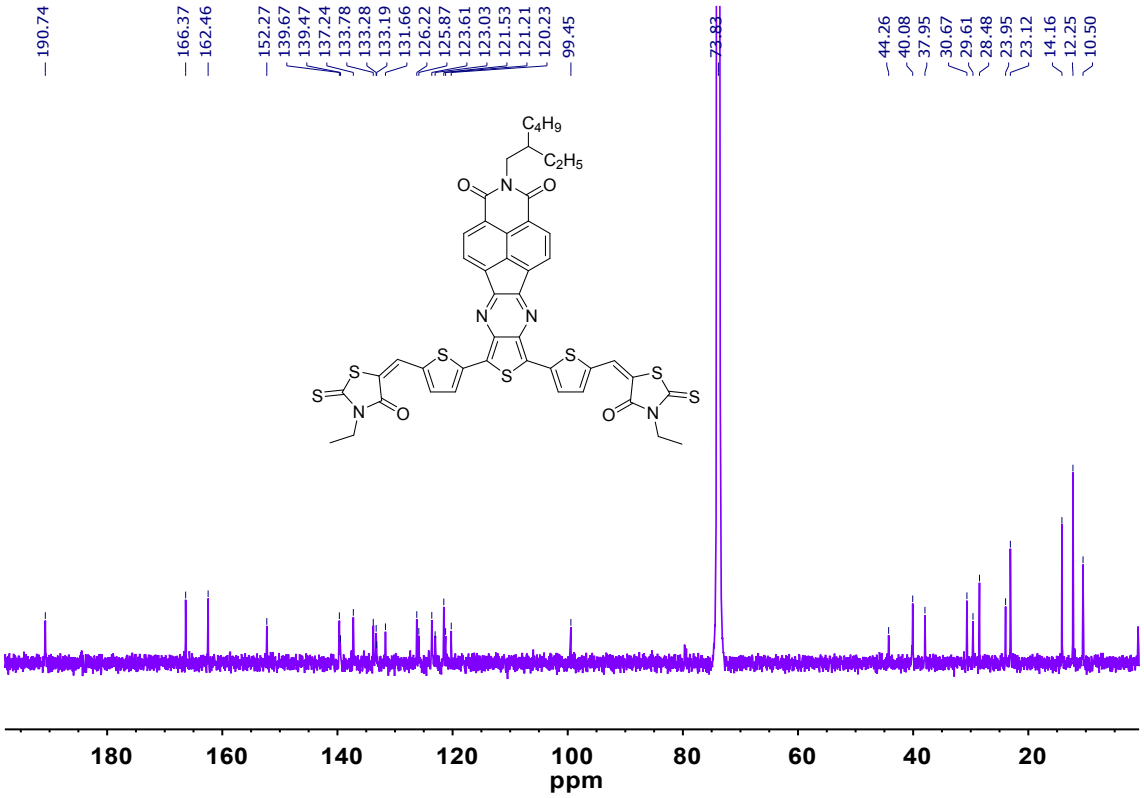

Figure S22 ^{13}C-NMR spectrum of **NIPa3T-Rd** in $C_2D_2Cl_4$.

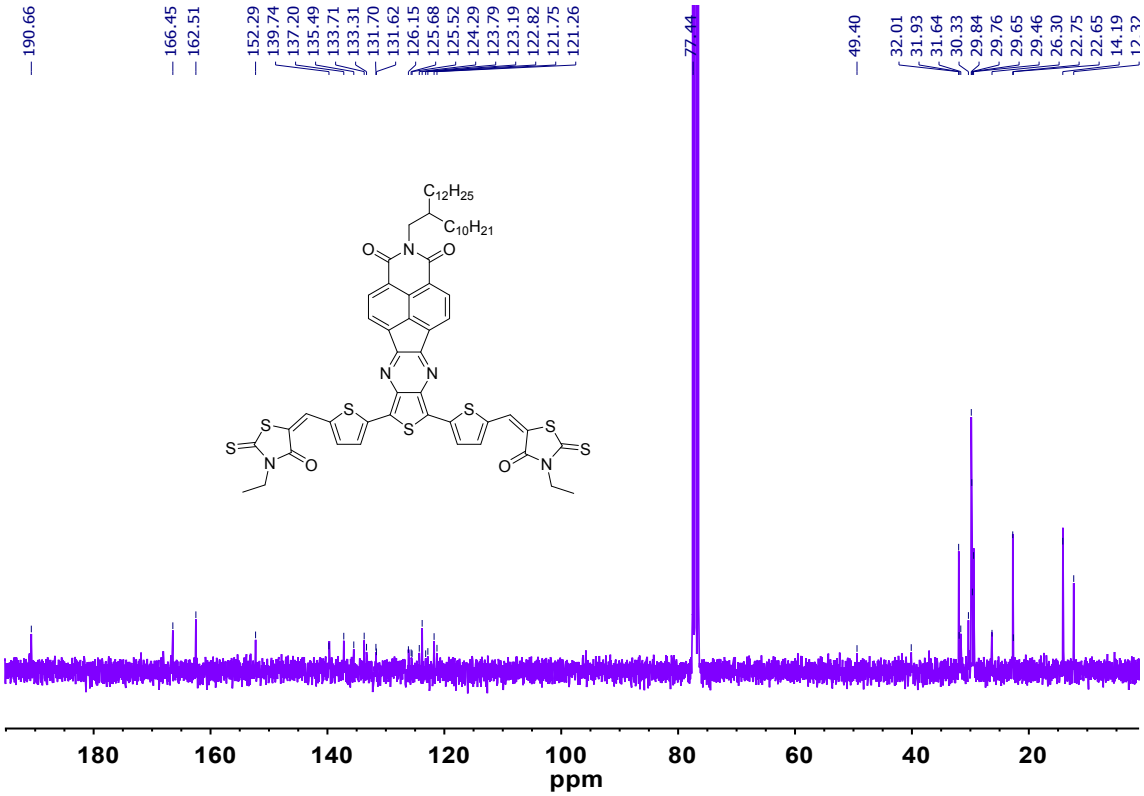

Figure S23 ^{13}C-NMR spectrum of **NIPb3T-Rd** in $CDCl_3$.

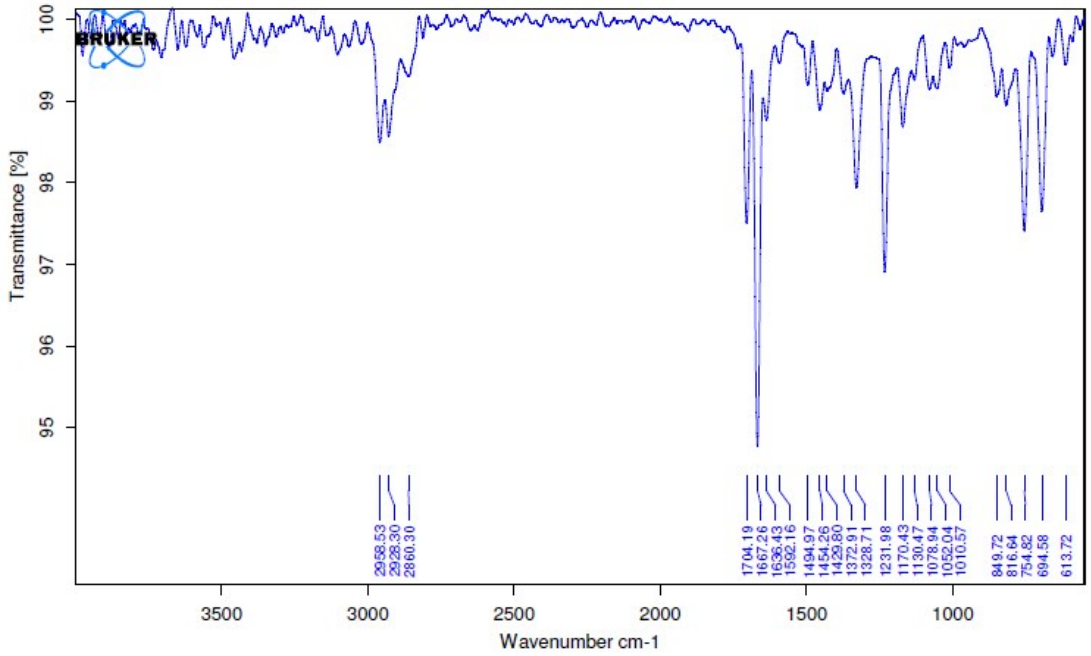

Figure S24 IR spectrum of **NIPa3T-Br**.

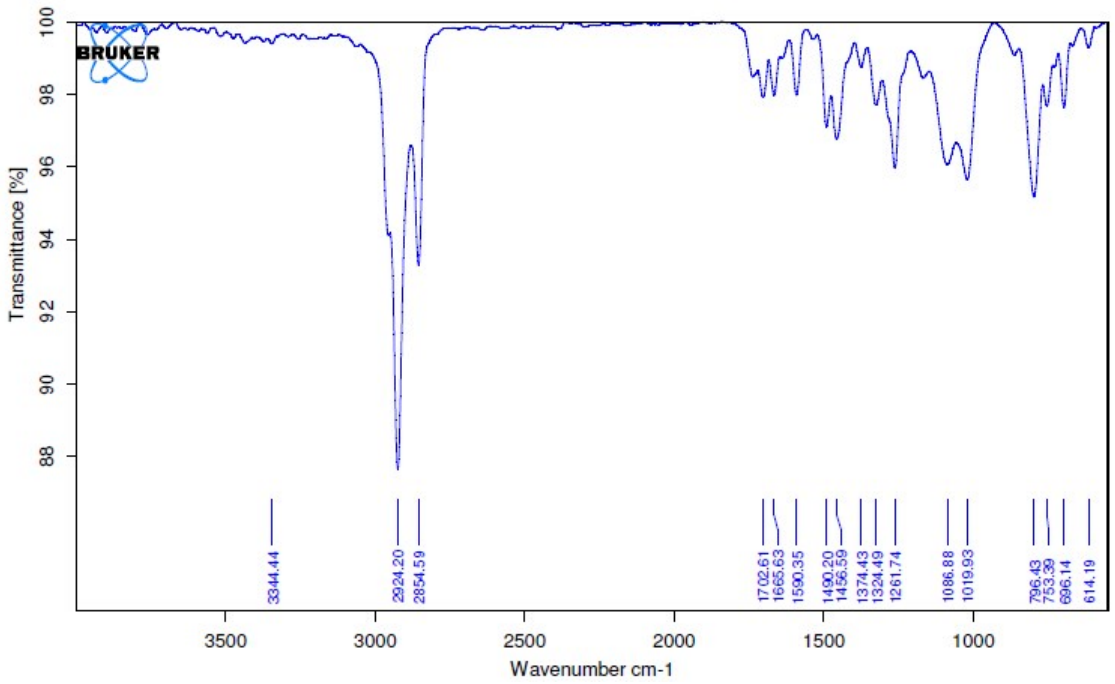

Figure S25 IR spectrum of **NIPa3T-TA**.

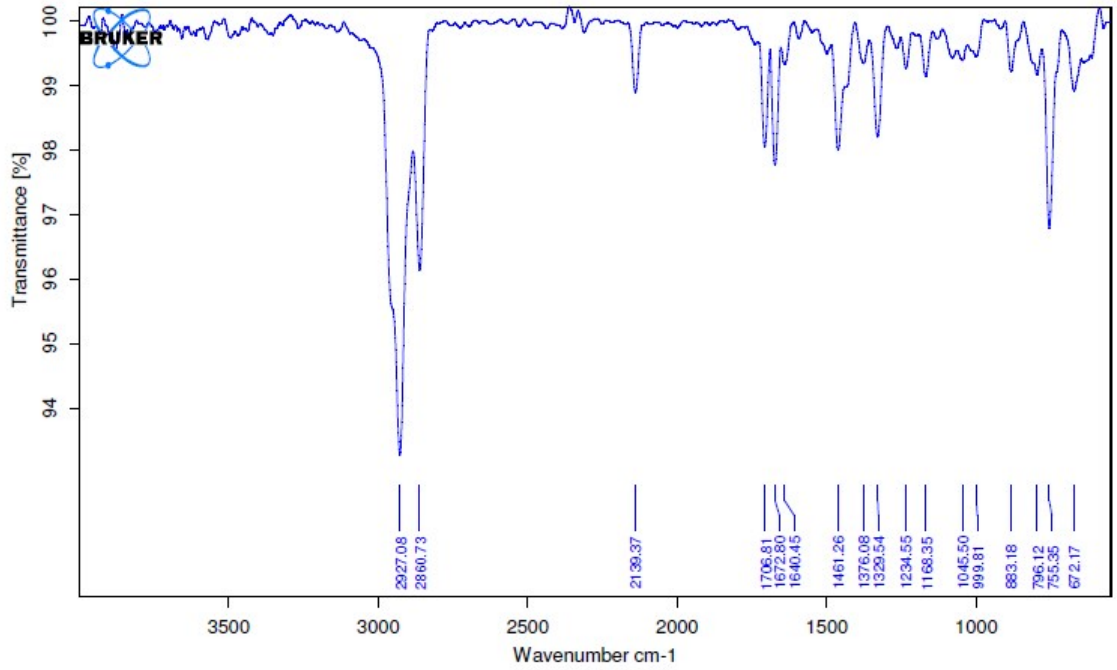

Figure S26 IR spectrum of **NIPa3T-TIPS**.

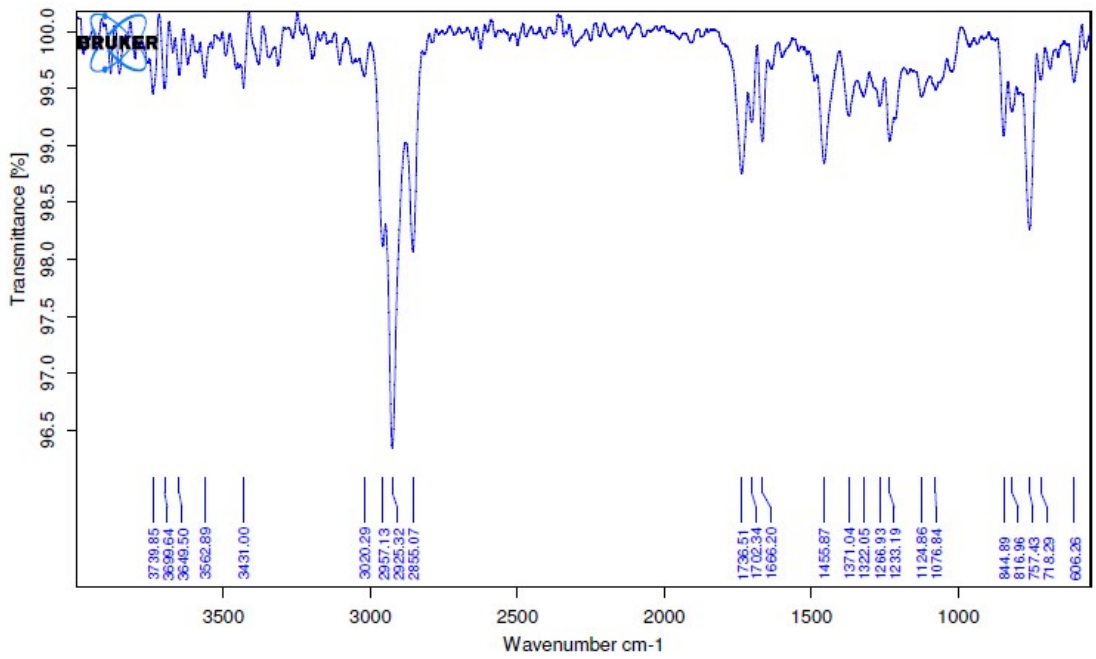

Figure S27 IR spectrum of **NIPa3T-Py**.

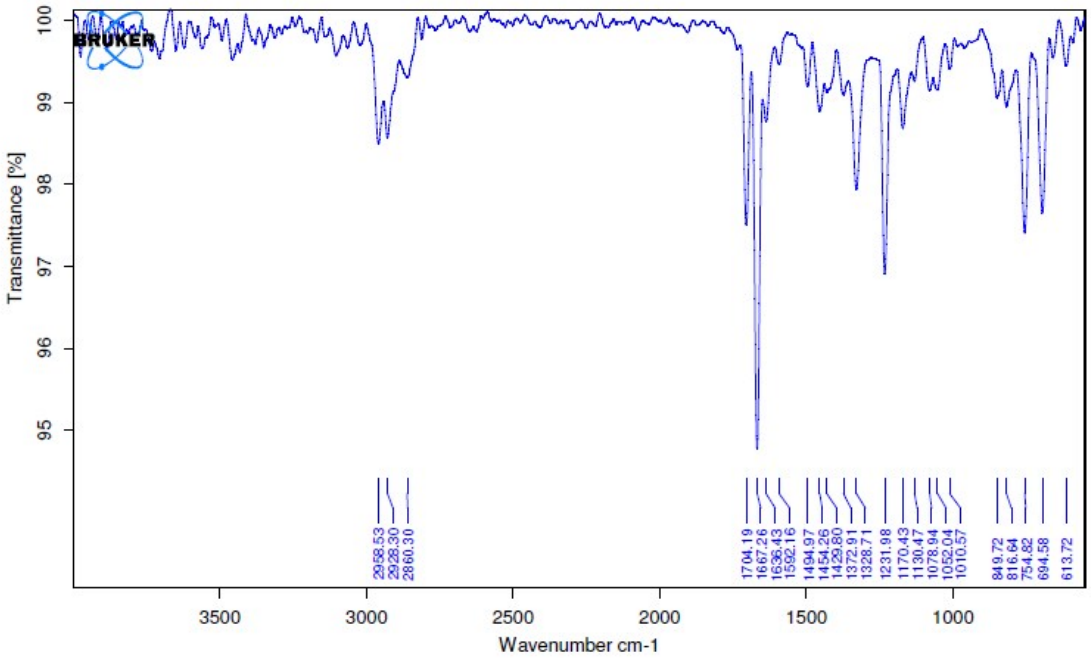

Figure S28 IR spectrum of **NIPa3T**.

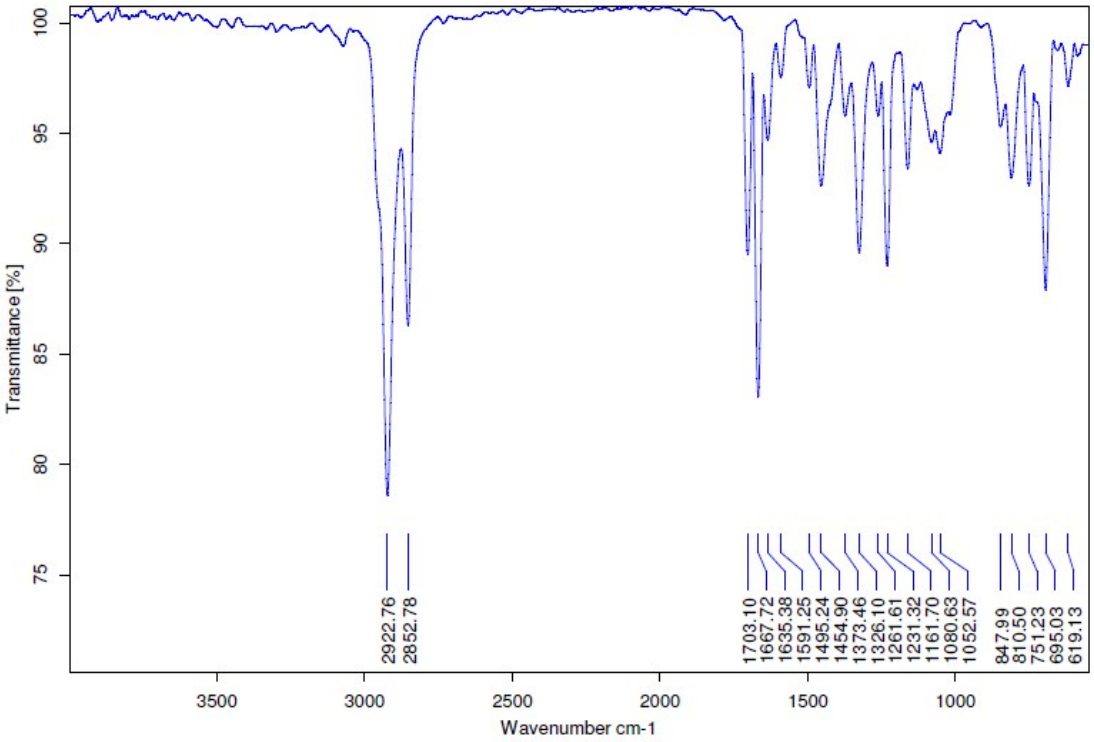

Figure S29 IR spectrum of **NIPb3T**.

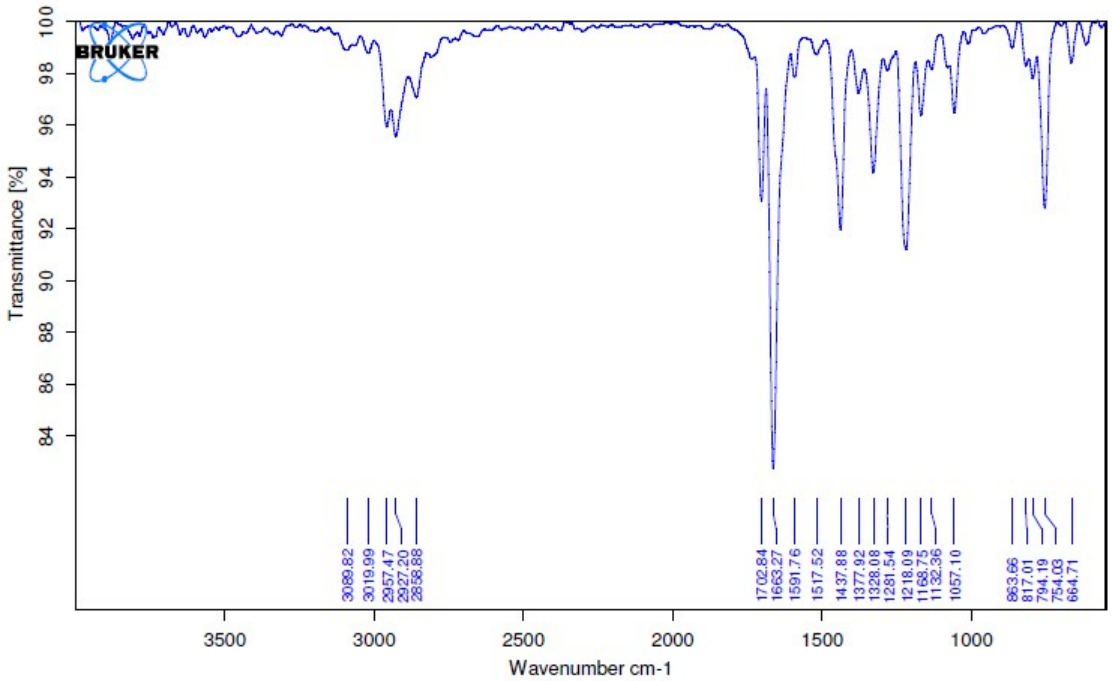

Figure S30 IR spectrum of **NIPa3T-CHO**.

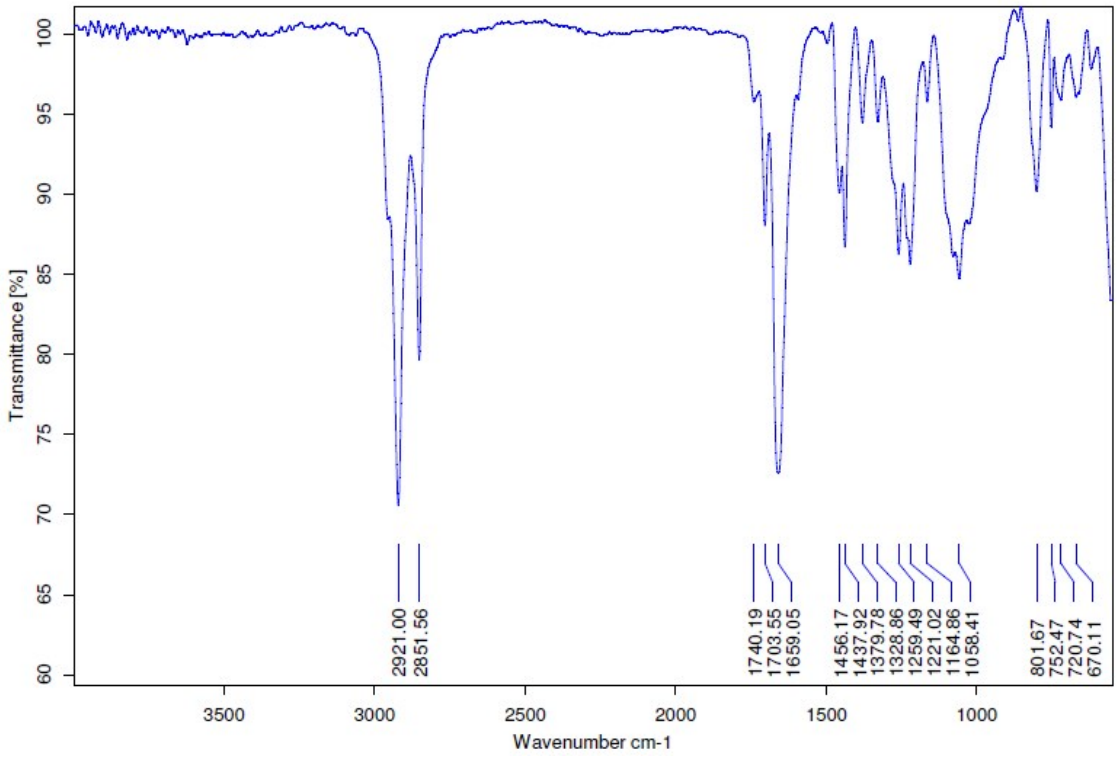

Figure S31 IR spectrum of **NIPb3T-CHO**.

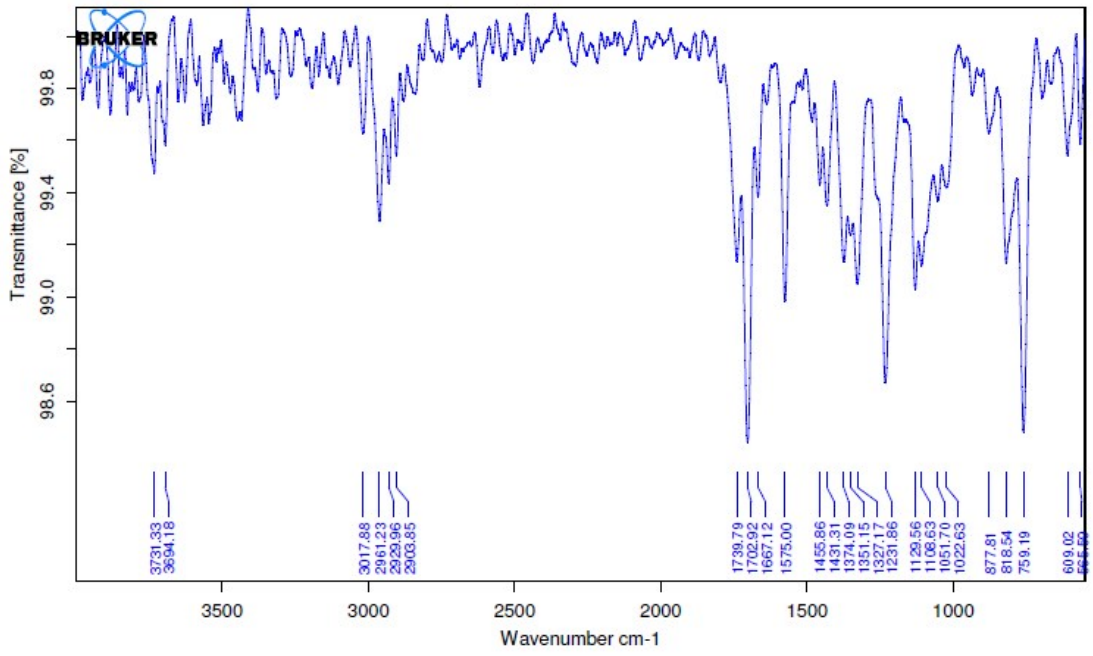

Figure S32 IR spectrum of **NIPa3T-Rd**.

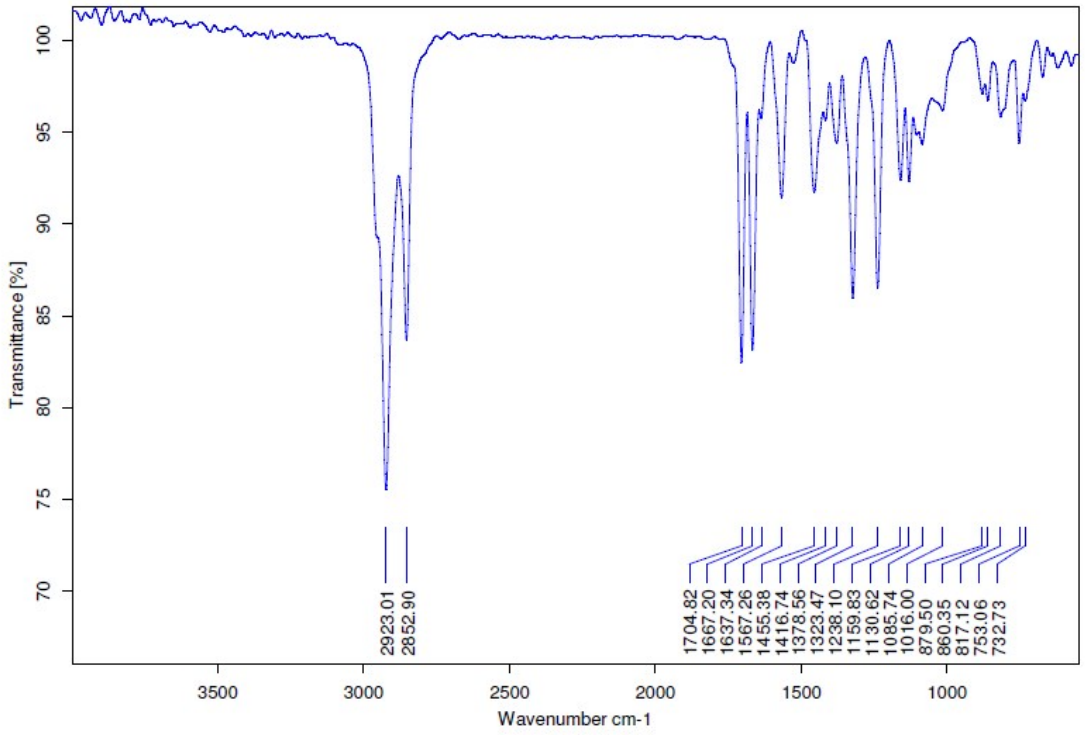

Figure S33 IR spectrum of **NIPb3T-Rd**.

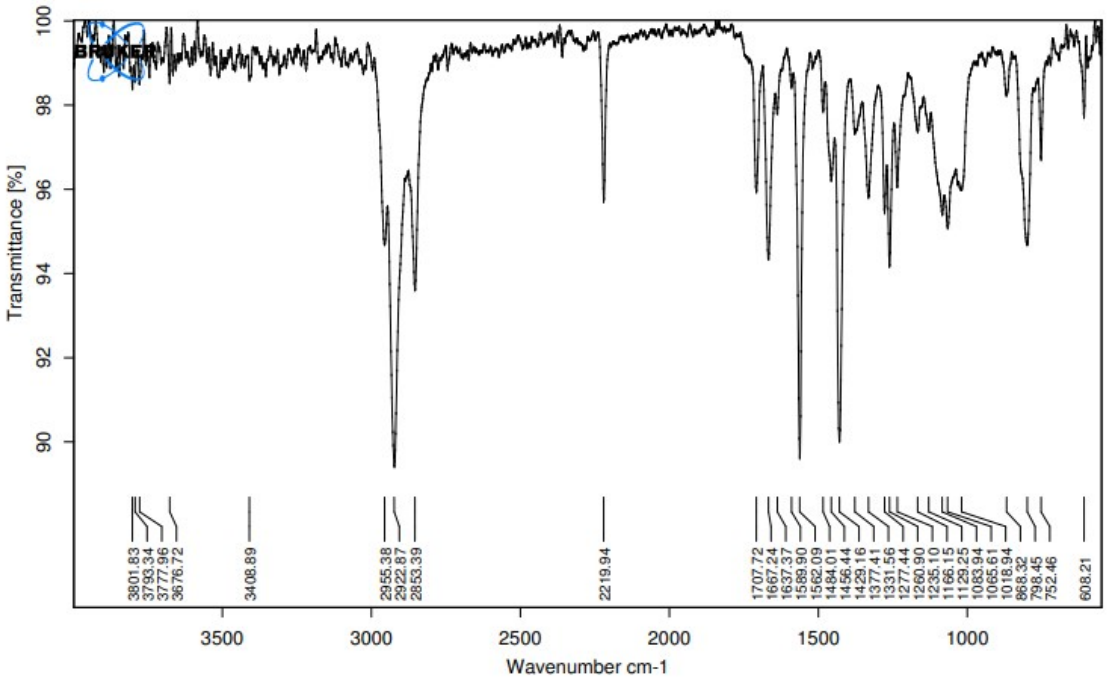

Figure S34 IR spectrum of **NIPa3T-DCV**.

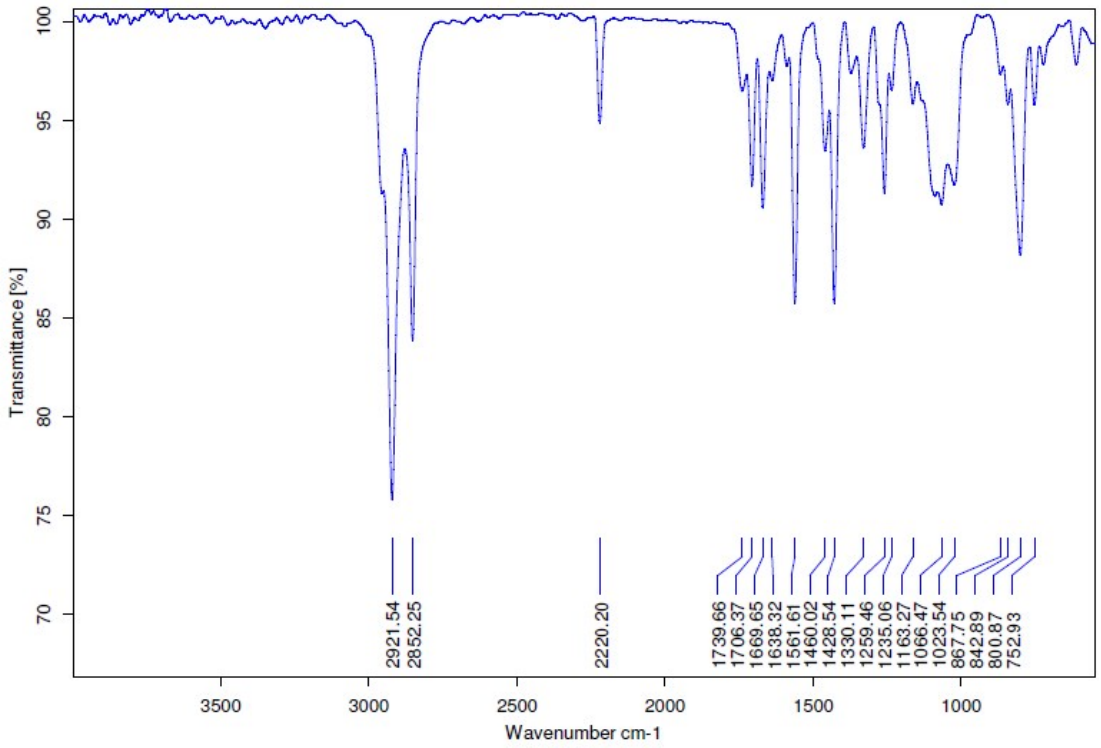

Figure S35 IR spectrum of **NIPb3T-DCV**.

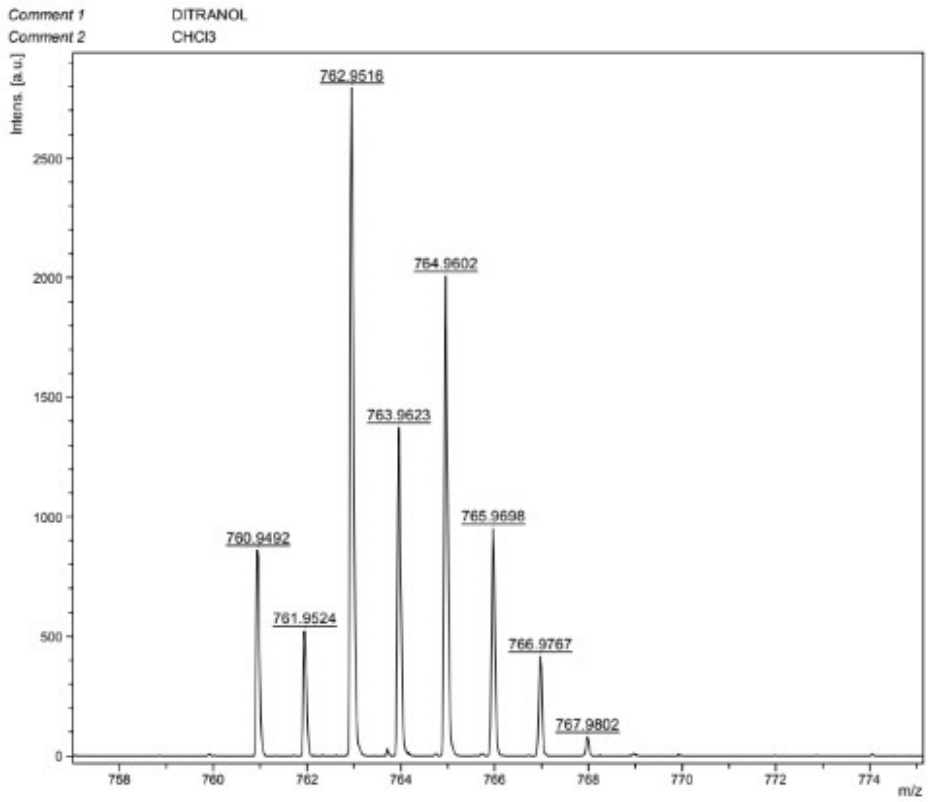

Figure S36 MALDI-HRMS (m/z) spectrum of **NIPa3T-Br**.

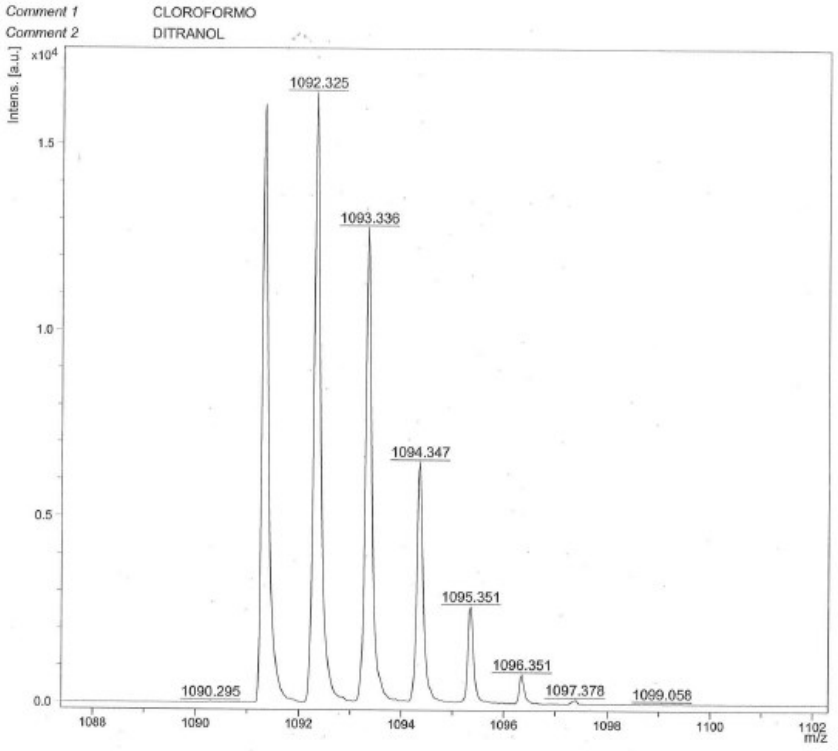

Figure S37 MALDI-HRMS (m/z) spectrum of **NIPa3T-TA**.

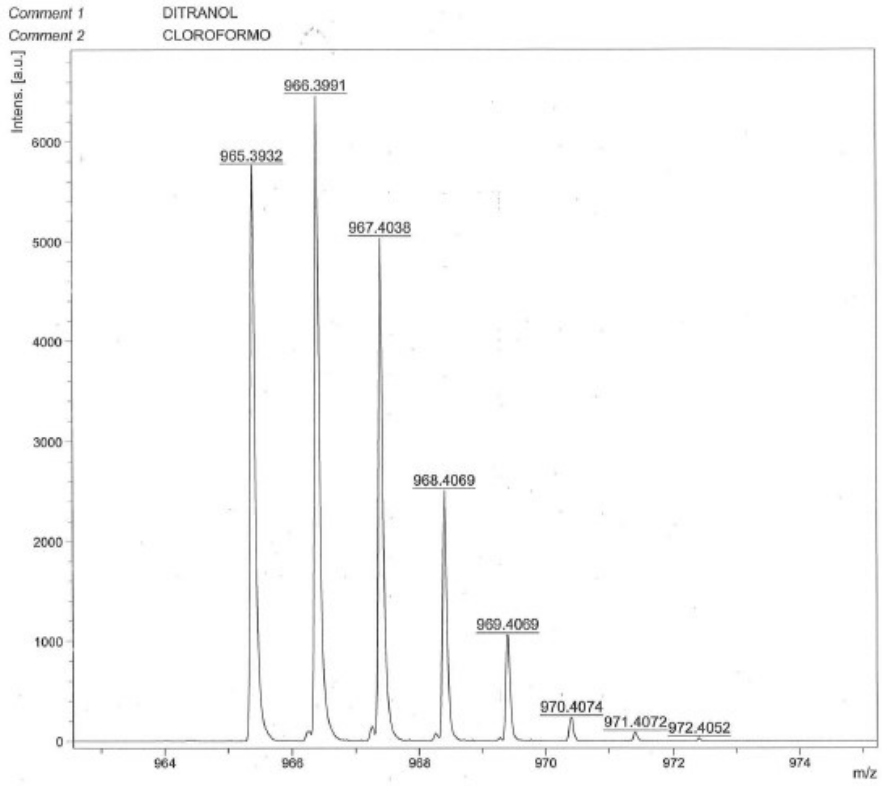

Figure S38 MALDI-HRMS (m/z) spectrum of **NIPa3T-TIPS**.

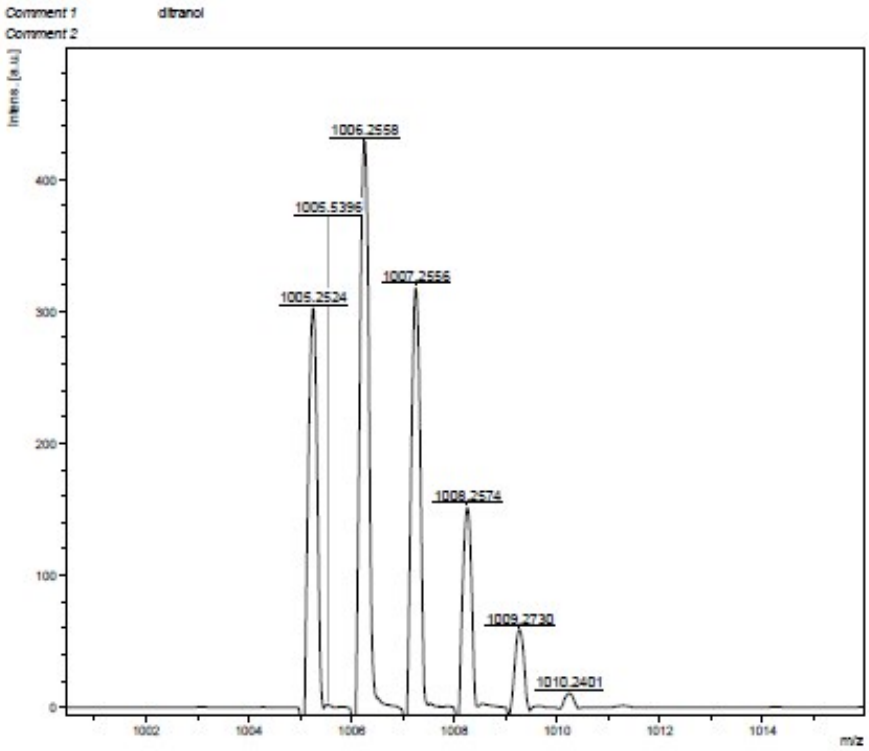

Figure S39 MALDI-HRMS (m/z) spectrum of **NIPa3T-Py**.

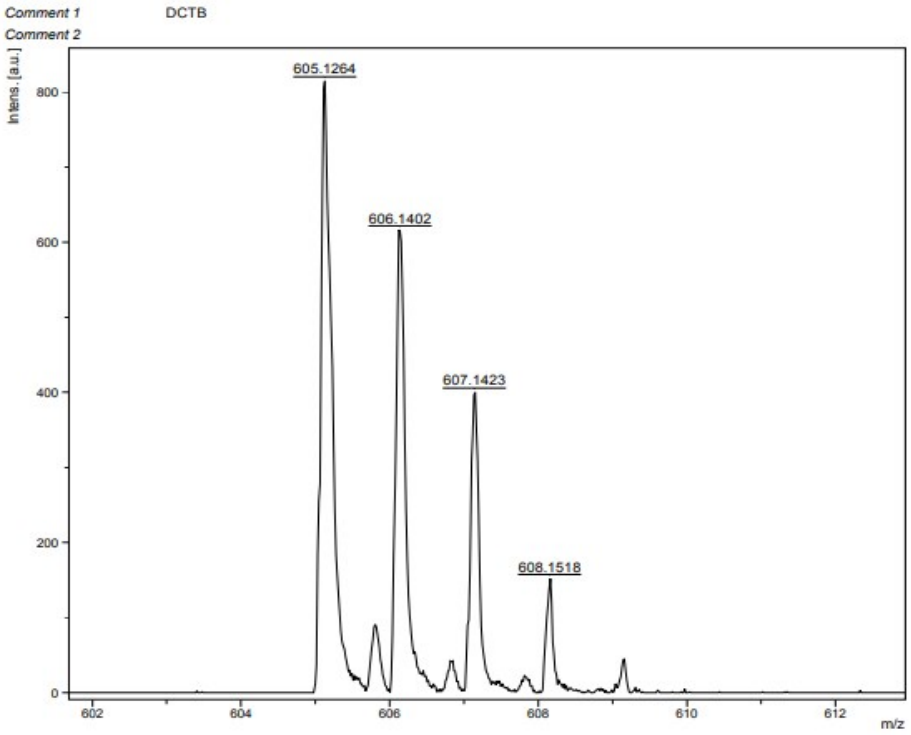

Figure S40 MALDI-HRMS (m/z) spectrum of **NIPa3T**.

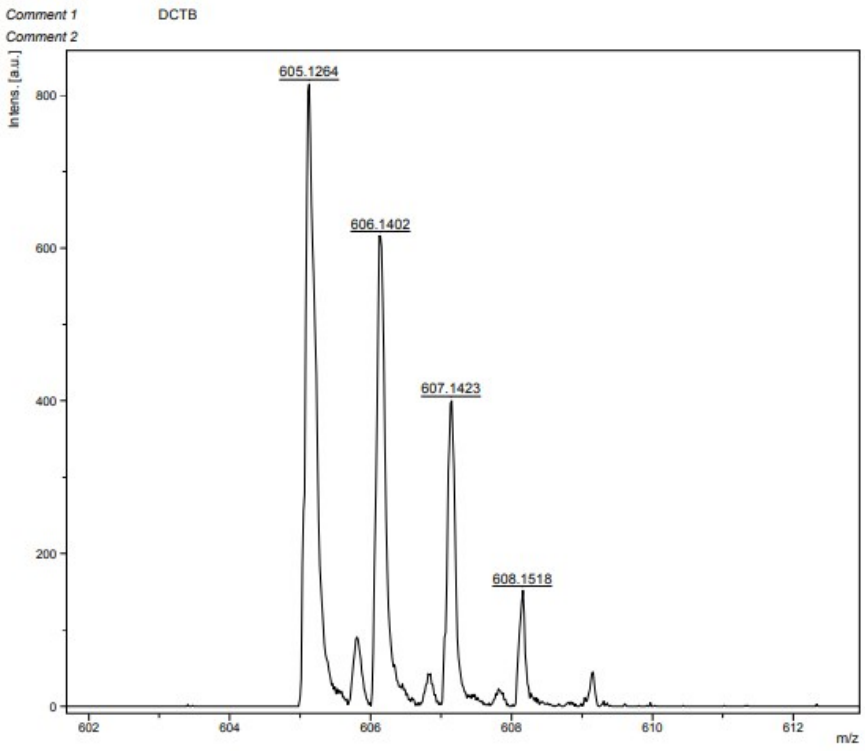

Figure S41 MALDI-HRMS (m/z) spectrum of **NIPb3T**.

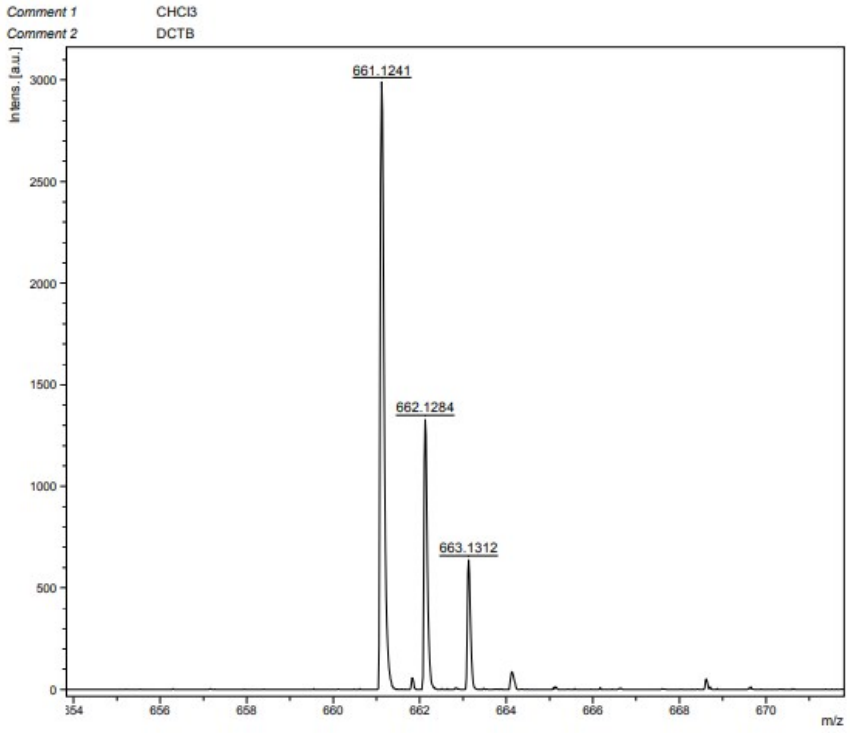

Figure S42 MALDI-HRMS (m/z) spectrum of **NIPa3T-CHO**.

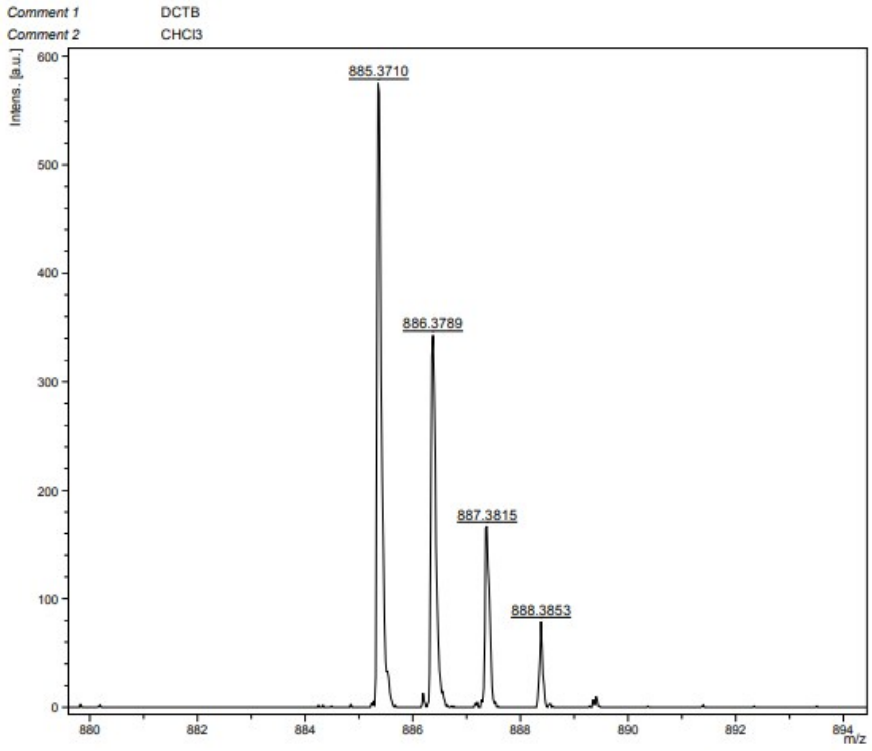

Figure S43 MALDI-HRMS (m/z) spectrum of **NIPb3T-CHO**.

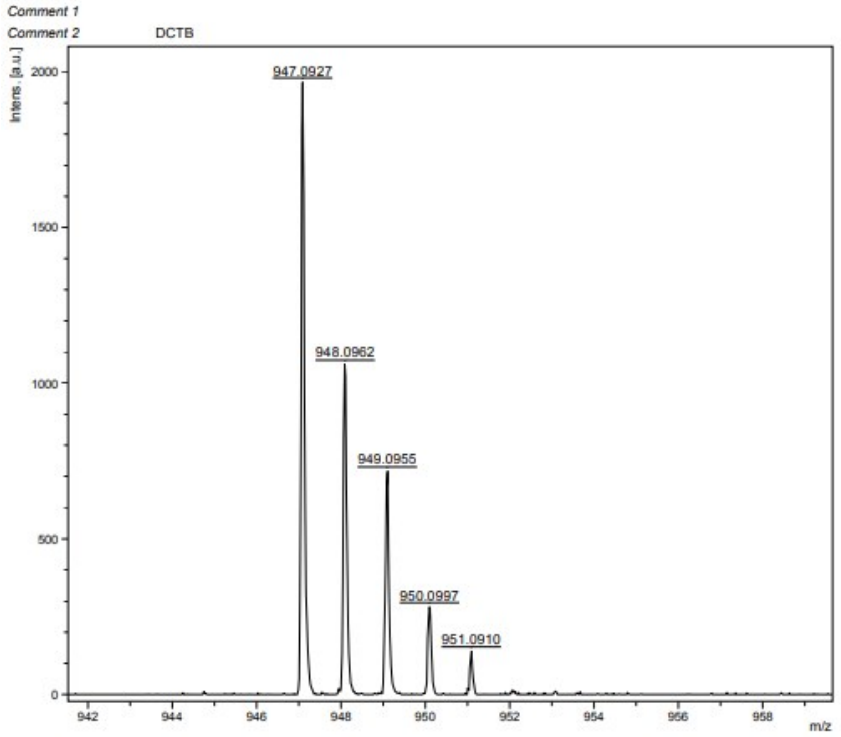

Figure S44 MALDI-HRMS (m/z) spectrum of **NIPa3T-Rd.**

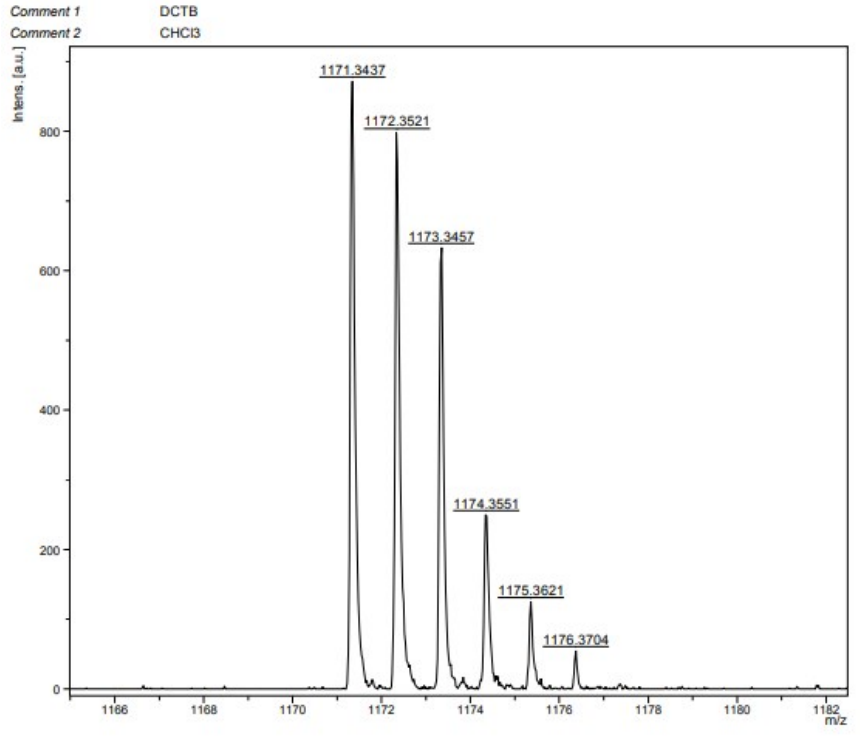

Figure S45 MALDI-HRMS (m/z) spectrum of **NIPb3T-Rd.**

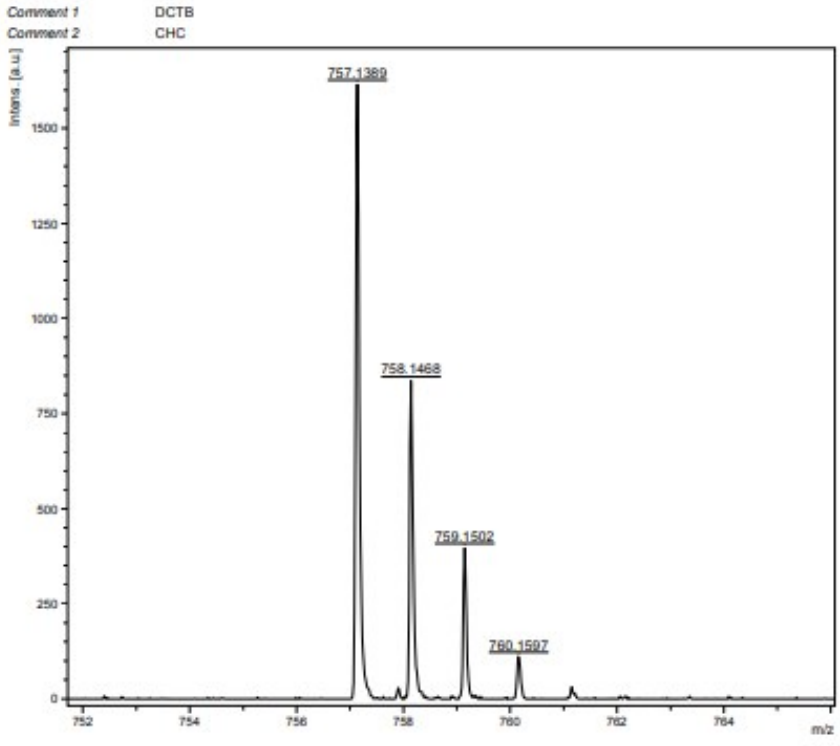

Figure S46 MALDI-HRMS (m/z) spectrum of **NIPa3T-DCV**.

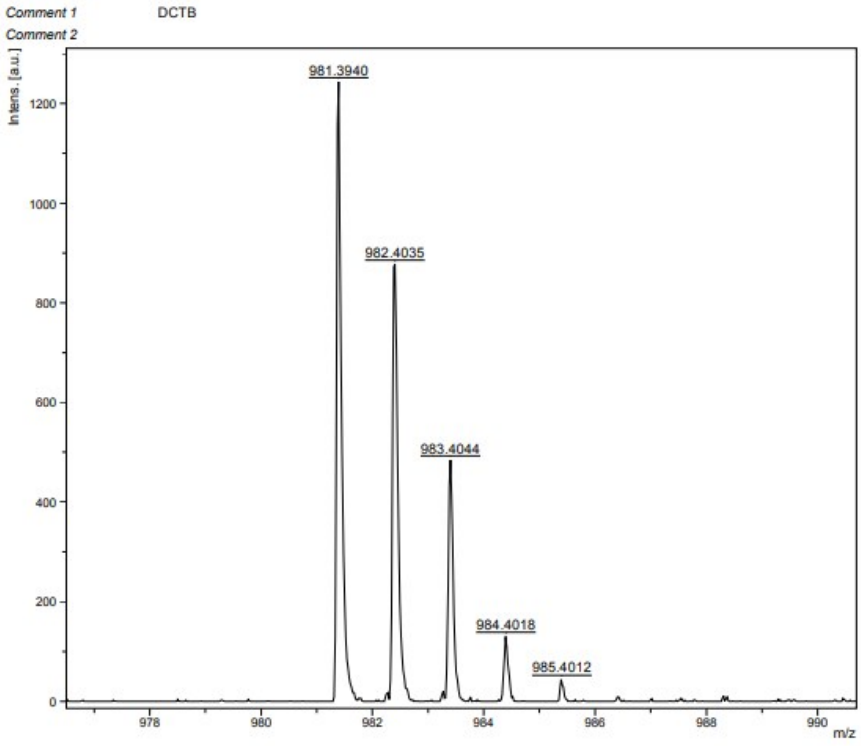

Figure S47 MALDI-HRMS (m/z) spectrum of **NIPb3T-DCV**.

3. DFT calculations

Theoretical calculations for the NIPs monomers were carried out in the frame of density functional theory (DFT), using the B3LYP functional[11-13] and the 6-31G** basis set[14, 15] as implemented in the Gaussian 16 program.[16] 2-decyltetradecyl chains on the N-imide group of NIPs were replaced with isopropyl chains to simplify the calculations, for this reason NIP3T acronym is used to simplify the nomenclature. Geometry optimizations were performed without any symmetry constrains. On the basis of the resulting ground-state geometries, harmonic vibrational frequencies were calculated at the same theoretical level. The reorganization energies were calculated directly from the relevant points on the potential energy surfaces by using previously reported standard procedures. The formation of dimeric structures for the different semiconducting systems were theoretically predicted at the wB97XD[17, 18]/6-31G*[19] level, the formation of dimeric structures.

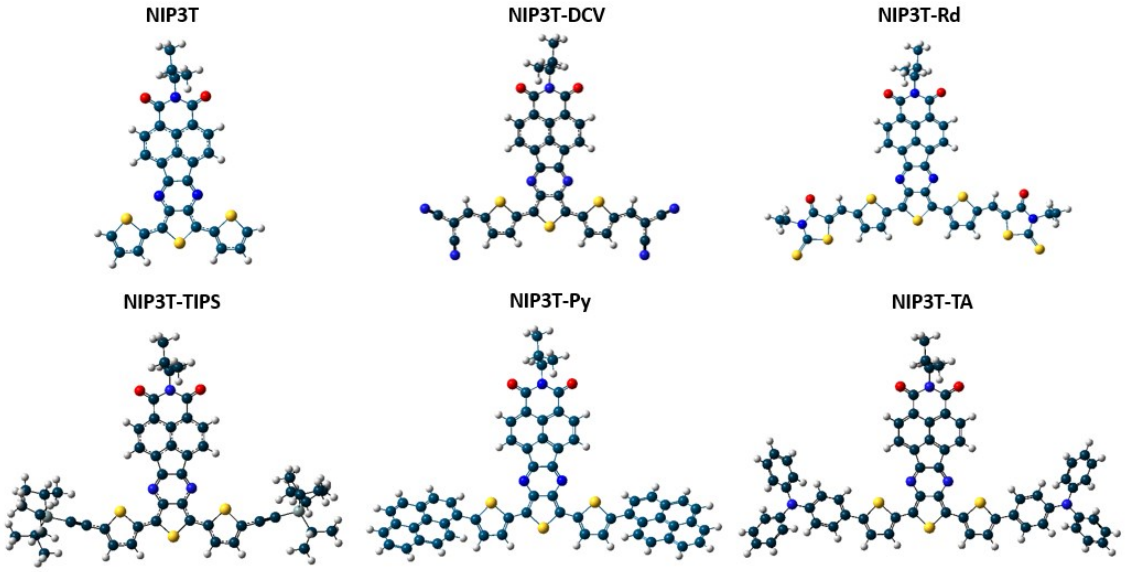

Figure S48 B3LYP/6-31G** optimized geometries of NIPs.

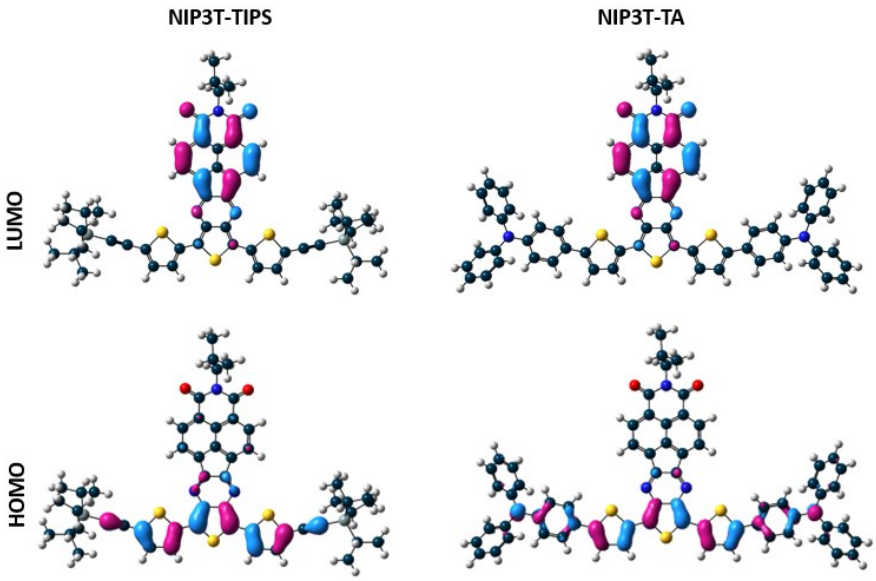

Figure S49 5 B3LYP/6-31G** molecular orbital topologies of **NIP3T-TIPS** and **NIP3T-TA**.

Table S1. HOMO-LUMO gap energies and TDDFT-calculated vertical transition energies with the corresponding description at B3LYP/6-31G** level of theory. The oscillator strength values are given in brackets.

	E_{H-L} (eV)	λ (f) (nm)	Description
NIP3T-TIPS	2.04	416 (1.18)	HOMO→L+2 (91%)
		695 (0.46)	HOMO→LUMO (99%)
NIP3T-Py	1.91	465 (1.06)	HOMO→L+2 (96%)
		739 (0.61)	HOMO→L+1 (99%)
NIP3T	1.73	327 (0.65)	H-5→L+1 (53%), H-3→L+1 (37%)
		357 (0.38)	H-3→LUMO (17%), H-1→LUMO (19%), HOMO→L+2 (48%)
		657 (0.23)	HOMO→LUMO (98%)
NIP3T-TA	2.17	456 (1.38)	HOMO→L+2 (94%)
		797 (0.65)	HOMO→LUMO (99%)
NIP3T-Rd	1.90	370 (0.28)	H-1→L+3 (59%), HOMO→L+4 (72%)
		508 (0.68)	HOMO→L+2 (89%)
		726 (1.04)	HOMO→LUMO (98%)
NIP3T-DCV	2.00	416 (0.51)	H-1→LUMO (31%), HOMO→L+3 (51%)
		609 (0.20)	HOMO→L+1 (98%)
		665 (0.85)	HOMO→LUMO (98%)

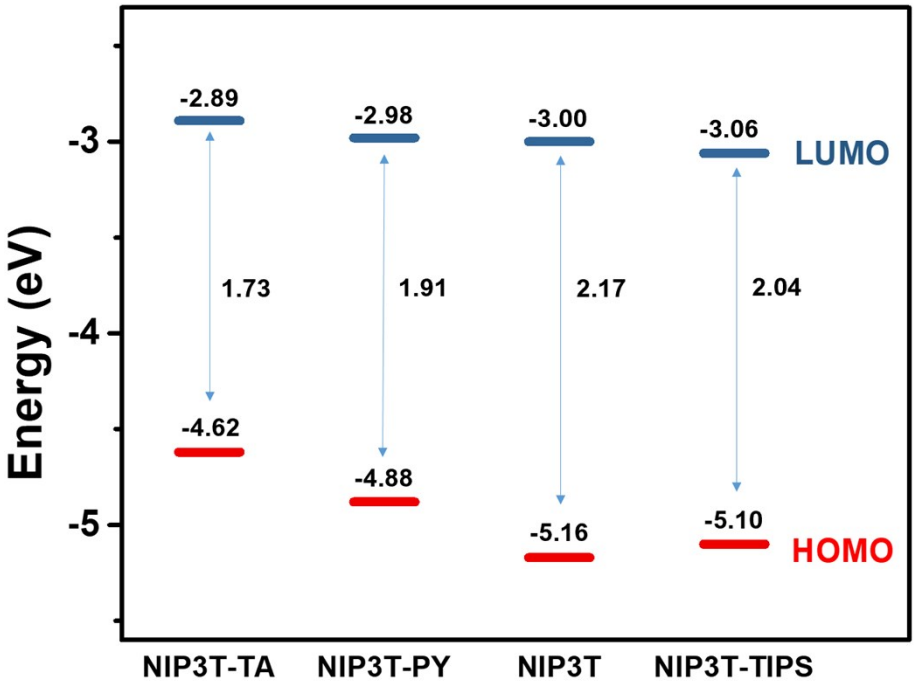

Figure S50 B3LYP/6-31G** frontier molecular orbital topologies predicted for **NIP3T-TA**, **NIP3T-Py**, **NIP3T** and **NIP3T-TIPS** and the energy gap values.

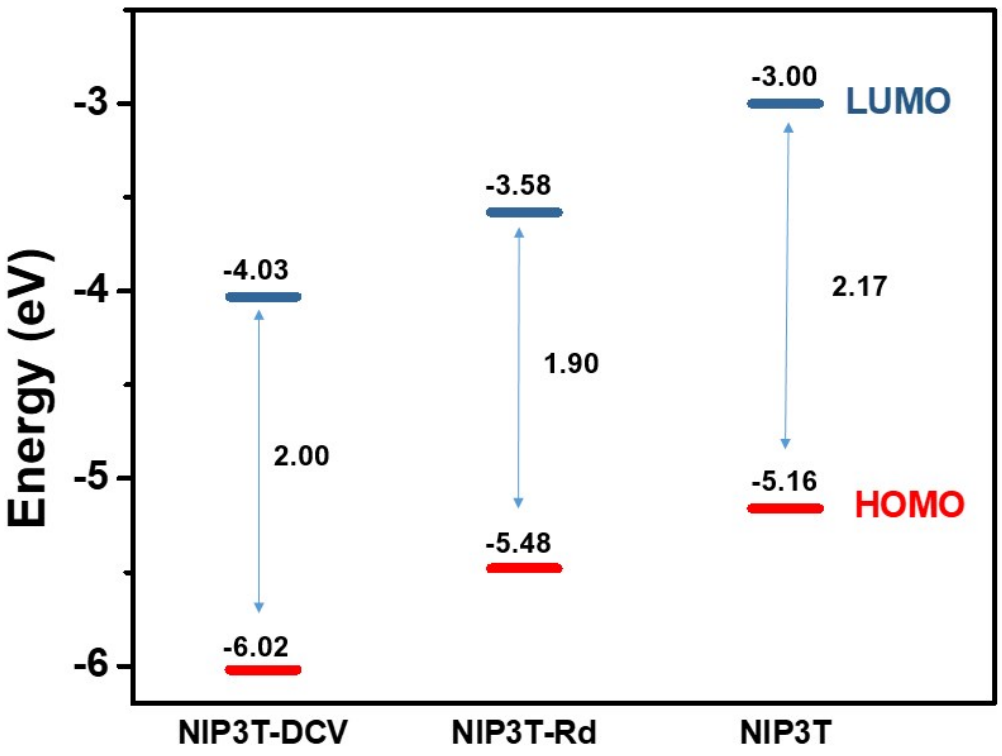

Figure S51 B3LYP/6-31G** frontier molecular orbital topologies predicted for **NIP3T-DCV**, **NIP3T-Rd** and **NIP3T** and the energy gap values.

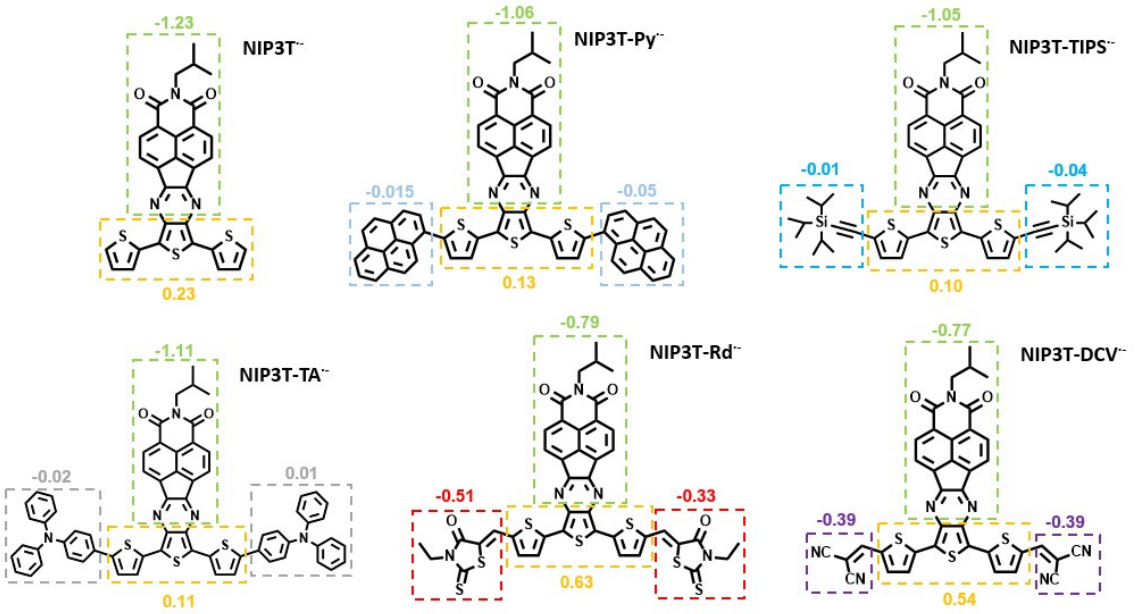

Figure S52 B3LYP/6-31G**-charge distributions for a) **NIP3T**, b) **NIP3T-Py**, c) **NIP3T-TIPS**, d) **NIP3T-TA**, e) **NIP3T-Rd** and f) **NIP3T-DCV** as anion species.

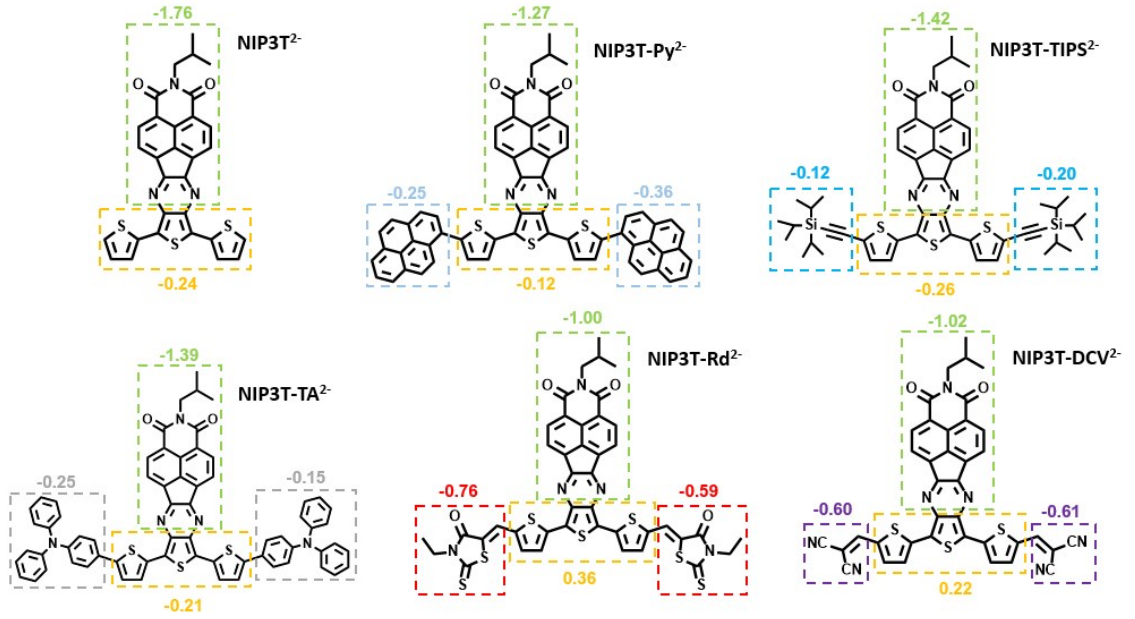

Figure S53 B3LYP/6-31G**-charge distributions for a) **NIP3T**, b) **NIP3T-Py**, c) **NIP3T-TIPS**, d) **NIP3T-TA**, e) **NIP3T-Rd** and f) **NIP3T-DCV** as dianion species.

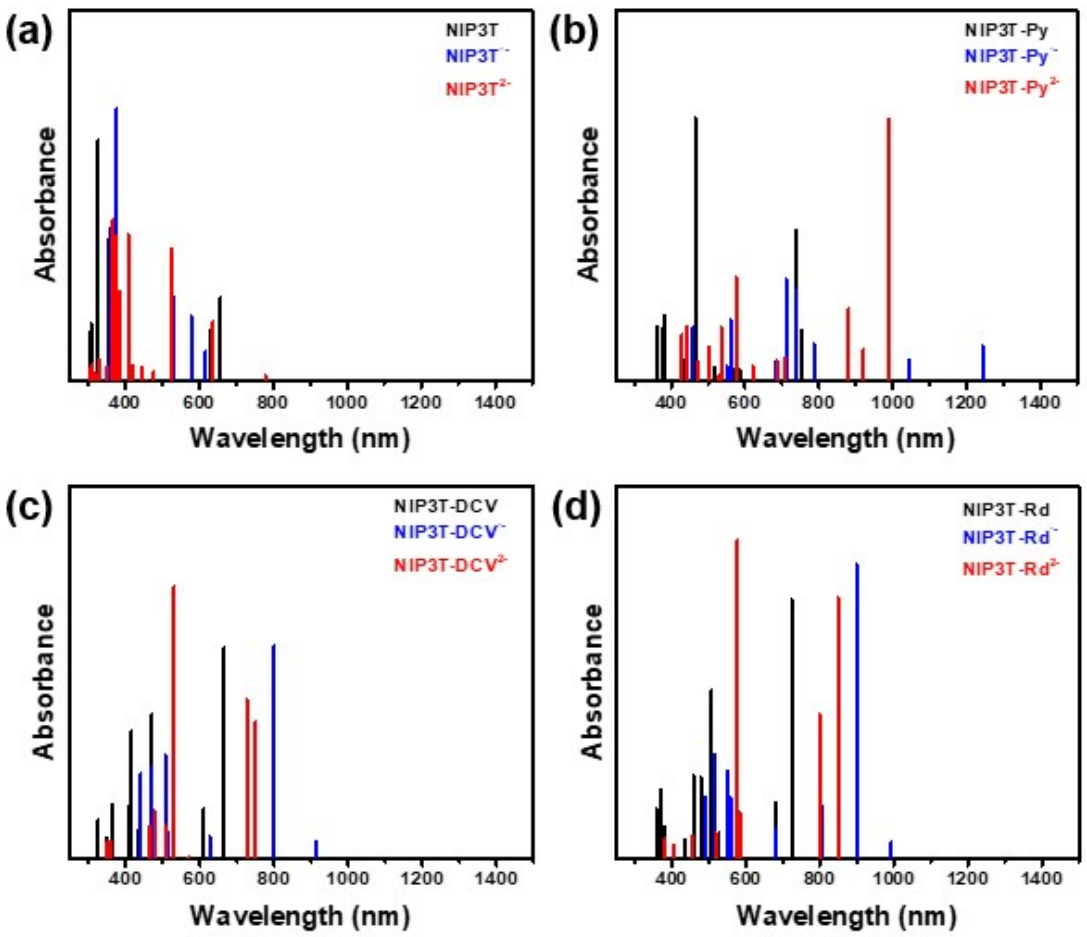

Figure S54 TDDFT-B3LYP/6-31G**-calculated vertical transition energies for a) **NIP3T**, b) **NIP3T-Py**, c) **NIP3T-DCV** and d) **NIP3T-Rd** with the different reduced species. See the comparison with the experimental results in Figures S77-80.

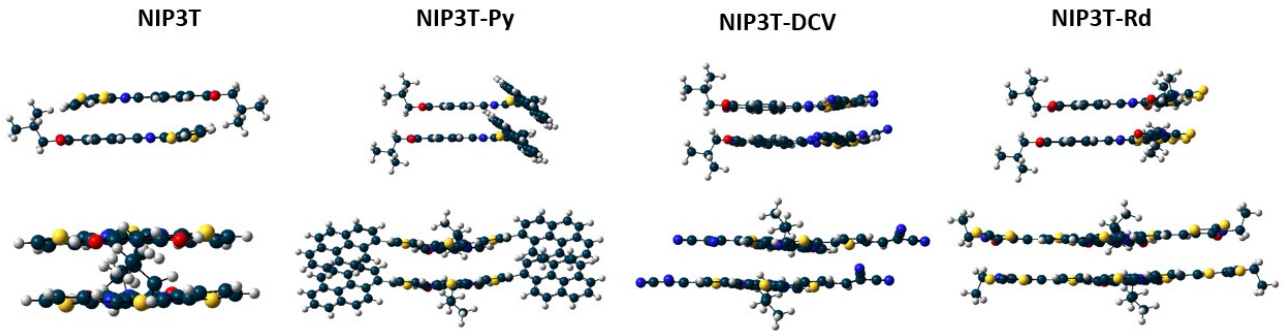

Figure S55 wB97XD/6-31G* optimized geometries of NIPs dimers.

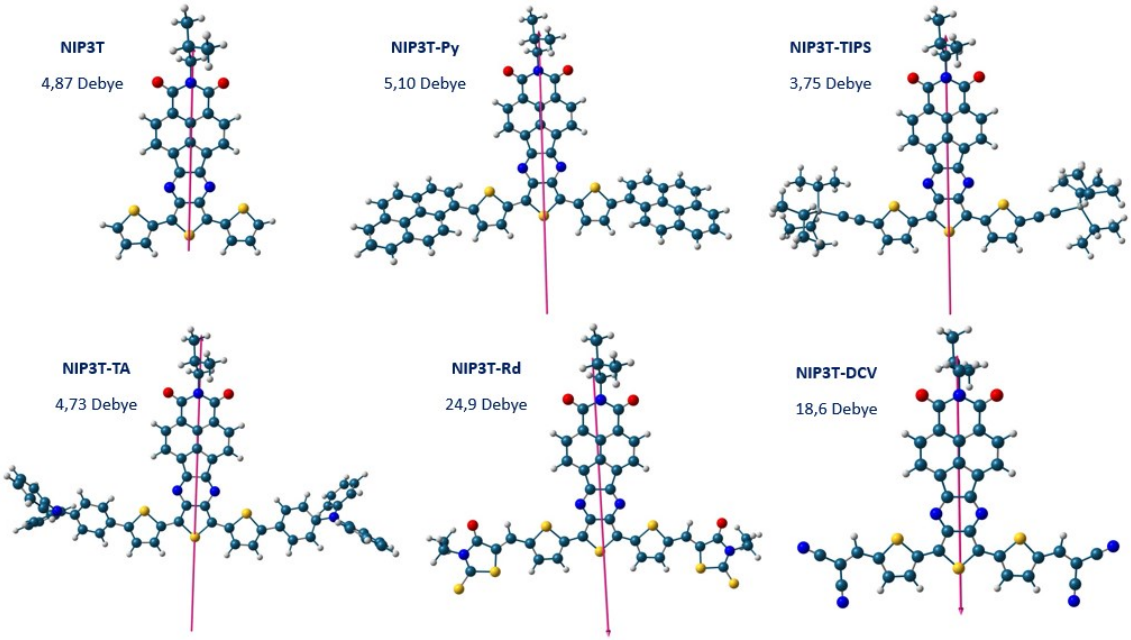

Figure S56 Calculated transition dipole moments of NIP derivatives.

4. FT-Raman

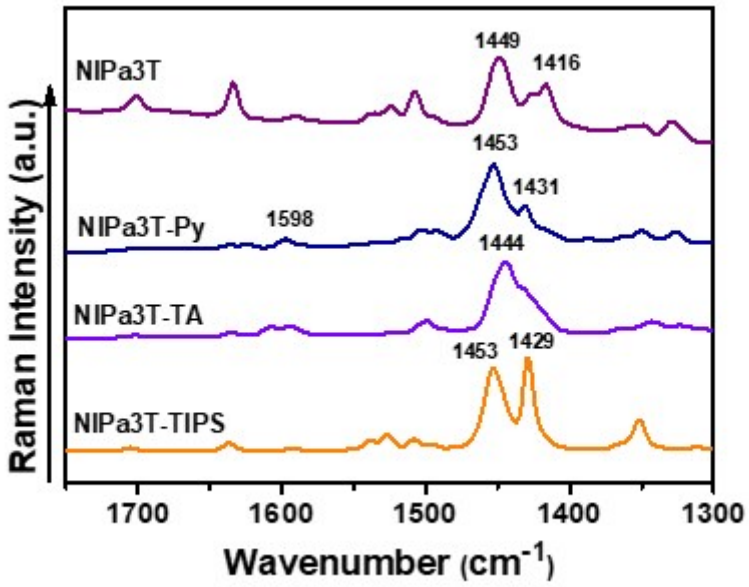

Figure S57 Raman spectra (λ=1064 nm) of **NIPa3T**, **NIPa3T-Py**, **NIPa3T-TA** and **NIPa3T-TIPS** derivatives as bulk materials.

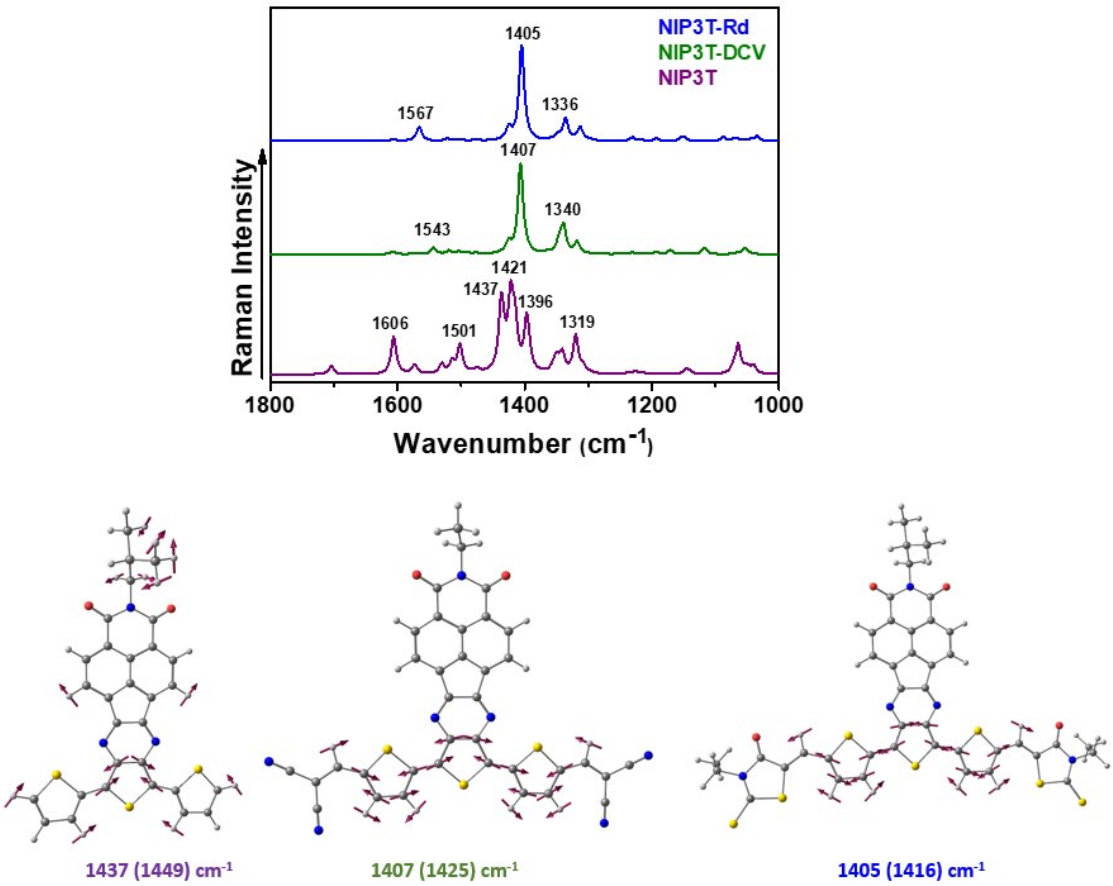

Figure S58 B3LYP/6-31G** predicted Raman spectra for **NIP3T-Rd**, **NIP3T-DCV** and **NIP3T** and the corresponding eigenvectors.

5. UV-Vis and electrochemical data

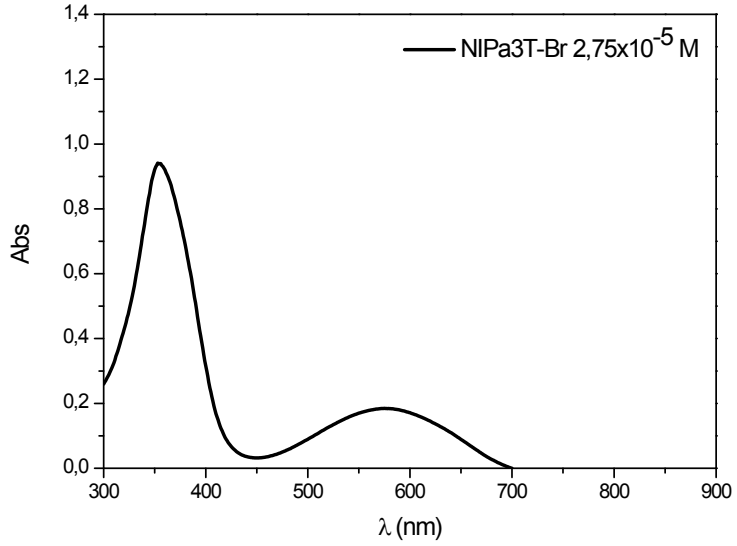

Figure S59 UV-Vis spectra of **NIPa3T-Br** 2.75x10^{-5} M in chloroform solution.

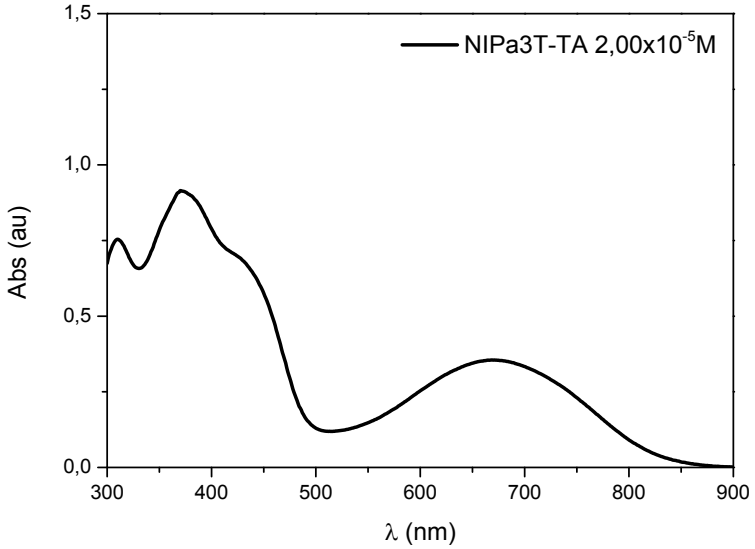

Figure S60 UV-Vis spectra of **NIPa3T-TA** 2.00x10^{-5} M in chloroform solution.

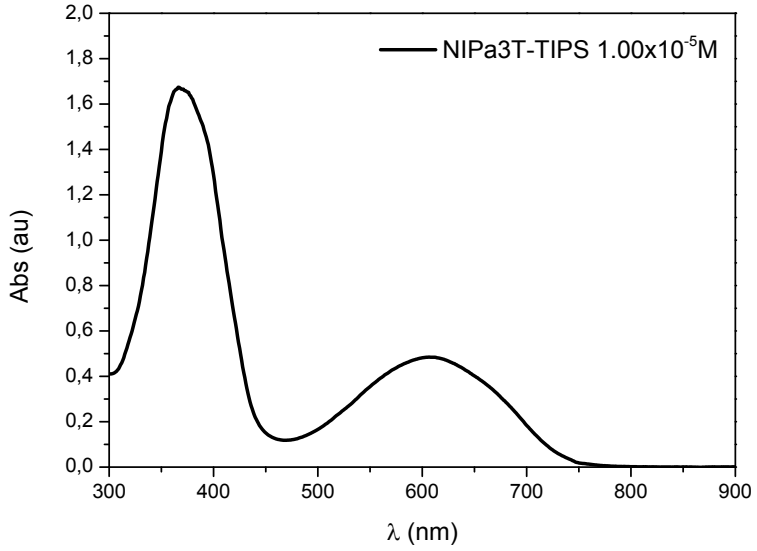

Figure S61 UV-Vis spectra of **NIPa3T-TIPS** 1.00x10^{-5} M in chloroform solution.

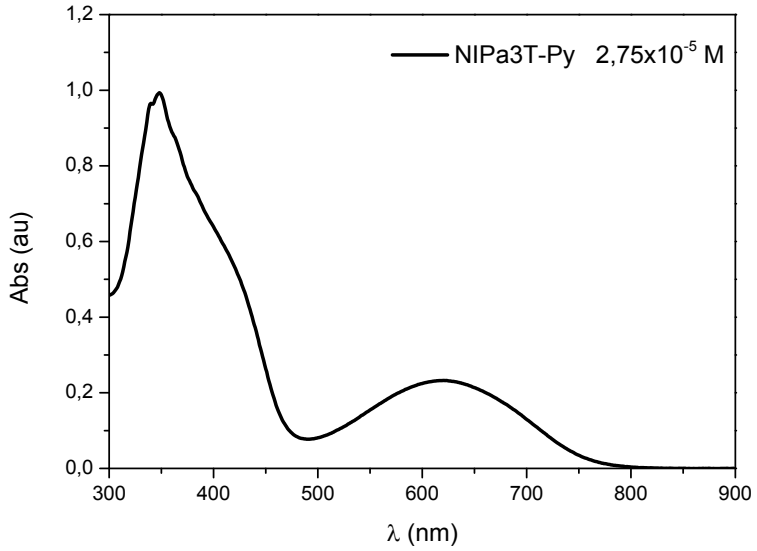

Figure S62 UV-Vis spectra of **NIPa3T-Py** 2.75x10^{-5} M in chloroform solution.

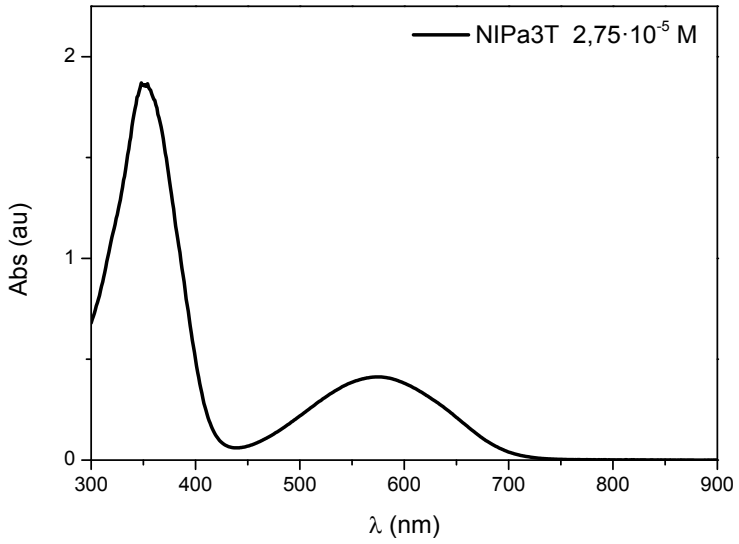

Figure S63 UV-Vis spectra of **NIPa3T** 2.75x10^{-5} M in chloroform solution.

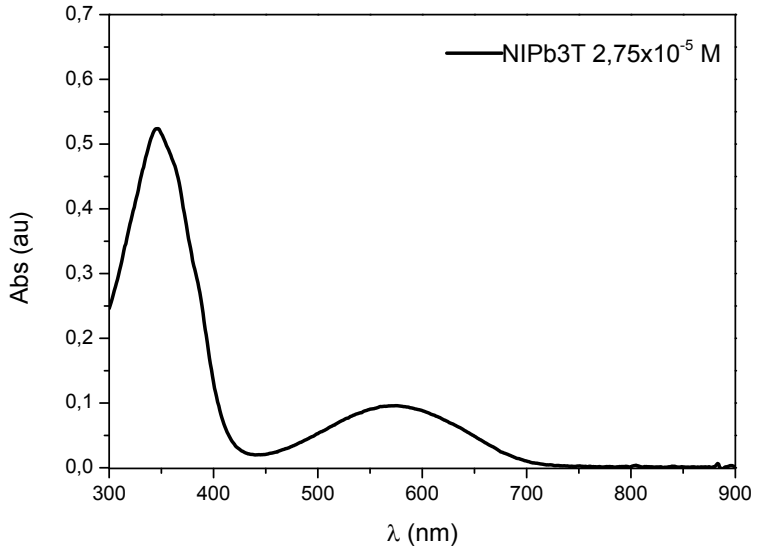

Figure S64 UV-Vis spectra of **NIPb3T** 2.75x10^{-5} M in chloroform solution.

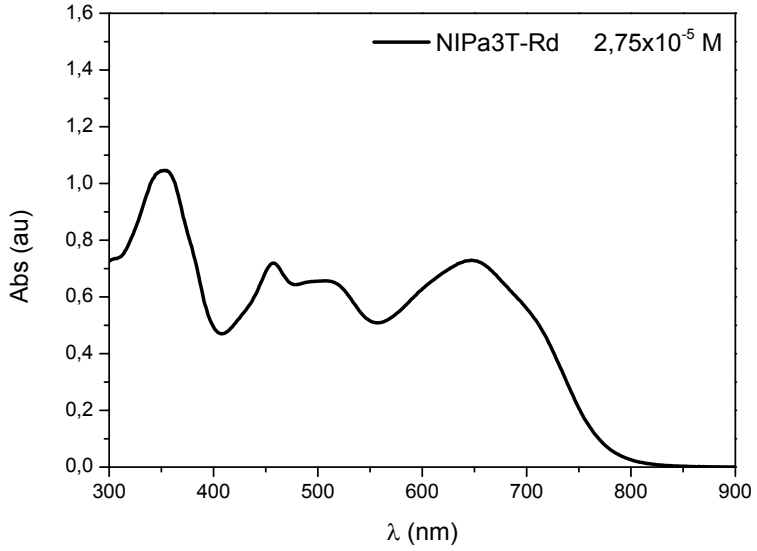

Figure S65 UV-Vis spectra of **NIPa3T-Rd** 2.75x10^{-5} M in chloroform solution.

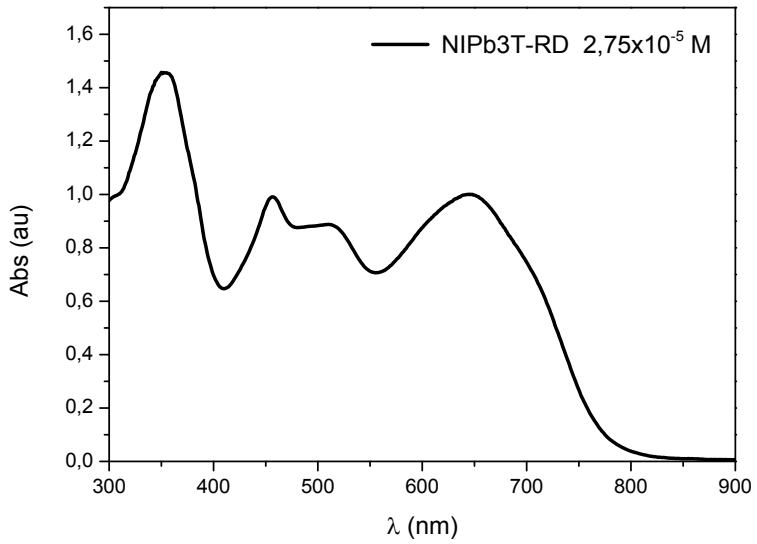

Figure S66 UV-Vis spectra of **NIPb3T-Rd** 2.75x10^{-5} M in chloroform solution.

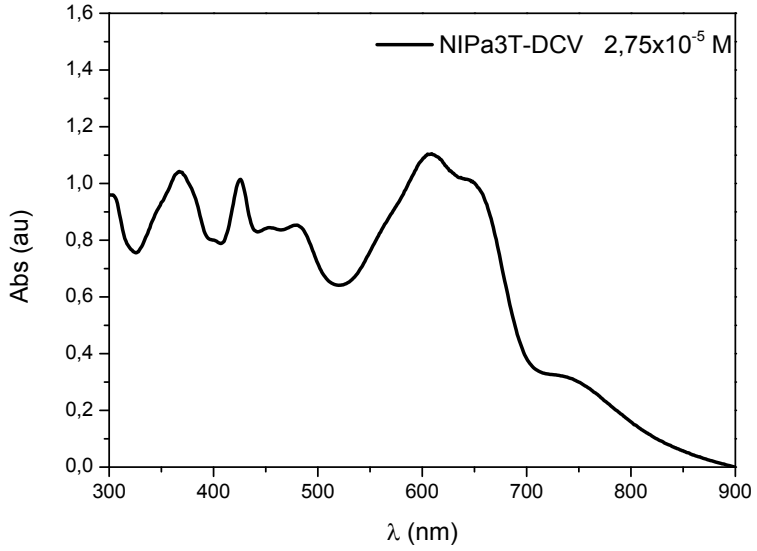

Figure S67 UV-Vis spectra of **NIPa3T-DCV** 2.75x10^{-5} M in chloroform solution.

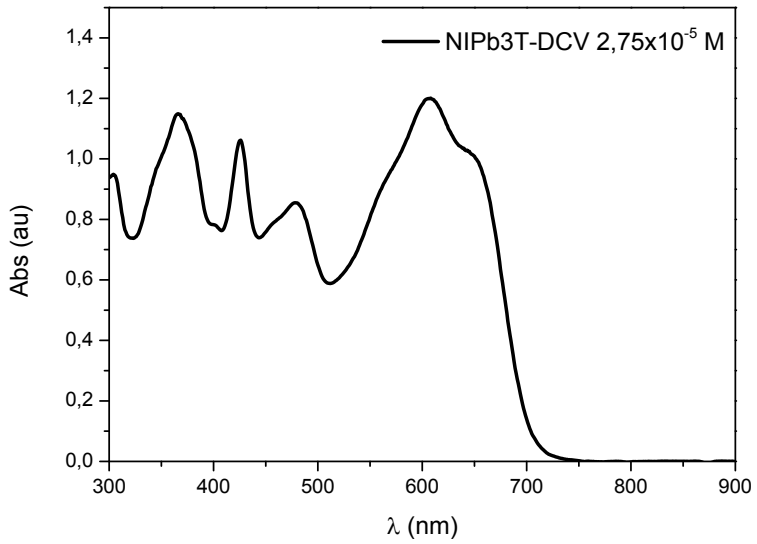

Figure S68 UV-Vis spectra of **NIPb3T-DCV** 2.75x10^{-5} M in chloroform solution.

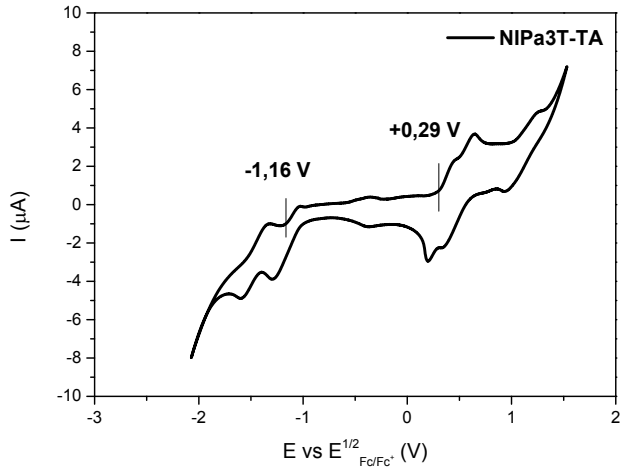

Figure S69 Cyclic voltammetry of **NIPa3T-TA** and TBAHFP 0.1M in dichloromethane solution.

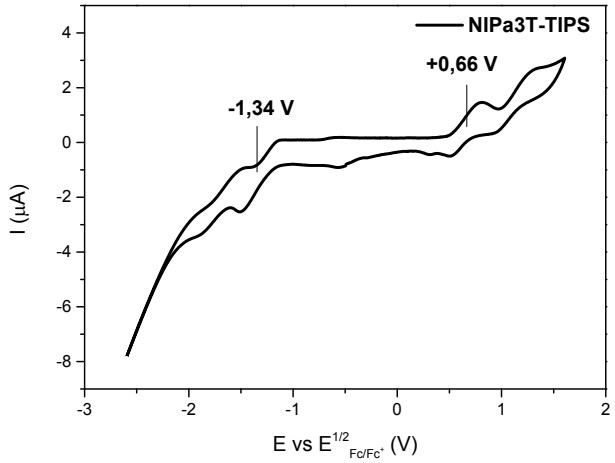

Figure S70 Cyclic voltammetry of **NIPa3T-TIPS** and TBAHFP 0.1M in dichloromethane solution.

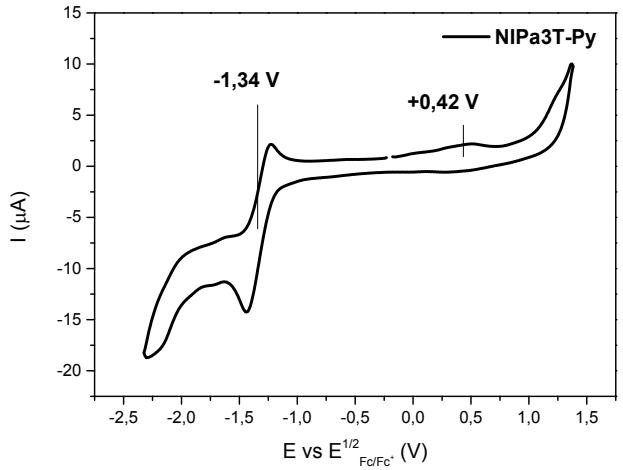

Figure S71 Cyclic voltammetry of **NIPa3T-Py** and TBAHFP 0.1M in dichloromethane solution.

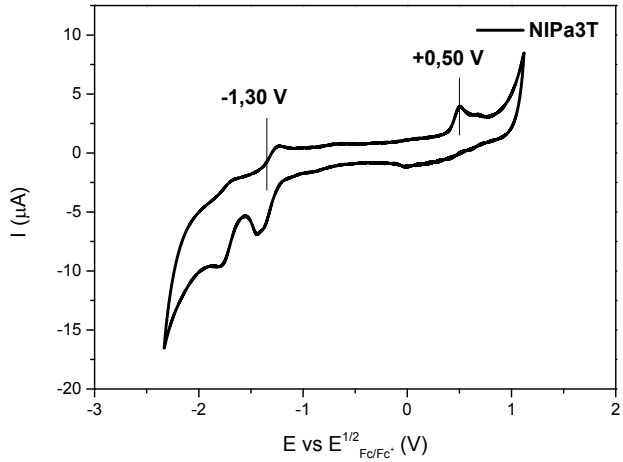

Figure S72 Cyclic voltammetry of **NIPa3T** and TBAHFP 0.1M in dichloromethane solution.

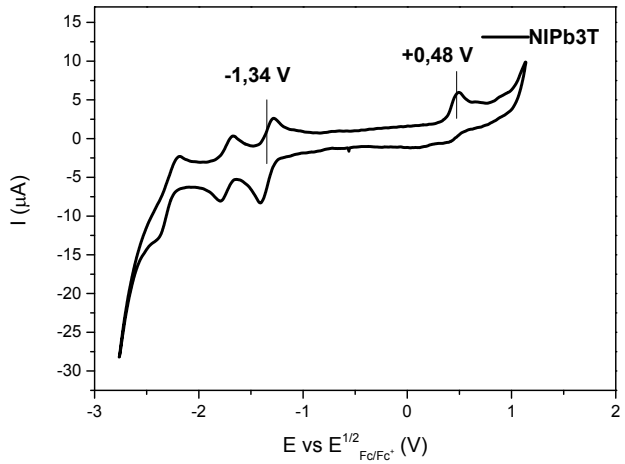

Figure S73 Cyclic voltammetry of **NIPb3T** and TBAHFP 0.1M in dichloromethane solution.

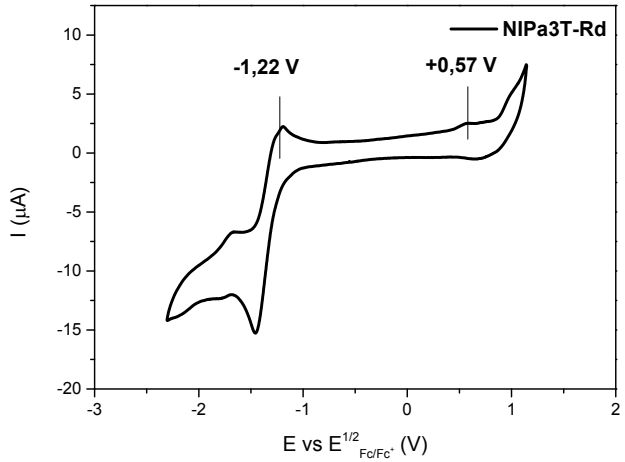

Figure S74 Cyclic voltammetry of **NIPa3T-Rd** and TBAHFP 0.1M in dichloromethane solution.

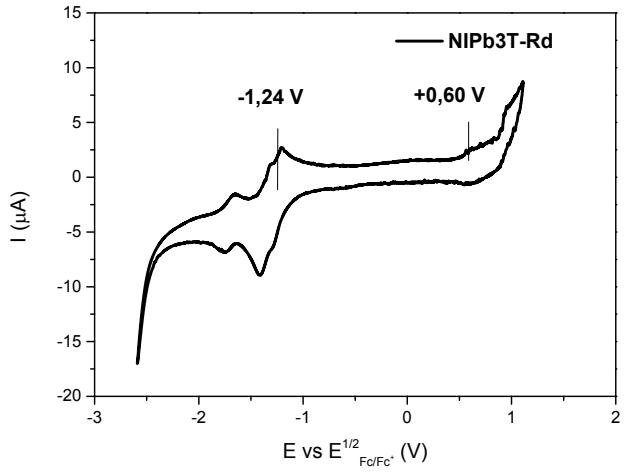

Figure S75 Cyclic voltammetry of **NIPb3T-Rd** and TBAHFP 0.1M in dichloromethane solution.

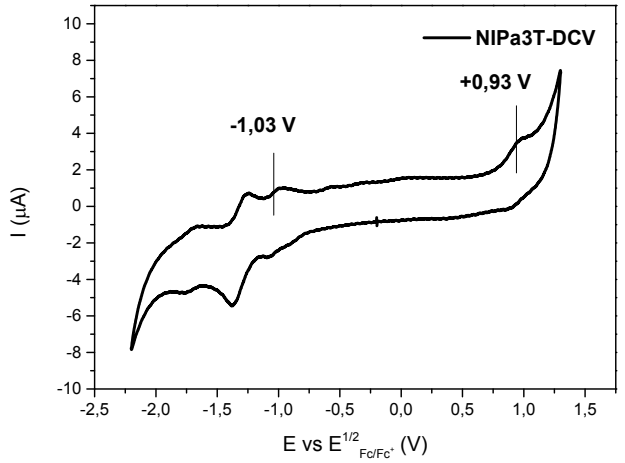

Figure S76 Cyclic voltammetry of **NIPa3T-DCV** and TBAHFP 0.1M in dichloromethane solution.

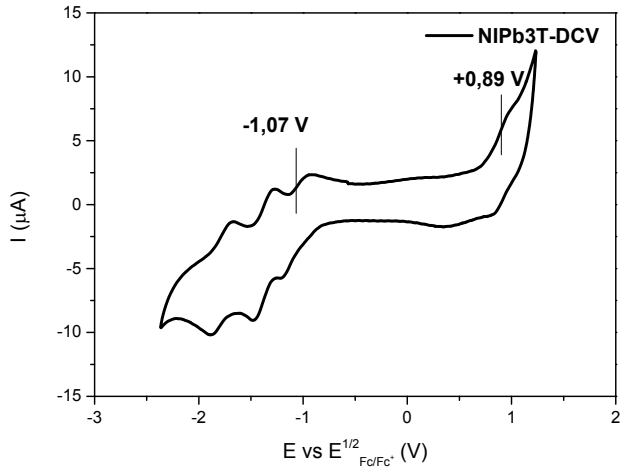

Figure S77 Cyclic voltammetry of **NIPb3T-DCV** and TBAHFP 0.1M in dichloromethane solution.

6. Spectroelectrochemical measurements

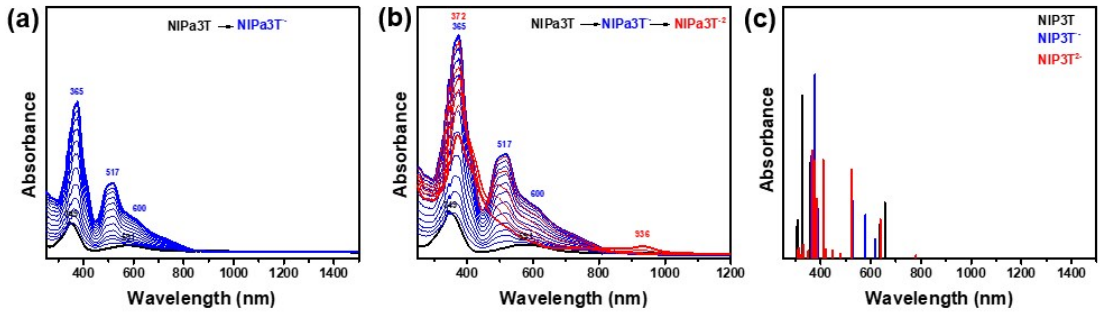

Figure S78 (a),(b) UV-Vis-NIR absorption spectra of **NIP3T** electrochemically reduced by progressive increase of the reduction potential; (c) TDDFT-B3LYP/6-31G**-calculated vertical transition energies.

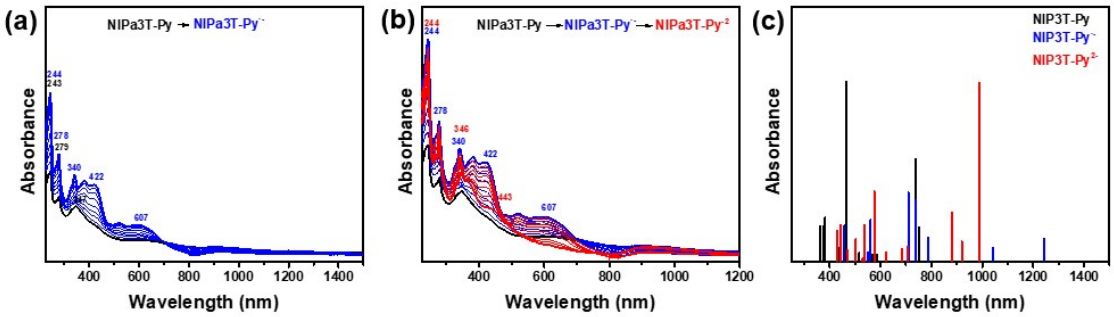

Figure S79 (a),(b) UV-Vis-NIR absorption spectra of **NIP3T-Py** electrochemically reduced by progressive increase of the reduction potential; (c) TDDFT-B3LYP/6-31G**-calculated vertical transition energies.

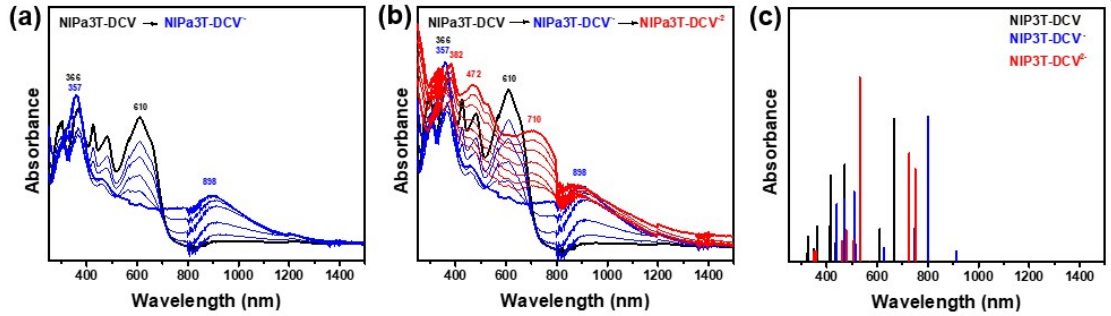

Figure S80 (a),(b) UV-Vis-NIR absorption spectra of **NIPb3T-DCV** electrochemically reduced by progressive increase of the reduction potential; (c) TDDFT-B3LYP/6-31G**-calculated vertical transition energies.

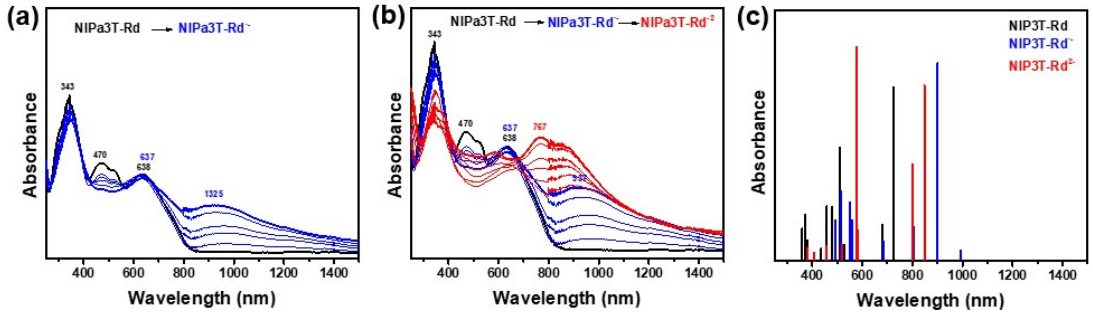

Figure S81 (a),(b) UV-Vis-NIR absorption spectra of **NIPb3T-Rd** electrochemically reduced by progressive increase of the reduction potential ; (c) TDDFT-B3LYP/6-31G**-calculated vertical transition energies.

7. XRD

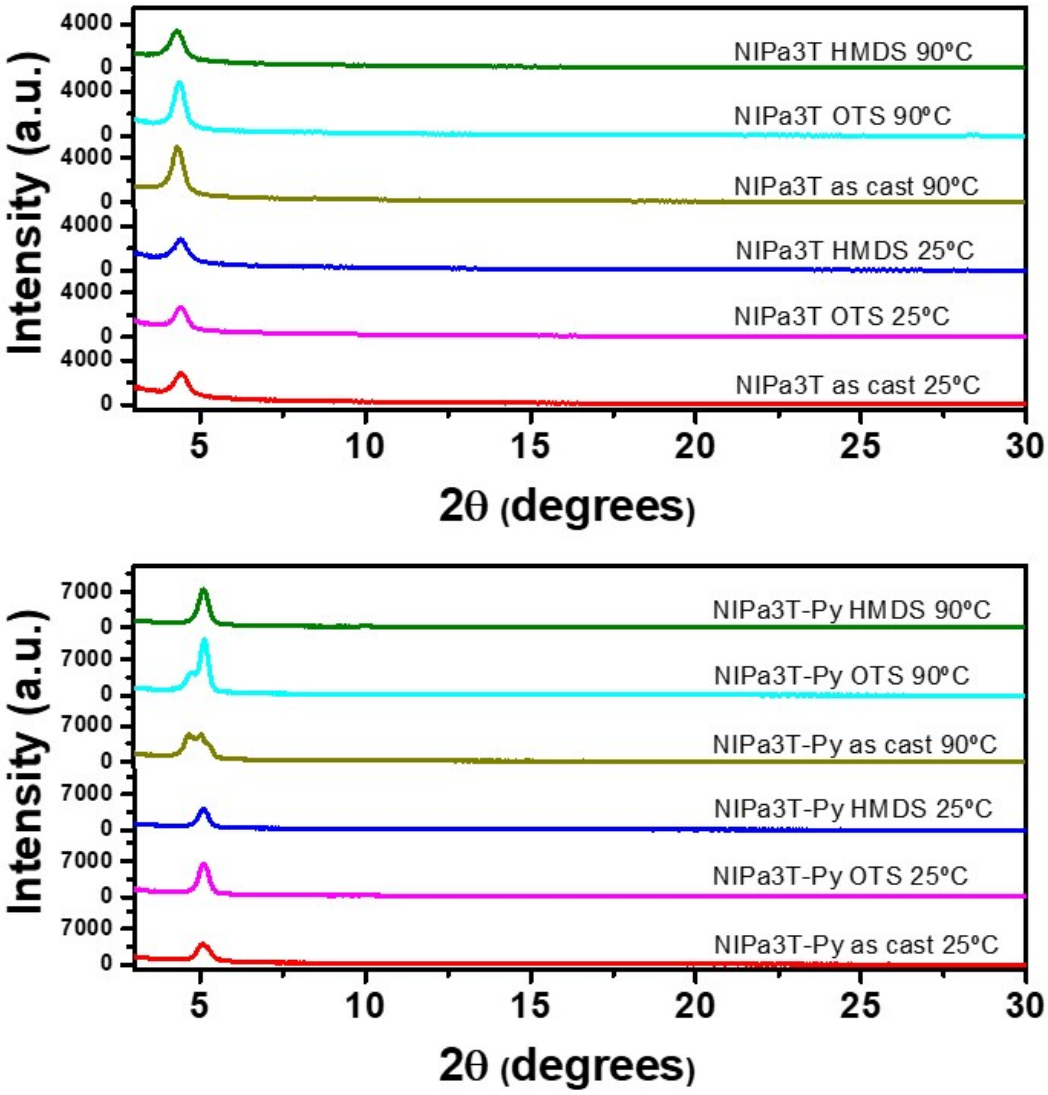

Figure S82. Θ-2Θ X-ray diffraction scans of vapor-deposited, **NIPa3T** and **NIPa3T-Py** thin films (Td = 25ºC and 90ºC) grown on as cast, OTS or HMDS-treated Si/SiO_2 substrates.

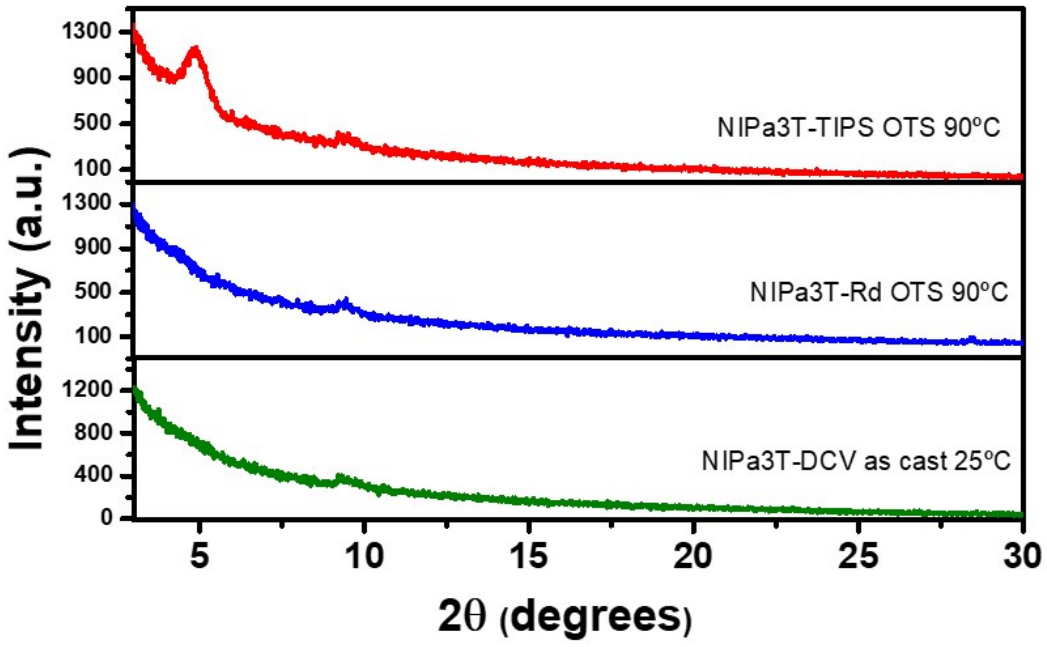

Figure S83. Θ-2Θ X-ray diffraction scans of vapor-deposited **NIPa3T-TIPS**, **NIPa3T-Rd** and **NIPa3T-DCV** thin films (Td = 90ºC) grown on OTS-treated Si/SiO_2 substrates.

8. AFM

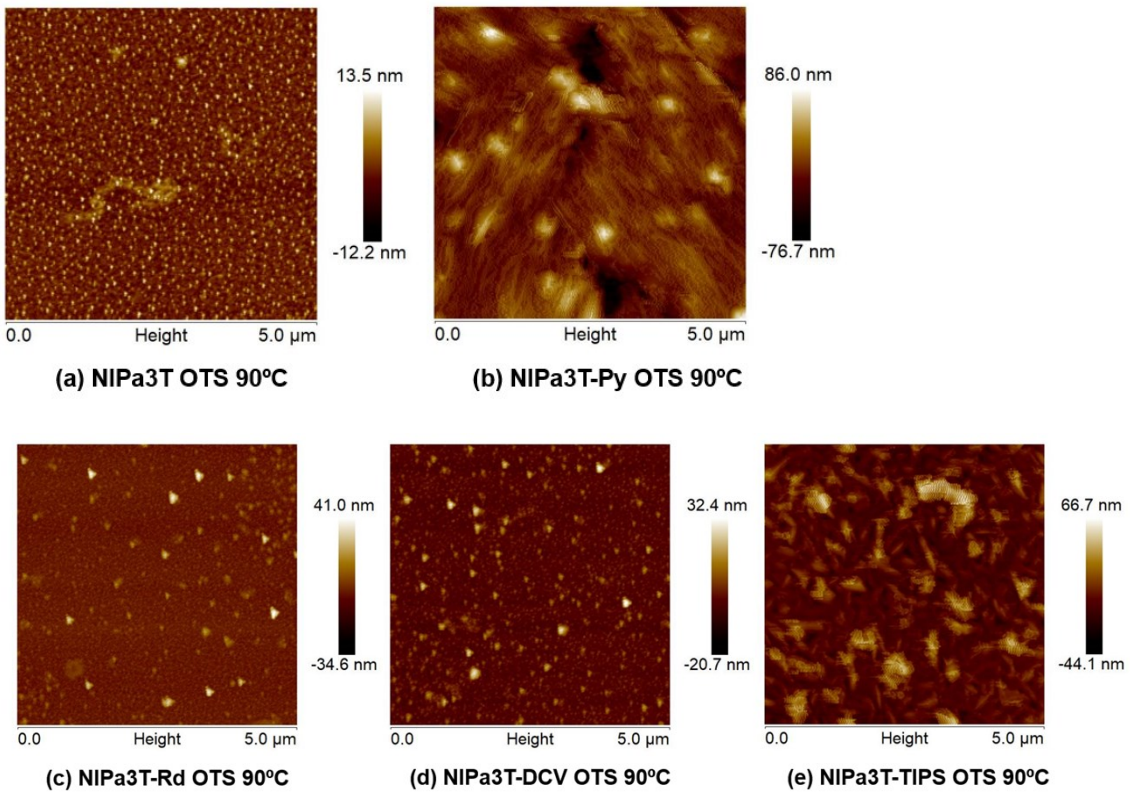

Figure S84. AFM images of the (a) NIPa3T, (b) NIPa3T-Py, (c) NIPa3T-Rd, (d) NIPa3T-DCV and (e) NIPa3T-TIPS vapor-deposited under conditions yielding optimum OFET performance. Image size: 5x5 mm.

9. Organic field effect transistor

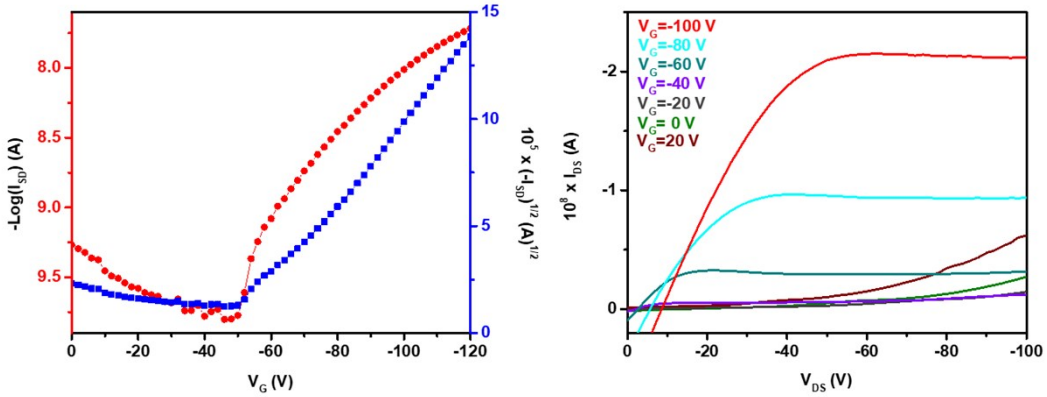

Figure S85. OFET transfer and output characteristics of **NIPa3T**.

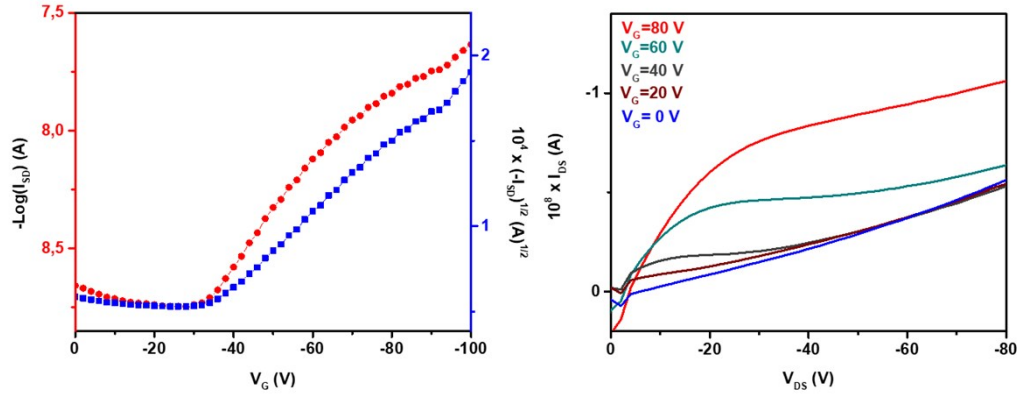

Figure S86. OFET transfer and output characteristics of **NIPa3T-TIPS**.

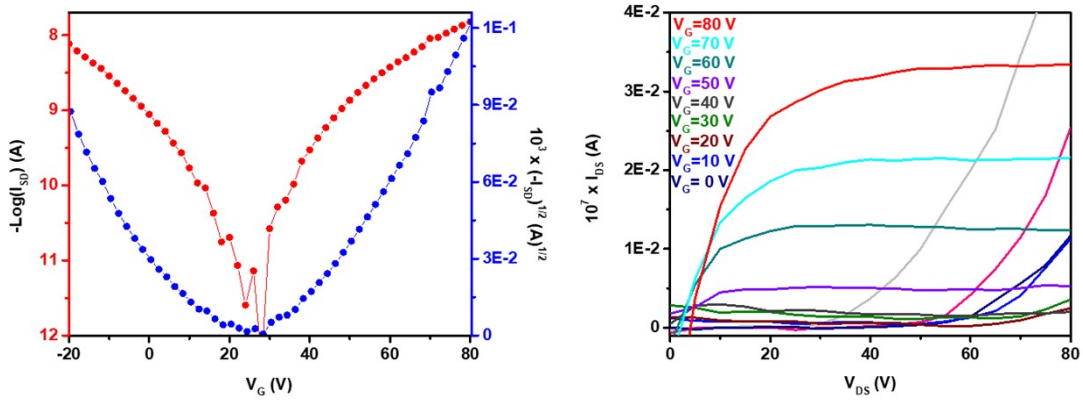

Figure S87. OFET transfer and output characteristics of **NIPa3T-Rd**.

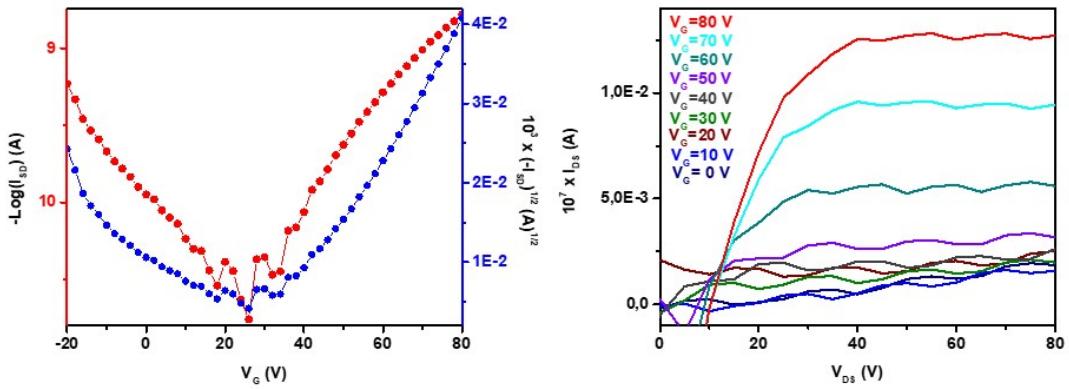

Figure S88. OFET transfer and output characteristics of **NIPa3T-DCV**.

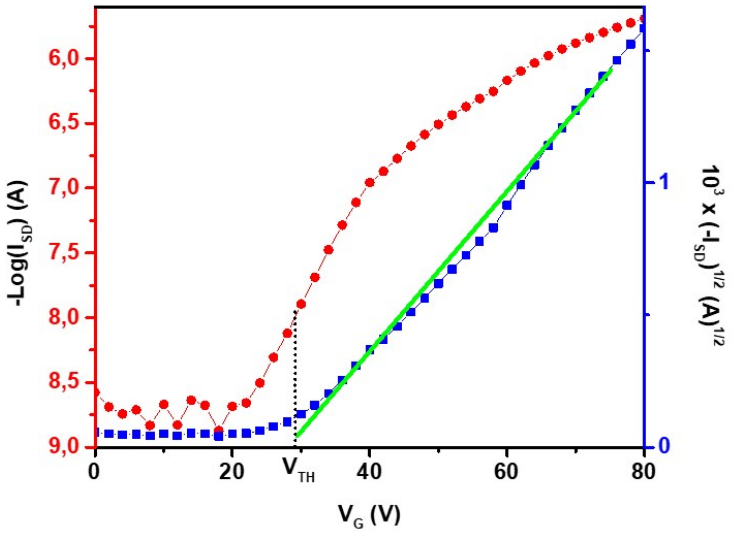

Figure S89. OFET transfer characteristics of **NIPa3T-Py** with the linear fitting used to calculate the electron mobility.

10. Organic solar cells (OSC)

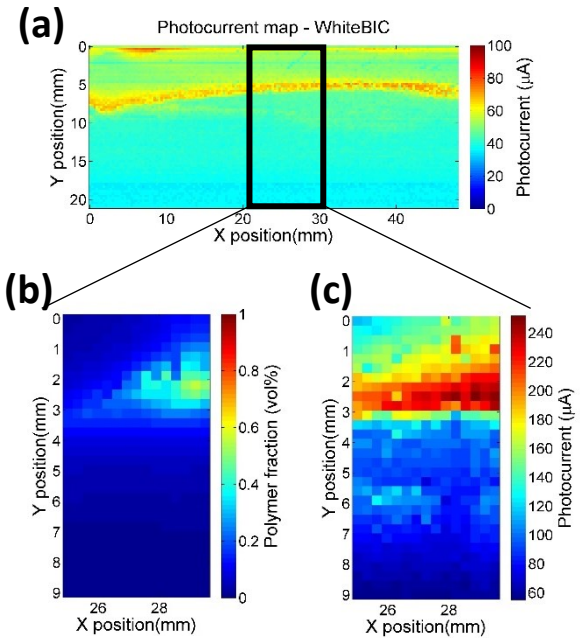

Figure S90. a) Local photocurrent under white light mapping of a **P3HT:NIPb3T-Rd** OSC with a composition gradient. b) P3HT fraction map, zoomed in. c) Local photocurrent under 488nm laser illumination, zoomed in.

One continuous organic solar cell (OSC) device was fabricated by blade coating, using a two-drop method to obtain a lateral composition gradient in order to efficiently explore all the possible compositions of donor:acceptor, following the method described in a previous work.[20]

The local photocurrent was extracted by illuminating the sample locally, and the local composition extracted by analyzing the Raman signal of the material.[21]

Raman cross-section for **NIPb3T-Rd** was calculated from the Raman signal of the pure material deposited as thin film with a thickness gradient on a glass slide, and the value obtained was $2.46*10^{-5}$. For this single sample, a first evaluation of the performance can be made. We deduced from here that the best efficiencies occurred for polymer rich compositions.

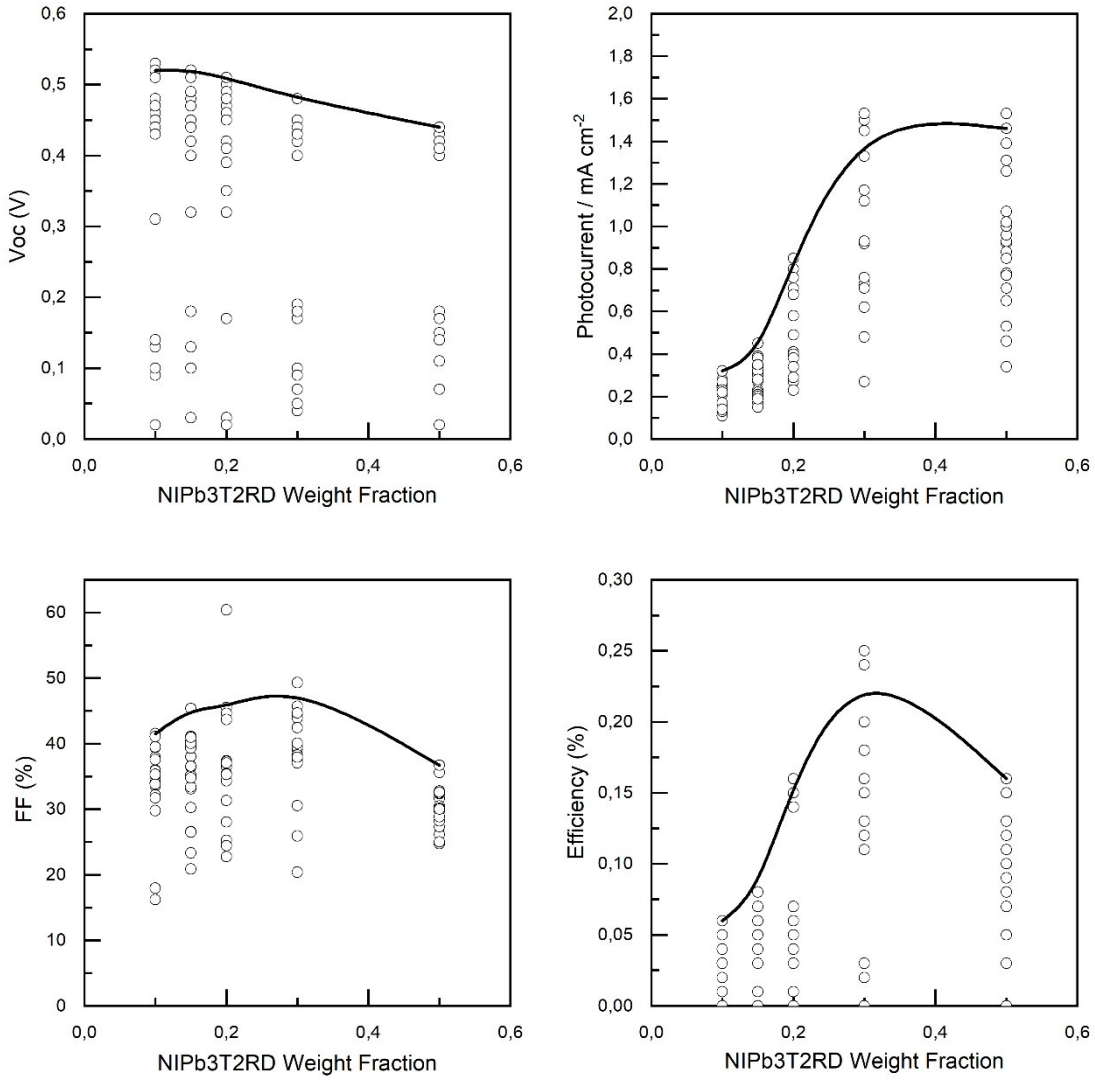

Figure S91. Electrical parameters of discrete OSC with a thickness gradient, for 5 different **P3HT:NIPb3T-Rd** composition ratios a) Open circuit voltage. b) Short circuit current c) Fill Factor d) Efficiency

In a second step, 5 discrete samples were fabricated in order to obtain all the electrical parameters for 5 different P3HT:NIPb3T-Rd composition ratios around the optimum found with the continuous sample above. Each sample contained 12 times 2 pixels. We fabricated the samples with a controlled thickness gradient, so each pixel had a slightly different local thickness, and thus the optimum thickness could be identified.

Both materials were premixed, dissolved in chlorobenzene, at 15mg/ml and stirred overnight at 80ºC, deposited in an inverted structure (Glass/ITO/ZnO/Active Layer/MoO_3/Ag) by blade coating at 80ºC, with a 200µm gap, applying a thickness gradient in each sample by varying linearly the deposition speed from 90 to 10 mm/s while depositing.[20]

11. References

1. P. de Echegaray, M. J. Mancheño, I. Arrechea-Marcos, R. Juárez, G. López-Espejo, J. T. López Navarrete, M. M. Ramos, C. Seoane, R. P. Ortiz and J. L. Segura, *J. Org. Chem.*, 2016, **81**, 11256-11267.
2. H. Li, F. S. Kim, G. Ren, E. C. Hollenbeck, S. Subramaniyan and S. A. Jenekhe, *Angew. Chem. Int. Ed.*, 2013, **52**, 5513-5517.
3. H. Herrera, P. de Echegaray, M. Urdanpilleta, M. J. Mancheño, E. Mena-Osteritz, P. Bäuerle and J. L. Segura, *Chem. Commun.*, 2013, **49**, 713-715.
4. R. C. DeCicco, A. Black, L. Li and N. S. Goroff, *Eur. J. Org. Chem.*, 2012, **2012**, 4699-4704.
5. W. Mammo, S. Admassie, A. Gadisa, F. Zhang, O. Inganäs and M. R. Andersson, *Sol. Energy Mater. Sol. Cells*, 2007, **91**, 1010-1018.
6. S. Ravi, K. K. Chiruvella, K. Rajesh, V. Prabhu and S. C. Raghavan, *Eur. J. Med. Chem.*, 2010, **45**, 2748-2752.
7. T. Wang, N. Zhang, K. Zhang, J. Dai, W. Bai and R. Bai, *Chem. Commun.*, 2016, **52**, 9679-9682.
8. W.-C. Yen, B. Pal, J.-S. Yang, Y.-C. Hung, S.-T. Lin, C.-Y. Chao and W.-F. Su, *J. POLYM. SCI. POL. CHEM.*, 2009, **47**, 5044-5056.
9. B. P. Karsten, R. K. M. Bouwer, J. C. Hummelen, R. M. Williams and R. A. J. Janssen, *J. Phys. Chem. B*, 2010, **114**, 14149-14156.
10. A. Riaño, P. Mayorga Burrezo, M. J. Mancheño, A. Timalsina, J. Smith, A. Facchetti, T. J. Marks, J. T. López Navarrete, J. L. Segura, J. Casado and R. Ponce Ortiz, *J. Mater. Chem. C*, 2014, **2**, 6376-6386.
11. C. Lee, W. Yang and R. G. Parr, *Phys. Rev. B Condens. Matter*, 1988, **37**, 785-789.
12. A. D. Becke, *J. Chem. Phys.*, 1993, **98**, 5648-5652.
13. A. D. Becke, *J. Chem. Phys.*, 1993, **98**, 1372-1377.
14. P. C. Hariharan and J. A. Pople, *Theoret. Chim. Acta*, 1973, **28**, 213-222.
15. W. J. Hehre and W. A. Lathan, *J. Chem. Phys.*, 1972, **56**, 5255-5257.
16. G. W. S. M. J. T. Frisch, H. B.; Scuseria, G. E.; Robb, M. A.; Cheeseman, J. R.; Scalmani, G.; Barone, V.; Petersson, G. A.; Nakatsuji, H.; Li, X.; Caricato, M.; Marenich, A. V.; Bloino, J.; Janesko, B. G.; Gomperts, R.; Mennucci, B.; Hratchian, H. P.; Ortiz, J. V.; Izmaylov, A. F.; Sonnenberg, J. L.; Williams-Young, D.; Ding, F.; Lipparini, F.; Egidi, F.; Goings, J.; Peng, B.; Petrone, A.; Henderson, T.; Ranasinghe, D.; Zakrzewski, V. G.; Gao, J.; Rega, N.; Zheng, G.; Liang, W.; Hada, M.; Ehara, M.; Toyota, K.; Fukuda, R.; Hasegawa, J.; Ishida, M.; Nakajima, T.; Honda, Y.; Kitao, O.; Nakai, H.; Vreven, T.; Throssell, K.; Montgomery, J. A., Jr.; Peralta, J. E.; Ogliaro, F.; Bearpark, M. J.; Heyd, J. J.; Brothers, E. N.; Kudin, K. N.; Staroverov, V. N.; Keith, T. A.; Kobayashi, R.; Normand, J.; Raghavachari, K.; Rendell, A. P.; Burant, J. C.; Iyengar, S. S.; Tomasi, J.; Cossi, M.; Millam, J. M.; Klene, M.; Adamo, C.; Cammi, R.; Ochterski, J. W.; Martin, R. L.; Morokuma, K.; Farkas, O.; Foresman, J. B.; Fox, D. J. Gaussian, Inc., Wallingford CT., 2016.
17. J. D. Chai and M. Head-Gordon, *J Chem Phys*, 2008, **128**, 084106.
18. L. M. d. Costa, *J. Comput.Chem.*, 2004, **25**, 1463.
19. R. Ditchfield, W. J. Hehre and J. A. Pople, *J. Chem. Phys.*, 1971, **54**, 724-728.
20. A. Sánchez-Díaz, X. Rodríguez-Martínez, L. Córcoles-Guija, G. Mora-Martín and M. Campoy-Quiles, *Adv. Electron. Mater.*, 2018, **4**, 1700477.

21. X. Rodríguez-Martínez, M. S. Vezie, X. Shi, I. McCulloch, J. Nelson, A. R. Goñi and M. Campoy-Quiles, *J. Mater. Chem. C*, 2017, **5**, 7270-7282.